

PL-TR-92-2115

AD-A256 687



2

HYDRODYNAMIC METHODS FOR MONITORING
UNDERGROUND NUCLEAR TESTS

F. K. Lamb
J. D. Sullivan
B. W. Calien
R. A. Fiedler

University of Illinois at Urbana-Champaign
Department of Physics
1110 West Green Street
Urbana, Illinois 61801

April 1992

SDTIC
ELECTE
AUG 20 1992
A D

Final Report
16 September 1988—31 December 1991

Approved for public release; distribution unlimited



PHILLIPS LABORATORY
AIR FORCE SYSTEMS COMMAND
HANSCOM AIR FORCE BASE, MASSACHUSETTS 01731-5000

92-23092



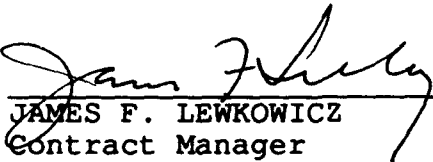
12 8 19 019

SPONSORED BY
Defense Advanced Research Projects Agency
Nuclear Monitoring Research Office
ARPA ORDER NO. 5307

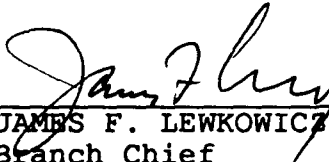
MONITORED BY
Phillips Laboratory
Contract No. F19628-88-K-0040

The views and conclusions contained in this document are those of the authors and should not be interpreted as representing the official policies, either expressed or implied, of the Defense Advanced Research Projects Agency or the U.S. Government.

This technical report has been reviewed and is approved for publication.



JAMES F. LEWKOWICZ
Contract Manager
Solid Earth Geophysics Branch
Earth Sciences Division



JAMES F. LEWKOWICZ
Branch Chief
Solid Earth Geophysics Branch
Earth Sciences Division



DONALD H. ECKHARDT, Director
Earth Sciences Division

This report has been reviewed by the ESD Public Affairs Office (PA) and is releasable to the National Technical Information Service (NTIS).

Qualified requestors may obtain additional copies from the Defense Technical Information Center. All others should apply to the National Technical Information Service.

If your address has changed, or if you wish to be removed from the mailing list, or if the addressee is no longer employed by your organization, please notify PL/IMA, Hanscom AFB, MA 01731-5000. This will assist us in maintaining a current mailing list.

Do not return copies of this report unless contractual obligations or notices on a specific document requires that it be returned.

REPORT DOCUMENTATION PAGE

FORM NO. 104 OTRR

This report contains information which is classified "Secret" or "Confidential" and is intended for the use of the Department of Energy and the Department of Defense. It is not to be distributed outside the Department of Energy and the Department of Defense. If you are not a member of the Department of Energy or the Department of Defense, you should not disseminate this report. If you are a member of the Department of Energy or the Department of Defense, you should not disseminate this report outside your organization. For more information on the classification of this report, contact the Office of Information Operations and Reports, U.S. Jefferson Building, Suite 1204, Washington, DC 20545.

1 AGENCY USE ONLY (Leave Blank)		2 REPORT DATE April, 1992	3 REPORT TYPE AND DATES COVERED Final Report 9/16/88-12/31/91	
4 TITLE AND SUBTITLE Hydrodynamic Methods for Monitoring Underground Nuclear Tests			5. FUNDING NUMBERS Contract F19628-88-K-0040 PE 62714E PR 8A10 TA DA WU AL	
6 AUTHOR(S) F. K. Lamb* B.W. Callen J. D. Sullivan* R. A. Fiedler				
7. PERFORMING ORGANIZATION NAME(S) AND ADDRESS(ES) University of Illinois at Urbana-Champaign Department of Physics 1110 West Green Street Urbana, IL 61801			8. PERFORMING ORGANIZATION REPORT NUMBER	
9 SPONSORING/MONITORING AGENCY NAME(S) AND ADDRESS(ES) Geophysics Laboratory Hanscom AFB, MA 01731-5000 Contract Manager: James Lewkowicz/GPEH			10. SPONSORING/MONITORING AGENCY REPORT NUMBER PL-TR-92-2115	
11. SUPPLEMENTARY NOTES * Co-investigators				
12a. DISTRIBUTION/AVAILABILITY STATEMENT Approved for public release; distribution unlimited			12b. DISTRIBUTION CODE	
13. ABSTRACT (Maximum 200 words) <p>Research performed under this contract is designed to improve the analysis and interpretation of shock-wave data in the hydrodynamic region gathered in the past or in the future to monitor agreed limitations on underground nuclear testing. Research accomplishments include: (1) refinement and comparison to numerical simulations and actual nuclear test data of an approximate analytical model of the shock-front radius vs. time relationship for a variety of geologic media; (2) assembly of a Hugoniot database for several important classes of geologic materials; (3) investigation—by means of the approximate analytical model—of the nature and physical basis of the insensitive interval discovered empirically in hydrodynamic data taken at US test sites; (4) a rigorous analysis of the conditions under which cube-root scaling is an exact condition in the hydrodynamic region; (5) detailed analysis using state-of-the-art, one-dimensional hydrodynamic numerical simulations of the effects of source parameters on hydrodynamic yield estimation; (6) the development of a state-of-the-art, two-dimensional hydrodynamic code suitable for simulating two-dimensional source and/or ambient medium effects.</p>				
14. SUBJECT TERMS Threshold Test Ban Treaty, hydrodynamic methods, shock waves, underground nuclear explosions			15. NUMBER OF PAGES 110	
			16. PRICE CODE	
17. SECURITY CLASSIFICATION OF REPORT Unclassified	18. SECURITY CLASSIFICATION OF THIS PAGE Unclassified	19. SECURITY CLASSIFICATION OF ABSTRACT Unclassified	20. LIMITATION OF ABSTRACT SAR	

I. OBJECTIVES

The overall objective of the project was to improve the analysis and interpretation of shock wave data gathered in the past or in the future to monitor agreed limitations on underground nuclear testing. Specific objectives were to explore the effects of the ambient geologic medium on yield estimates made using shock wave methods; to investigate the effects of different test geometries; and to explore the possibility of using shock wave methods to monitor limitations well below the current yield limit of 150 kt.

II. ACHIEVEMENTS

The overall and specific objectives of this project have been achieved. In particular:

(1) We refined and fully analyzed a simple analytical model for shock-wave propagation in homogeneous media proposed earlier by one of the investigators (FKL) to understand the usefulness of the model in exploring the sensitivity of shock-front radius vs. time (RVT) relationships to variations in the properties of ambient geologic media. As part of our evaluation, we used the model to estimate the yield of six underground nuclear explosions, using unclassified radius vs. time data, as well as numerical simulations of explosions in two different media. (The RVT data from the six actual explosions represent all currently available unclassified data applicable to studies in the hydrodynamic region.) When we used the best piecewise-continuous representation of Hugoniot data available in the open literature, we found that the analytical model gave yield estimates accurate to eight percent or better for all cases studied.

(2) In order to exploit capabilities offered by the analytical model for carrying out simple sensitivity and error analyses, we collected Hugoniot data from the open literature for a wide range of geologic media believed to be characteristic of U.S. and (former) Soviet test sites.

(3) Using the analytical model, we carried out a two-part study of the insensitive interval. This interval, which was discovered empirically in studies of U.S. test data, is a portion of the hydrodynamic region for which the shock-front radius vs. time relationship is relatively insensitive to the properties of geologic media, yet still sensitive to the yield. Using a first-order approximation to the crossing point predicted by the analytical model for the radius vs. time curves for two different media, we first demonstrated that the existence of an insensitive interval is related to the existence of a simple power-law correlation between the parameters describing the Hugoniot in the linear (high-pressure) region for silicates and, similarly, for carbonates. (These two classes are representative of media encountered in the majority of U.S. underground tests.) Next, without making any approximations, we used the analytical model together with a simple representation of experimental uncertainties to study further the characteristics of the insensitive interval and to map its location

for silicate and carbonate ambient media. These latter studies are illustrative of the results one would expect from a full error and uncertainty analysis of hydrodynamic yield determination. To carry out a full analysis one must have detailed knowledge of the experimental apparatus employed to gather data in the hydrodynamic region (currently unavailable in the open literature) and of uncertainties in parameters characterizing the ambient medium. The product of such an analysis would be an optimal set of weights to be assigned to experimental data throughout the hydrodynamic region; the most heavily weighted region would correspond to the insensitive interval.

(4) Essentially all models—empirical, numerical, or otherwise—used to reduce data taken in the hydrodynamic region assume cube-root-of-yield scaling, yet previous theoretical studies of this scaling are incomplete and, in some cases, are in error. Accordingly, we carried out a rigorous examination of the conditions necessary for cube-root scaling to obtain in the hydrodynamic region. We find that the initial value data (source data) must also scale if cube-root scaling is to be exact.

(5) We modified an existing one-dimensional, state-of-the-art hydrodynamic code (Zeus) at the UIUC National Center for Supercomputing Applications (NCSA) in two important ways: (i) the code was modified to accept tabular representations of the equation-of-state of source and ambient media, and (ii) the code was changed to explicitly conserve total energy. The resultant code permits distinct equation-of-state choices to be made for the source and ambient medium and is optimized to run efficiently in a vector processing mode. The modified code was carefully checked against the analytic Sedov-Taylor blast wave solution, which is asymptotically correct for explosions in an ideal gas medium. Finally, we used the modified one-dimensional code to simulate a set of underground explosions in order to study the dependence of hydrodynamic yield estimates on the mass, size, and composition of the source. These simulations were carried out for two different ambient media and three different source equations of state.

(6) We developed a modified version of the state-of-the-art, two-dimensional Zeus code at NCSA. The changes and characteristics of Zeus-2D-Mod are similar to Zeus-1D-Mod described just above. Zeus-2D-Mod can be utilized to simulate two-dimensional source and/or ambient medium effects, such as cylindrical sources and layered media.

Accession For	
NTIS CRA&I	<input checked="" type="checkbox"/>
DTIC TAB	<input type="checkbox"/>
Unannounced	<input type="checkbox"/>
Justification	
By	
Distribution/	
Availability Codes	
Dist	Avail and/or Special
A-1	

DTIC QUALITY INSPECTED 5

III. PAPERS PREPARED UNDER THIS CONTRACT

1. F. K. Lamb, B. W. Callen, and J. D. Sullivan, "Yield Estimation Using Shock Wave Methods," *Explosion Source Phenomenology, Geophysical Monograph 65*, edited by S. R. Taylor, P. G. Richards, and H. J. Patton, American Geophysical Society, Washington, D. C., pp. 73-89, 1991.
2. F. K. Lamb, B. W. Callen, and J. D. Sullivan, "An Approximate Analytical Model of Shock Waves from Underground Nuclear Explosions," *Journal of Geophysical Research*, Vol. 97, No. B1, pp. 515-535, 1992.
3. B. W. Callen, F. K. Lamb, and J. D. Sullivan, "Insensitive Interval in the Evolution of Shock Waves," *Shock Compression in Condensed Matter-1989*, edited by S. C. Schmidt, J. N. Johnson, and L. W. Davidson, Elsevier Science, New York, pp. 241-244, 1990.
4. F. K. Lamb, B. W. Callen, and J. D. Sullivan, "Insensitive Interval in the Evolution of Shock Waves from Underground Nuclear Explosions," presented at the 11th Annual AFGL/DARPA Seismic Research Symposium (GL-TR-90-0301, ADA229228), San Antonio, Texas, 2-4 May 1989.
5. B. W. Callen, F. K. Lamb, and J. D. Sullivan, "Hydrodynamic Determination of the Yield of Underground Nuclear Explosions," presented at the 12th Annual DARPA/GL Seismic Research Symposium (GL-TR-90-0212, ADA226635), Key West, Florida, 18-20 September 1990.
6. B. W. Callen, R. A. Fiedler, F. K. Lamb, and J. D. Sullivan, "Effects of Source Parameters on Hydrodynamic Yield Estimation and New Results on the Insensitive Interval," presented at 13th Annual PL/DARPA Seismic Research Symposium (PL-TR-91-2208, ADA241325), Keystone, Colorado, 8-10 October 1991.
7. F. K. Lamb, R. A. Fiedler, B. W. Callen, and J. D. Sullivan, "Effects of Source Parameters on Hydrodynamic Yield Estimation," detailed manuscript in preparation for submission to *Journal of Geophysical Research*.
8. B. W. Callen, F. K. Lamb, J. D. Sullivan, and R. A. Fiedler, "The Insensitive Interval and Optimal Weighting of Experimental Data from the Hydrodynamic Region," detailed manuscript in preparation for submission to *Journal of Geophysical Research*.

Copies of papers (1)-(6) are contained in Appendix A to this report.

Appendix A

.

.

.

.

YIELD ESTIMATION USING SHOCK WAVE METHODS

Frederick K. Lamb¹, Bruce W. Callen, and Jeremiah D. Sullivan

Department of Physics and Program in Arms Control, Disarmament, and International Security
University of Illinois at Urbana-Champaign, Urbana, Illinois 61801

Abstract. The yields of underground nuclear explosions can be estimated using shock wave methods. These methods make use of the fact that the strength of the expanding shock wave produced by an underground explosion increases with the yield. We first discuss the basis of shock wave yield estimation methods, including the properties of shock waves in rock, the evolution of the shock waves produced by underground nuclear explosions, and the dependence of the evolution on the properties of the ambient medium. We then describe several techniques that have been developed in the United States to measure the shock front position as a function of time, including the so-called CORTEX technique. Finally, we consider several of the algorithms that have been used to derive yield estimates from measurements of the shock front position as a function of time, the application of these algorithms to low-yield explosions, and the expected accuracy of shock wave methods.

1. Introduction

Shock wave methods have long been used to estimate the yields of nuclear explosions, both in the atmosphere (see, for example, Sedov [1946, 1959] and Taylor [1950a, 1950b]) and underground (see, for example, Johnson, Higgins, and Violet [1959], Nuckolls [1959], Butkovich [1965]). Shock wave methods were introduced as a treaty-monitoring tool in the original 1976 Protocol of the Peaceful Nuclear Explosions Treaty (PNET), which explicitly established such methods as among those that could be used to monitor the yield of any salvo of underground explosions with a planned aggregate yield greater than 150 kilotons (kt) (U. S. Arms Control and Disarmament Agency, 1990a). The United States and the Soviet Union have recently ratified new verification protocols for both the PNET and the Threshold Test Ban Treaty (TTBT) that allow the use of shock wave yield estimation methods for explosions having a planned yield greater than 50 kt (the texts of these protocols may be found in U. S. Arms Control and Disarmament Agency [1990b]).

In this article, we review shock wave yield estimation methods and their application to nuclear test monitoring. Such methods make use of the fact that the strength of the shock wave produced by an underground nuclear explosion increases with the yield of the explosion, other things being equal. As a result, the speed of the shock front and the particle speed and pressure just behind it are greater at a given radius for explosions of greater yield. The yield of the

explosion can therefore be estimated by comparing measurements of these quantities with a model of the evolution of the shock wave in the ambient geologic medium. Although in principle the yield can be estimated from measurements of the post-shock particle speed or pressure, in practice constructing and emplacing transducers to measure these quantities and obtaining reliable measurements has proved difficult. For this reason, U. S. efforts to develop shock wave yield estimation methods have for the past 15 years emphasized techniques for sensing the position of the shock front as a function of time and for analyzing such position measurements to obtain a yield estimate. Hence, in the present review we focus primarily on this approach.

We begin in §2 by summarizing some of the relevant properties of shock waves in rock and reviewing the phases of an underground nuclear explosion. We then introduce a simplified model and use it to illustrate how the shock wave produced by a spherically-symmetric point explosion would evolve. Finally, we discuss the more complex evolution of the shock waves produced by actual underground nuclear tests. In §3 we explain the CORTEX technique currently used by the United States to measure the position of the shock front as a function of time. In §4 we describe several of the algorithms that have been used to derive yield estimates from shock front position measurements, the application of these algorithms to low-yield explosions, and the expected accuracy of shock wave methods. Our conclusions are summarized in §6. For a discussion of the implications of using shock wave methods to monitor present and possible future limitations on underground nuclear testing, see Lamb [1988].

2. Shock Waves from Underground Nuclear Explosions

In this section, we summarize briefly the general properties of shock waves in rock, describe the phases of an underground nuclear explosion, and discuss the evolution of the spherical shock wave produced by a point explosion in a uniform solid medium. Finally, we describe the sometimes quite complex shock waves in rock produced by actual nuclear tests.

Shock Waves in Rock

Shock waves in rock behave differently from shock waves in air, primarily because the atoms in rock are close together and interact strongly (see Zel'dovich and Raizer [1967], pp. 685-705), that is, the equation of state is fundamentally different.

Elastic and plastic waves.—The strength of a shock wave can be characterized by the peak pressure that it produces. Weak shock waves and acoustic waves in rock propagate at a constant speed, the so-called elastic wave speed (see Zel'dovich and Raizer [1967], pp. 741-746)

$$c_t = \left(\frac{K_0 + \frac{4}{3}G_0}{\rho_0} \right)^{1/2} \quad (1)$$

¹Also, Department of Astronomy

Explosion Source Phenomenology
Geophysical Monograph 65
Copyright 1991 American Geophysical Union

Here K_0 and G_0 are the bulk and shear moduli, respectively, of the rock in its standard state, and ρ_0 is the mass density. The speed c_t is also sometimes called the longitudinal sound speed. For granite, $K_0 \approx 36$ GPa and $G_0 \approx 32$ GPa [Holzer, 1965] giving $c_t \approx 5.5$ km s⁻¹ for $\rho_0 = 2.65$ Mg m⁻³.

Shock waves that are strong enough to produce a peak radial stress p_1 greater than the critical shear stress p_{crit} of the rock cause the rock to become plastic (for granite, p_{crit} is about 4 GPa for high strain rates [Holzer, 1965]). Such waves are called plastic waves. The speed of a plastic wave increases with its strength. The weakest such waves propagate at the low-pressure plastic wave speed [Zel'dovich and Raizer, 1967, pp. 741-746]

$$c_0 = \left(\frac{K_0}{\rho_0} \right)^{1/2}, \quad (2)$$

which is determined by the compressibility of the rock in its standard state. The speed c_0 is also sometimes called the bulk sound speed. Since only the bulk modulus contributes to c_0 , it is necessarily less than c_t . For solid granite, $c_0 \approx 4$ km s⁻¹.

If a plastic shock wave is strong enough that the shear strength of the rock can be neglected, it is called a *hydrodynamic* shock wave. If, further, a shock wave is so strong that the speed of the wave front is much greater than the acoustic wave speed in the undisturbed rock, the pressure behind the wave front is predominantly thermal pressure, and the ratio of the density just behind the wave front to the density just ahead of the front is close to its limiting value, it is called a *strong* shock wave (see Zel'dovich and Raizer [1967], pp. 685-705). As discussed below, shock waves in hard rocks such as granite are strong only when the peak pressure p_1 is ≥ 1 TPa.

Shock compression.—The equation of state of a rock may be written as a relation between the pressure p , the specific volume $V = 1/\rho$, and the specific internal energy ϵ . Before the shock front arrives, the rock is at rest with specific volume V_0 , specific internal energy ϵ_0 , and pressure p_0 . As the shock front arrives, the pressure rises rapidly and the rock is severely compressed. We denote the specific volume, specific internal energy, and pressure just after the shock front has passed by V_1 , ϵ_1 , and p_1 , respectively. The changes in these thermodynamic variables occur over such a small distance that the shock front often may be approximated as a mathematical discontinuity. Henceforth we shall assume, unless otherwise stated, that the shock wave is strong enough that it is hydrodynamic.

The curve on the equation of state surface $p = p(V, \epsilon)$ that is relevant for determining the thermodynamic state of rock subjected to shock compression may be seen as follows. Although the shock wave produced by an underground nuclear explosion evolves with time, the time scale of this evolution is much longer than the time required for the shock front to pass through a given fluid element. Thus, the change in the thermodynamic state of a given element as the shock front passes through it may be found by considering a steady shock wave with the instantaneous speed of the actual shock wave. In the frame in which the unshocked material is at rest, conservation of mass, momentum, and energy across the front of a steady shock wave give (see Zel'dovich and Raizer [1967], pp. 45-50 and 705-710)

$$\epsilon_1 - \epsilon_0 = \frac{1}{2}(p_0 + p_1)(V_0 - V_1) = \frac{1}{2}u_1^2 + \left(\frac{p_0 u_1}{\rho_0 D} \right), \quad (3)$$

where D and u_1 are, respectively, the speed of the shock front and the particle speed just behind the shock front. When combined with the equation of state $\epsilon = \epsilon(p, V)$, equation (3) gives the pressure just behind the shock front in terms of the specific volume just behind the front and the pressure and specific volume just ahead of the front, that is,

$$p_1 = p_H(V_1, p_0, V_0) \quad (4)$$

This relation is called the *Hugoniot*. It is *not* the thermodynamic path followed by a fluid element during shock compression, but rather the locus of all final states (p, V) that can be reached by shock compression from a given initial state (p_0, V_0) . The final thermodynamic state depends on the strength of the shock wave.

By analogy with the equation that relates the pressure of a fluid after adiabatic compression to the specific volume after compression, and the pressure and specific volume before compression, relation (4) is sometimes called the "shock adiabat". However, the "shock adiabat" is *not* an isentrope, since shock compression of a fluid increases its entropy (the stronger the shock wave, the greater the increase in the entropy). Thus, the Hugoniot curve crosses isentropes, as shown in Figure 1. The final pressure p_1 produced by shock compression is a function of *two* parameters, such as p_0 and V_0 , as well as the final specific volume V_1 , whereas the pressure p along an isentrope is a function only of the specific volume and the entropy (see Zel'dovich and Raizer [1967], pp. 49-50 and 705-710).

The Hugoniot may also be expressed as a relation between D and u_1 , that is

$$D = D(u_1) \quad (5)$$

To see that this implies a relation of the form (4), note that in the frame in which the undisturbed rock is at rest conservation of momentum across the front of a hydrodynamic shock wave implies

$$p_1 - p_0 = \rho_0 D u_1. \quad (6)$$

Using relation (5), D can be eliminated from equation (6) in favor of u_1 , p_1 , p_0 , and V_0 . The post-shock particle speed u_1 can then be eliminated from equation (3), giving a relation of the form (4). Figure 2 shows a Hugoniot for solid quartz expressed in this way. The step in the curve at $u_1 \approx 2$ km s⁻¹ reflects a phase transformation that occurs at about 40 GPa. Hugoniot for granite are generally similar to this quartz Hugoniot, although they differ in detail. In general the Hugoniot of rock in the field depends on the bulk density, grain density, chemical composition, fracture pattern, porosity, and water

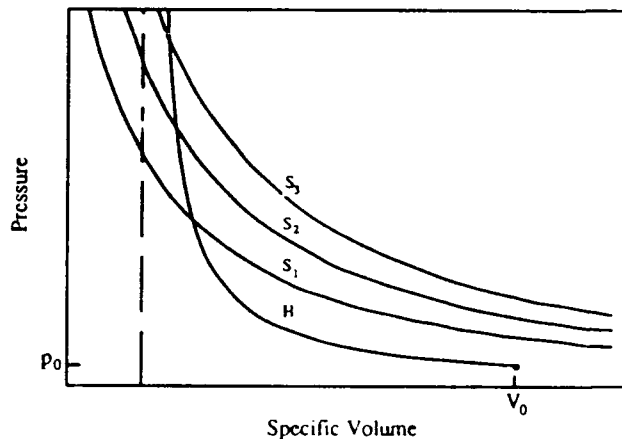


Fig. 1. Hugoniot (labeled H) for a hypothetical non-porous material initially in the state (p_0, V_0) (dot) and several isentropes (labeled by their entropies $S_1 < S_2 < S_3$) for the same material. All final states (p_1, V_1) that can be reached via shock compression from (p_0, V_0) lie along H . The stronger the shock wave, the smaller the final specific volume and the higher the final pressure. The Hugoniot crosses isentropes of increasing entropy as the final specific volume decreases, showing that the entropy of the final state increases with the strength of the shock wave. The vertical dashed line indicates the limiting specific volume for a strong shock wave in this material.

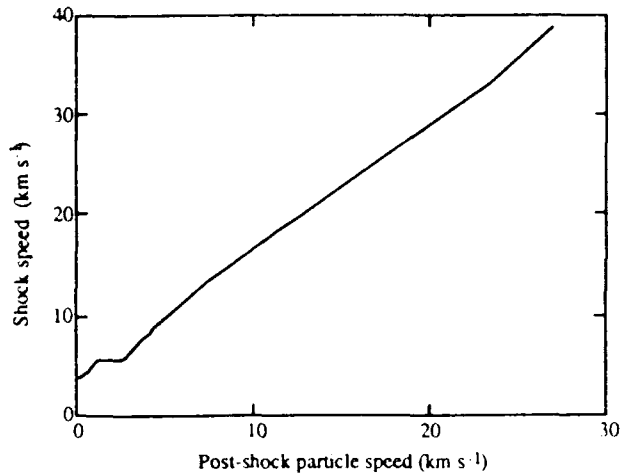


Fig. 2. Relation between shock speed D and particle speed u_1 just behind the shock front for solid quartz. The curve is a piecewise-linear approximation by Lamb, Callen, and Sullivan [1990] to Hugoniot data compiled by King et al. [1989] from Al'tshuler et al. [1977], Chung and Simmons [1969], McQueen, Fritz, and Hopson [1977], Wackerle [1962], and Ragan [1984]. Note the approximate linearity of the Hugoniot at large u_1 . The step in the curve at $u_1 \approx 2 \text{ km s}^{-1}$ reflects a phase transformation that occurs at about 40 GPa.

content, and may differ from the Hugoniot of the small samples that can be tested in laboratories.

For some rocks, the Hugoniot at high particle speeds (high pressures) may be adequately represented by a linear relation of the form (see Zel'dovich and Raizer [1967], pp. 705-710)

$$D = A + Bu_1 \quad (7)$$

for some constants A and B . As shown below, the ambient pressure p_0 is negligible compared to p_1 for all depths and times of interest here. Relation (7) then implies that

$$pH = \frac{A^2(V_0 - V)^2}{(B-1)^2 V^2 \left[\frac{B}{B-1} - \frac{V_0}{V} \right]^2} \quad (8)$$

(see Zel'dovich and Raizer [1967], pp. 705-710). Table 1 lists values of A , B , and ρ_0 for granite and wet tuff that were derived by fitting a Hugoniot of the form (8) to high-pressure equations of state for similar materials.

For Hugoniot of the form (8), the ratio ρ_1/ρ_0 of the material density immediately behind the shock front to the material density ahead of the shock front increases with the strength of the shock wave until it reaches a certain value $(\rho/\rho_0)_{\max} = (V_0/V)_{\max} = B/(B-1)$. Once the shock has become this strong, any further increase in its strength does not produce any increase in the ratio ρ/ρ_0 . For this reason, the density ratio $(\rho/\rho_0)_{\max}$ is referred to as the limiting density ratio. For the granite Hugoniot listed in Table 1, the limiting density ratio is ~ 3 . Peak pressures ~ 1 -10 TPa are required to achieve density ratios near the limiting value. For extremely strong shock waves, changes in material properties caused by ionization, relativistic corrections to the electron pressure, and radiation affect the Hugoniot and alter the limiting density.

If a single linear D vs u_1 relation adequately describes the Hugoniot at large u_1 and if this relation could be extrapolated to small u_1 , the constant A would correspond to the low-pressure plastic wave

TABLE 1. Approximate Hugoniot for Granite and Wet Tuff^a

Rock	ρ_0 (Mg m^{-3})	A (km s^{-1})	B	L_1 (m)	L_{150} (m)
Granite	2.67	2.80	1.45	3.8	20
Wet tuff	1.95	1.45	1.62	7.0	37

^aThe parameters ρ_0 , A , and B are from Moss [1988] and were obtained by fitting a Mie-Grüneisen equation of state to tabulated equations of state [King et al., 1989] for quartz and wet tuff at high pressures. L_1 and L_{150} are characteristic shock wave transition radii (see eq. [12]) for 1 kt and 150 kt explosions.

speed c_0 . However, the large- u_1 relation usually is not valid for small u_1 , and hence A usually does not equal c_0 . In granite, for example, A is about 3 km s^{-1} whereas c_0 is about 4 km s^{-1} .

Even if the Hugoniot is not linear over the range of u_1 that is of interest, a curve consisting of piecewise-linear segments of the form (7) may serve as a practical approximation to $H(u_1)$ for many purposes.

Release—After the shock front has passed, the pressure falls and the fluid expands. This is often referred to as "release". For a shock front of given strength, the curve on the equation of state surface that describes the evolution of the thermodynamic state of the material during release is very nearly an isentrope, since heat conduction is almost always negligible. This curve is therefore frequently called the release adiabat (see, for example, Murri et al. [1974]).

Phases of an Underground Nuclear Explosion

For present purposes, the time development of an underground nuclear explosion may be divided into three phases (see Glasstone and Dolan [1977] or Germain and Kahn [1968]):

Initial phase.—The energy released by a nuclear explosion initially emerges as nuclear radiation, fission fragments, and thermal electromagnetic radiation. The temperature in the nuclear charge rises steeply, reaching 10^7 K within a microsecond or so. At the very earliest times, energy is carried outward by the expanding weapon debris and radiation. As a result, the vaporized nuclear charge and nearby rock form a bubble of hot gas in which the initial pressure is of order 10 TPa. The enormous pressure in the bubble causes it to expand rapidly, creating a cavity and driving a shock wave into the rock surrounding the emplacement canister. The radial stress produced by the shock wave greatly exceeds the critical stress at which the rock becomes plastic. Thus, to a good approximation the strength of the rock can be neglected and the rock can be treated as a fluid. During the initial phase the evolution of the explosion can be followed using the equations of hydrodynamics and radiation transport.

Hydrodynamic phase.—Within ~ 10 -100 μs , depending on the design and yield of the nuclear charge and the composition and distribution of the matter surrounding it, the outward flow of energy via radiation becomes unimportant and the explosion can be described by the equations of hydrodynamics alone. At this point the explosion enters the (purely) hydrodynamic phase. As the shock wave expands, it weakens. Eventually, the radial stress produced by the shock wave is not much greater than the critical stress of the rock. At this point the rock can no longer be treated as a fluid and the hydrodynamic phase of the explosion ends.

Final phase.—The final radius R_c of the cavity produced by an underground nuclear explosion depends somewhat on the depth of the explosion and the composition of the surrounding rock, as well as the yield. For a burst of yield W , a useful approximate expression is [Terhune et al., 1979]

$$R_c \approx 14(W/1 \text{ kt})^{1/3} \text{ m} \quad (9)$$

The cavity reaches its final radius in about $90(W/1 \text{ kt})^{1/3} \text{ ms}$ [Ter-

hune et al., 1979]

Even after the compression wave is no longer hydrodynamic, the rarefaction wave that follows is still strong enough to fracture rock. Intense fracturing typically occurs out to a radius $\sim 3R$. [Terhune et al., 1979]. Beyond this point, the degree of fracturing caused by the expanding shock wave drops dramatically until, at $\sim 5R$, fracturing essentially stops. (Rarefaction waves caused by reflection of the shock wave from the surface or collapse of the roof of the cavity may cause fracturing beyond this radius.) The shock wave then continues to expand nearly elastically, eventually evolving into the leading wave of a train of elastic (seismic) waves.

In the remainder of this section we focus on the evolution of the shock wave during the hydrodynamic phase and somewhat beyond.

Approximate Model

For pedagogical purposes, it is useful to consider the shock wave that would be produced by a spherically-symmetric explosion in a uniform medium before confronting the full complexity of the shock waves produced by actual underground nuclear tests. The shock wave produced by such an idealized explosion is spherically-symmetric at all times. Even so, tracking accurately the change in the thermodynamic state of an element of rock as it undergoes shock compression and release requires knowledge of the equation of state of the rock over a wide range of densities and internal energies. Such an equation of state is usually quite complicated, and often can be presented only in tabular form. Hence, for pedagogical purposes it is also useful to consider first a simpler, more approximate description of the behavior of rock subjected to a shock wave.

In fact, the basic features of the evolution of the shock wave produced by a spherically-symmetric explosion in a uniform solid medium are illustrated by a simple analytical model. This model was proposed by Lamb [1987], who showed that it is exact for strong, self-similar shock waves and that the shock-front radius vs. time curves it predicts agree fairly well with data from several underground nuclear tests and numerical simulations of underground nuclear explosions. The model was proposed independently by Moss [1988], who showed that the particle-speed vs. radius relationship it predicts agrees fairly well with data from underground nuclear explosions and numerical simulations. A detailed description and assessment of the model has been given by Lamb, Callen, and Sullivan [1990], who find that the model provides a remarkably accurate description of the motion of the shock front throughout the hydrodynamic phase.

Without loss of generality, the particle speed u_1 just behind the shock front can be related to the hydrodynamic yield W of the explosion and the radius R of the front via the expression

$$u_1 = \left(\frac{3fW}{4\pi R^3 \rho_0} \right)^{1/2} \quad (10)$$

where f is a dimensionless factor that generally depends on the equation of state of the ambient medium and the radius of the shock front. An important assumption of the model is that f is independent of the shock front radius R for all shock front radii of interest.

In this model, the compression of the ambient medium at the shock front is treated exactly, via the Rankine-Hugoniot jump conditions and the Hugoniot of the medium. In contrast, the rarefaction that occurs as a shocked fluid element is left behind is treated only approximately, via the parameter f . The value of this parameter depends on the density, velocity, and specific internal energy distributions within the shocked volume. These distributions, and thus f , could be determined from a full hydrodynamic simulation of the shock wave evolution. However, such a simulation requires knowledge of the equation of state for substantial ranges of pressure and density, not just along

the Hugoniot. This requirement is sidestepped in the model by assuming that f is independent of R .

The factor f is independent of R for self-similar shock waves (see below) but need not be independent of R for shock waves produced by actual underground nuclear explosions [Lamb, 1987; Lamb, Callen, and Sullivan, 1990]. Nevertheless, shock wave radius and particle-speed data from actual underground nuclear tests as well as from computer simulations of such tests indicate that relation (10) with f constant is fairly well satisfied for explosions in quartz and wet tuff until relatively late times [Lamb, 1987; Moss, 1988; Lamb, Callen, and Sullivan, 1990]. The best value of f to use for explosions in a given rock can be determined by fitting the post-shock particle speed relation (10) (or the relations for the shock speed, shock front radius, and post-shock pressure that follow from it) to data from numerical simulations or actual underground explosions in that rock. For shock waves in quartz and wet tuff, $f \approx 0.53$ provides a relatively accurate description of the evolution during the hydrodynamic phase and somewhat beyond [Moss, 1988; Lamb, Callen, and Sullivan, 1990].

For simplicity, let us assume that the Hugoniot of the medium can be adequately represented by a single linear relation of the form (7) over the whole range of u_1 of interest. Then $c_0 = A$. Therefore, in the following discussion we refer to A as the low-pressure plastic wave speed. Given the ansatz (10), the Hugoniot (7) can be rewritten as [Lamb, 1987, 1988]

$$D \equiv \frac{dR}{dt} = A \left[1 + \left(\frac{L}{R} \right)^{3/2} \right], \quad (11)$$

where

$$L \equiv \left(\frac{3fWB^2}{4\pi\rho_0 A^2} \right)^{1/3} \quad (12)$$

is a characteristic length that separates the region where $D \propto R^{-3/2}$ from the region where $D \approx A$. Typical values of L for 1 kt and 150 kt explosions in granite and wet tuff are listed in Table 1 for the values of A and B given there.

Given the shock-front radius R_0 at the time t_0 at which the explosion becomes purely hydrodynamic, the first-order differential equation (11) can be integrated to obtain a simple, closed expression for $R(t)$, from which one can calculate $D(t)$, $u_1(t)$, $p_1(t)$, and $\rho_1(t)$ [Lamb, 1987; Moss, 1988; Lamb, Callen, and Sullivan, 1990]. This model shows in a qualitative way how the evolution of the shock wave depends on the yield of the explosion and the Hugoniot of the rock. As an example, the peak pressure, peak density, and radius of the shock front at various times are listed in Table 2, for 1 kt and 150 kt

TABLE 2 Shock Wave Evolution in Granite^a

Pressure (GPa)	Density (ρ_{max})	1 kt Explosion		150 kt Explosion	
		Time (μ s)	R (m)	Time (μ s)	R (m)
7,000	0.9	4	0.5	20	3
1,000	0.8	10	0.9	80	5
400	0.7	40	1.4	200	8
150	0.6	90	2	500	11
50	0.5	200	3	1,200	17
15	0.4	600	5	3,000	30

^aFor the model of a spherically-symmetric, point explosion described in the text. The Hugoniot (7) was used, with the values of A and B given in Table 1. The phase transformation that occurs when the post-shock pressure p_1 is ~ 30 –40 GPa (see Fig. 2) has been neglected. The post-shock density ρ_1 is expressed in terms of the limiting density ρ_{max} of granite (see text), which is 9.4 Mg m^{-3} for this Hugoniot. From Lamb [1988].

point explosions in granite. (A point explosion is one in which a large amount of energy is released instantaneously in an infinitesimal volume.) For simplicity we have assumed that both explosions are purely hydrodynamic after the initial energy release at time $t = 0$. The corresponding initial condition for equation (11) is $R = 0$ at $t = 0$. As discussed below, the hydrodynamic phase ends in granite when the post-shock pressure p_1 has fallen to about 1 GPa. Thus, the pressure p_0 of the overburden, which is ≈ 20 MPa at the depths that are relevant here (≤ 1 km), is negligible compared to p_1 throughout the hydrodynamic phase of the explosion.

More generally, the model can be used to obtain a closed-form expression for $R(t)$ for any piecewise linear Hugoniot $D(u)$. Thus, the model can be used with more realistic Hugoniot like that shown in Figure 2. When currently available Hugoniot data is used, the model predicts post-shock particle speeds and pressures, shock-front speeds, and shock-front radii that agree quite well with data from underground nuclear explosions and with numerical simulations of such explosions [Lamb, Callen, and Sullivan, 1990].

Characteristic Intervals

During the hydrodynamic phase, the shock wave produced by a spherically-symmetric point explosion in a uniform medium evolves differently in the strong-shock, transition, and low-pressure plastic-wave intervals.

Strong-shock interval.—Initially, the speed of the shock front is much greater than the speed of sound in the undisturbed rock, the pressure behind the shock front is predominantly thermal pressure, and the ratio of the density immediately behind the shock front to the density ahead of the front is close to its limiting value. Thus, the shock wave is strong.

The shock wave produced by a point explosion in a uniform medium is self-similar as long as it remains strong (see Zel'dovich and Raizer [1967], Chap. I and XII, Sedov [1959], Barenblatt [1979]). In such a motion, the distributions with radius of the pressure, density, and particle velocity evolve with time in such a way that only the scales of the distributions change, while their shapes remain unaltered. For such a strong, self-similar shock wave, the radius as a function of time depends in a simple way on the properties of the medium and the yield of the explosion. This simple radius vs. time curve could be used to estimate the yield of actual underground nuclear explosions, if there were an interval of strong, self-similar motion and if data from this interval could be obtained.

For example, the simplified model described above predicts that the radius of the shock front produced by a point explosion satisfies [Lamb, 1987, 1988]

$$R(t) \approx W^{1/3} \left(\frac{75fB^2}{16\pi\rho_0} \right)^{1/5} \left(\frac{t}{W^{1/3}} \right)^{2/5} \propto W^{1/3} \left(\frac{t}{W^{1/3}} \right)^{2/5}, \quad (13)$$

during the strong-shock interval ($R \ll L$). This expression illustrates the more general result that the radius of a strong, self-similar shock wave varies as the two-fifths power of the time since the beginning of the explosion, independent of the properties of the medium. In the simplified model, the radius of the shock front depends only on ρ_0 and B , for a given choice of f .

Unfortunately, as explained below, strong, self-similar motion does not develop in actual underground nuclear tests, given current testing practices and the yields permitted by the TTBT.

Transition interval.—As the shock wave expands, it weakens and slows, and the peak pressure and density drop. When the peak density ratio has fallen to ≈ 8 times the limiting value, we say that the shock wave has entered the transition interval.¹ For an explosion in granite, this occurs when the peak pressure has fallen to ~ 1 TPa

(see Table 2). We denote the shock front radius at which this occurs by R_t . For a 1 kt explosion in granite R_t is ~ 1 m, whereas for a 150 kt explosion R_t is ~ 5 m.

Over most of the transition interval, the thermal pressure just behind the shock front is not much greater than the cold pressure of the compressed rock, although the speed D of the shock front is still much larger than the low-pressure plastic wave speed A . In this interval, the motion of the shock wave is more sensitive to the properties of the medium than it is in the strong shock interval. For example, the motion of the shock front in the simplified model discussed above depends on A as well as B and ρ_0 during the transition interval. Consequently, more knowledge of the ambient rock is required in order to make accurate yield estimates using data from this interval.

As the shock wave expands and weakens, the minerals in the rock behind the shock front may undergo polymorphic transitions. For example, the mineral constituents of granitic rocks appear to undergo several polymorphic transitions when the peak post-shock pressure falls below ~ 30 –40 GPa (see Fig. 2).

When the shock speed falls below the elastic wave speed c_t , the shock wave splits into an elastic wave followed by a plastic wave (see Zel'dovich and Raizer [1967], pp. 741–746). In granites, this is expected to occur when the peak pressure has fallen to ~ 20 –30 GPa (see Butkovich [1965], Holzer [1965], and Fig. 2). Since the plastic wave slows as it weakens whereas the elastic wave travels at the nearly constant speed c_t , the plastic wave falls further and further behind the elastic wave. This two-wave structure is clearly seen in laboratory experiments on small samples of granite and other rocks. Whether it persists in rock in the field is not as certain.

The elastic precursor raises the pressure of the rock to p_{crit} , which is ≈ 4 GPa for granite [Holzer, 1965], and accelerates it. The following plastic shock wave therefore propagates through rock that is already moving at ~ 1 –10 ms^{-1} . However, the speed of the plastic shock wave is at least c_0 , which is several kms^{-1} (see above). Thus, even after the shock wave has split, the acceleration of the rock by the elastic precursor can usually be neglected and low-pressure plastic wave taken to propagate at the plastic wave speed relative to the undisturbed ambient medium, as was done in writing eq. (6).

Low-pressure plastic wave interval.—As the shock wave expands and weakens further, the thermal pressure behind the shock front becomes a small fraction of the total pressure and the shock speed D approaches the low-pressure plastic wave speed A . At a certain radius R_{pw} ($\sim L$), the shock speed has fallen to 1.2 times the low-pressure plastic wave speed and we say that the shock wave has entered the low-pressure plastic wave interval.² For an explosion in granite, this occurs when the peak pressure has fallen to ~ 15 GPa, corresponding to a peak density ratio ~ 0.4 times the maximum (see Table 2). For a 1 kt explosion in granite R_{pw} is ~ 5 m, whereas for a 150 kt explosion R_{pw} is ~ 30 m.

For the simplified Hugoniot of equation (11), the low-pressure plastic wave interval corresponds to $R \geq 3L$. In this interval,

$$R \approx \text{const.} + At, \quad (14)$$

where the constant is determined by the motion in the strong shock and transition intervals.

When the peak pressure in the plastic wave is no longer much greater than the critical shear stress p_{crit} , the shear strength of the rock can no longer be neglected in treating the evolution of the plastic shock wave. In granite, for example, p_{crit} is ≈ 4 GPa, and hence the hydrodynamic approximation begins to fail when the peak pressure behind the plastic wave falls below about 15 GPa, which occurs soon after the shock wave has split. For granite, the hydrodynamic zone extends about $5(W/1 \text{ kt})^{1/3}$ meters from the center of the explosion (see Table 2).

Underground Nuclear Tests

The evolution of the shock wave produced by an actual underground nuclear test is generally more complex than the evolution just described. For one thing, the shock wave is produced by an aspherical source of finite size rather than a spherically symmetric point source. For another, natural or man-made geological or geophysical structures near the emplacement point may significantly distort the evolution.

Test geometries.—In preparation for a nuclear test, one or more nuclear explosives are customarily placed in each container or covering. These containers are called explosive canisters. Explosive canisters as long as 12 m with diameters as large as 3 m are permitted in the standard test geometries defined in the recently adopted TTBT verification protocol [U. S. Arms Control and Disarmament Agency, 1990b]. Larger canisters may be used in nonstandard tests.

Any drill-hole, shaft, adit, or tunnel in which one or more explosive canisters, associated cables, and other equipment have been installed is called an emplacement hole. Emplacement holes may be vertical shafts drilled deep into the ground, horizontal tunnels carved into the sides of mesas or mountains, or large underground cavities (see U. S. Congress [1989], pp. 15–18).³ The standard vertical and horizontal geometries defined by the TTBT verification protocol allow the use of vertical emplacement holes with diameters up to 4 m and horizontal emplacement holes with cross sections as large as 5 m by 5 m. Tests with planned aggregate yields less than 35 kt may be conducted in cavities as large as 20,000 cubic meters (the radius of a hemispherical cavity with this volume is about 20 m). Nonstandard tests may be carried out in larger emplacement holes or cavities if the parties agree on verification measures [U. S. Arms Control and Disarmament Agency, 1990b]. Historically, about 90% of U. S. nuclear tests have been conducted in vertical shafts, the remainder have been conducted in tunnels or cavities.

Cableways and cables as well as open or partially-open pipes are typically installed in the emplacement hole to carry signals or radiation away from the explosive canister or canisters. There have been as many as 250 or more such cables and pipes in recent U. S. nuclear weapon tests. Once the explosive canister, diagnostic equipment, pipes, and cables have been positioned in the emplacement hole, the emplacement hole is stemmed with sand, gravel, and plugs (if it is vertical) or grout (if it is horizontal) in order to prevent escape of radioactive gases (for an example of a stemming plan for a vertical shaft, see Glenn et al. [1983] or Glenn et al. [1986], for an example of a filling plan for a horizontal tunnel, see U. S. Congress [1989], p. 43). For tests conducted in tunnels, an ancillary tunnel (called the bypass drift) is constructed parallel to the emplacement tunnel to allow access to the room in which the nuclear explosive is to be placed and to other parts of the tunnel system close to the time of the test. After the nuclear explosive has been positioned, the bypass drift is filled with grout.

Source effects.—Unless impeded, vaporized weapon debris and radiation would fill many meters of the emplacement hole soon after the nuclear charge is detonated, producing a shock wave that would be highly aspherical initially (see Lamb [1988]). As such a shock wave expands, it tends to become more spherical if the surrounding medium is uniform. However, the shock wave will remain significantly aspherical until it has propagated a distance from the center of the explosion greater than the length of the source. Such an aspherical shock wave would make accurate yield estimation much more difficult than for a spherical shock wave, particularly if shock front position data were obtained from only one set of sensing cables (see below).

For this reason, the TTBT verification protocol restricts the dimensions of explosive canisters and any attached canisters containing diagnostic equipment [U. S. Arms Control and Disarmament

Agency, 1990b]. The TTBT protocol also requires that any pipe or cableway connected to an explosive canister pass through a "choke section" designed to restrict the flow of energy out of the canister. The distortion of the shock front caused by a canister, open pipe, or cableway of a given size is less for higher-yield than for lower-yield explosions, since the hydrodynamic zone extends further from the canister and emplacement hole for a higher-yield explosion (recall that the hydrodynamic zone extends about $5(W/1\text{ kt})^{1/3}$ meters from the center of the explosion). Moreover, higher-yield charges usually are not exploded in tunnels.

The shock wave produced by a test involving multiple explosive canisters could be very complex, creating a daunting verification problem. For this reason the TTBT protocol specifies that a test involving multiple explosives can be considered to have a standard geometry only if the explosives are placed in a single canister or the positions of the explosive canisters and their detonation times are arranged so that a shock-wave yield estimate can be made for each canister separately.

Even the shock wave from a test having a standard geometry and conducted in a uniform medium may not be completely spherical at the relatively small distances where hydrodynamic measurements must be made. For example, the hydrodynamic zone of a 150 kt explosion in granite extends only about 20 m from the center of the explosion. Shock front position measurements must therefore be made ~10–20 m from the center of the explosion in order to be usable in hydrodynamic yield estimation algorithms. These distances are comparable to the dimensions of the largest explosive canisters allowed in standard test geometries. Thus, even the shock wave from a standard test may be somewhat aspherical in the region where hydrodynamic measurements are made.

The shock wave from an underground nuclear explosion cannot become self-similar until it has enveloped a mass of rock much greater than the mass of the nuclear explosive and canister, and energy transport by radiation is negligible [Barenblatt, 1979, Ch. 2]. The radius R_0 at which this occurs is necessarily larger than the radius of the emplacement hole or cavity and depends on the design of the nuclear charge and surrounding equipment. Unless there is a range of radii satisfying $R_0 \ll R \ll R_1$, where R_1 is the radius at which the transition interval begins, the shock wave will not have time to become self-similar before entering the transition interval. Since R_0 is ≥ 2 m for current U. S. practices and allowed yields, no such range exists in granite even for explosions as large as 150 kt, as shown by the data in Table 2. Thus, the simplicity of estimating yields from an interval of self-similar motion cannot be realized. Furthermore, the structure of the shock wave in the hydrodynamic measurement zone is more sensitive to the properties of the source than it would be if it were evolving from a self-similar wave.

For example, even if the shock waves produced by two nuclear tests with the same yield were spherically symmetric at all radii, they could have different speeds at a given radius, because the effective size of the shock wave source could differ from one explosion to another. Moreover, the design and composition of the nuclear explosive and canister affects the equation of state of the effective hydrodynamic source, which is different from the equation of state of the surrounding rock. As a result, the fraction of the total device energy that couples to the shock wave can vary from one device to another. Indeed, Moran and Goldwire [1990] have shown that the yields of spherically-symmetric explosions inferred from data taken in the hydrodynamic measurement zone may differ from the actual yields by 20%, for hydrodynamic sources that they present as models of the hydrodynamic sources produced by nuclear explosions. Similar results have been obtained by Callen, Fiedler, Lamb, and Sullivan (in preparation).

Inhomogeneities in the ambient medium.—In addition to its depen-

dence on the properties of the source, the evolution of the shock wave produced by an underground nuclear explosion will be affected by any natural or man-made structures in the surrounding medium. In order to identify potentially disturbing structures, the TTBT protocol requires that the testing party provide a geological and geophysical description of the test location, including the depth of the water table, lithographic descriptions of each formation, and any known geological or geophysical discontinuities within the hydrodynamic measurement zone. The protocol also requires the testing party to make available the planned cross-sectional dimensions of each emplacement hole in each hydrodynamic measurement zone as well as a description of the materials that will be used to stem each such emplacement hole. In order to minimize the effects of voids on the evolution of the shock wave, the protocol requires that the locations and volumes of all voids within the hydrodynamic measurement zone be determined, using methods such as electromagnetic measurements, radar, and acoustic sounding, any voids within the hydrodynamic measurement zone with volumes greater than ten cubic meters and any voids near the emplacement hole with volumes greater than one cubic meter must then be filled with dense stemming material.

Explosions of nuclear charges in vertical shaft or tunnel complexes or in cavities may be accompanied by complicated (and unanticipated) energy flows and complex shock wave patterns. In order to minimize these effects, the TTBT protocol specifies that if a test involves explosions in more than one emplacement hole, no more than one such hole may depart from the standard vertical or horizontal configuration. If a test is to be conducted in a cavity, the protocol gives the verifying party the right to measure the shape and volume of the cavity.

3 Measuring Shock Waves

As noted in the Introduction, the evolution of the shock wave produced by an underground nuclear explosion can in principle be measured using either sensing elements or transducers (see Holzer [1965]). In the present context a sensing element is any switch, cable, or cable segment that provides data on the position of the shock front as a function of time, whereas a transducer is a device that converts a physical property of the shock wave, such as the radial stress, strain, or particle speed, into a recordable signal. In practice, constructing, emplacing, and obtaining reliable data from transducers has proved difficult.

For this reason, U. S. efforts to develop shock-wave yield estimation methods have for the past 15 years emphasized sensing elements. This approach is also the one that the TTBT protocol allows for shock-wave monitoring of nuclear tests with standard vertical or horizontal geometries. Hence, in the present section we focus primarily on shock-front sensing techniques. The TTBT protocol allows the use of transducers as well as sensing elements for monitoring tests with nonstandard geometries [U. S. Arms Control and Disarmament Agency, 1990b].

Use of Sensing Cables

One way of measuring the position of the shock front is to place an electrical sensing cable near the site of the explosion and then measure the point where it is being crushed at a given time by the pressure peak at the shock front. The crushing point is measured by electrical equipment attached to the cable but positioned a safe distance from the explosion. This technique has been utilized in the United States since the early 1960s.

Sensing cables may be inserted in the emplacement hole before it is filled or placed in one or more "satellite holes" that have been drilled or excavated nearby specifically for this purpose. Use of a

satellite hole requires sophisticated drilling capabilities in order to make sure that the satellite hole maintains the proper separation from the nuclear charge emplacement hole at the depth of the nuclear charge (see below and §4). Conversion of the uncrushed cable length to the position of the shock front is more complicated if the cable is placed in a satellite hole than if it is positioned in the emplacement hole. On the other hand, the satellite-hole geometry reduces the intrusiveness of the method and "jetting" and other phenomena that can crush or short sensing cables ahead of the hydrodynamic shock front. In the discussion that follows, we shall assume that the sensing cables have been placed in a satellite hole unless otherwise stated. The satellite-hole geometry is shown in Figure 3a.

If a sensing cable is strong enough that it is not crushed by the elastic precursor (if present) or other unwanted signals, but weak enough that it is crushed by the pressure peak at the hydrodynamic shock front, the cable will be electrically shorted or its impedance substantially changed near the point where the hydrodynamic shock front intersects it. As the shock front expands with time, the length of cable from the electrical equipment to the nearest point at which it has been crushed is measured, as shown in Figure 3b. If the path of the sensing cable relative to the center of the explosion is known and the time at which the explosion began can be determined, then the length of the uncrushed cable can be used to determine the position of the shock front along the path traced by the sensing cable, as a function of the elapsed time since the beginning of the explosion.

In order to sample a substantial portion of the hydrodynamic measurement zone for explosions with yields near the 150 kt limit of the TTBT, the sensing cable must pass within ~ 10 m of the center of the explosion. For this reason, the TTBT protocol requires that for standard tests, the axis of any satellite hole must be located 11 ± 3 meters from the axis of its associated emplacement hole throughout the hydrodynamic measurement zone. For standard vertical tests with yields near 150 kt, this requires drilling the emplacement and satellite holes to depths ≥ 650 m while maintaining a lateral separation of about 10 m.

Voids or excavations near the satellite hole can distort the shock front, causing the sensing cables to be crushed in complex patterns. For this reason, the TTBT protocol requires that for standard tests, any void that is near a satellite hole and that has a volume greater than one cubic meter must be filled with dense stemming material.

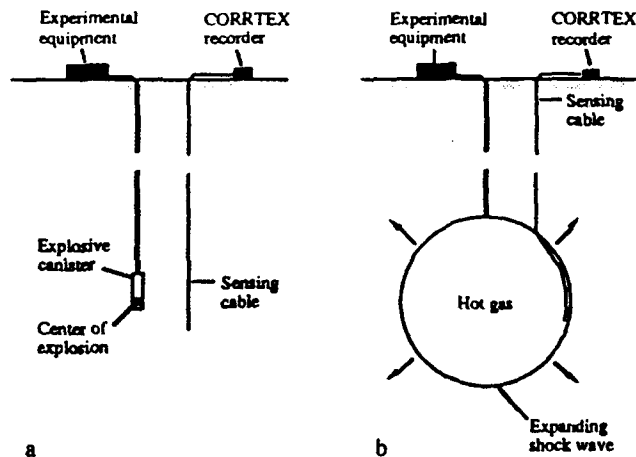


Fig. 3. Schematic drawings illustrating (a) placement of a shock front sensing cable in a satellite hole and (b) progressive shortening of the cable by the expanding shock front produced by a nuclear explosion. From Lamb [1988].

Also, a satellite hole must be at least as close to its associated emplacement hole as to any other holes or excavations. For standard horizontal tests, the axis of a satellite hole must be at least 6 m from any other drilled or excavated cavities or holes, in order to minimize the disturbing effects of such holes. Moreover, if drilled, a satellite hole must have a diameter of no less than 0.3 m and no more than 0.5 m; if excavated, it must have a cross section no greater than 2.5 m by 2.5 m. Similar restrictions apply to satellite holes for nonstandard tests [U. S. Arms Control and Disarmament Agency, 1990b].

If hydrodynamic methods are to be used to monitor a 10 kt low-threshold test ban, the sensing cable will have to pass within ~ 4 m of the center of the explosion in order to sample a substantial portion of the hydrodynamic measurement zone. For a standard vertical test geometry, this would require drilling vertical emplacement and satellite holes to depths ≥ 200 m while maintaining a 4 m lateral separation between them.

Sensing cables with crushing strengths ranging from as little as 3 MPa to as much as 3 GPa have been used [Schmitt and Dick, 1985]. However, even cables with crushing strengths as high as 3 GPa can be crushed by the elastic precursor in granite, since p_{crit} is ~ 4 GPa. Thus, once the shock wave has split, the length of uncrushed cable may indicate the position of the elastic precursor rather than the position of the trailing hydrodynamic shock front [Virchow et al., 1980; Deupree et al., 1980]. If so, the sensing cable will not provide data about the position of the hydrodynamic shock front [Holzer, 1965]. If the data is incorrectly interpreted as showing the position of the hydrodynamic shock front, the estimated yield of the explosion will be erroneously high. In some cases the cable may be crushed by the elastic precursor in some regions and by the plastic wave in others. Thus, use of sensing cable data from regions where the peak pressure of the shock front has fallen below ~ 20 GPa requires special care.

Further information on the use of sensing cables may be found in the U. S.-Soviet agreement on the conduct of the 1988 Joint Verification Experiment [U. S. Department of State, 1988].

Measuring the Length of the Sensing Cable

During the 1960s and 1970s, the position of the crushing point was measured in the United States using a technique called SLIFER⁴ [Heusinkveld and Holzer, 1964; Holzer, 1965]. In this approach, the cable is used as the inductive element of a resonant oscillator. As the cable is progressively crushed, the frequency of the oscillator changes. By knowing the propagation velocity of electromagnetic signals in the cable and the frequencies of the oscillator that correspond to at least two cable lengths, one can convert measurements of the change in oscillator frequency during the explosion to estimates of the change in the length of the cable.

In the late 1970s, an improved technique for measuring the length of sensing cables, called CORRTEX⁵, was developed [Virchow et al., 1980; Deupree et al., 1980; Storey et al., 1982; Los Alamos Natl. Lab., 1986]. In this approach, a sequence of electrical pulses is sent along the cable at preselected time intervals. At the crushing point, these pulses are reflected back along the cable to the recording equipment. By knowing the speed at which the pulses propagate along the cable, the round-trip travel time of each pulse can be converted into an estimate of the length of uncrushed cable at the time the pulse was reflected.

Current (CORRTEX III) equipment can store up to 4,000 data points. Pulse separations from 10 μ s to 90 μ s can be selected in 10 μ s steps, giving a record of the changing cable length that is 40 ms to 360 ms in length. The pulses typically propagate down and up the sensing cable at about 2×10^8 km s⁻¹. A typical uncertainty in the round-trip travel time during a nuclear explosion is 500 ps, corresponding to an uncertainty of about 0.1 m in the round-trip distance

to the crushing point or about 0.05 m in the distance to the crushing point.

Determining the Shock Front Position vs. Time

In order to understand how the evolution of the shock front produced by an underground explosion can be followed using CORRTEX or SLIFER measurements, it is helpful to consider first an idealized spherically-symmetric explosion in a uniform medium and a single sensing cable in a satellite hole that is relatively straight within the hydrodynamic measurement zone.

After the nuclear charge is detonated, the spherical shock front produced by the explosion expands away from the center of the explosion (see Fig. 3b). Some time elapses before the shock front begins to crush the sensing cable. This time depends on the distance between the center of the explosion and the point where the cable is closest to the center of the explosion.

At the instant of first crush, the length of uncrushed cable decreases discontinuously from its original length to the length to the point of first crush (see Fig. 4). As the shock front continues to expand, the crushing point nearest the electrical recording equipment moves steadily along the cable, reducing its uncrushed length. If the time at which the explosion began and the path of the cable relative to the center of the explosion are both known, the radius of the shock front as a function of the time since the beginning of the explosion can be calculated from the recorded change in the length of the cable as a function of time.

Accurate knowledge of the time at which the nuclear charge was detonated is required in order to determine accurately the shock front radius as a function of time. For this reason, the TTBT protocol requires the testing party to provide the verifying party with an electric

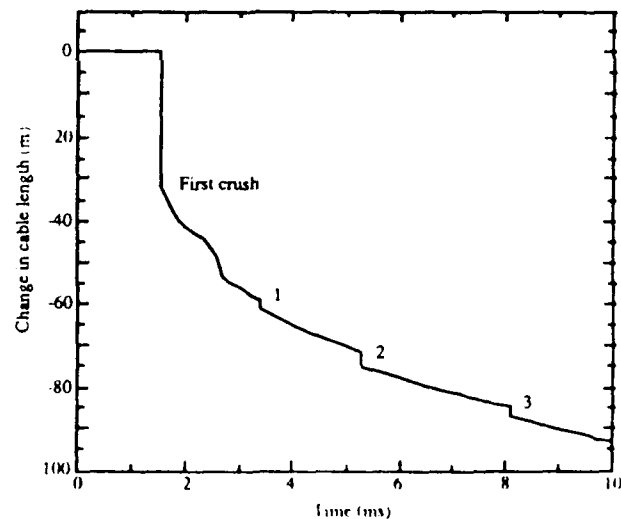


Fig. 4. Curve of uncrushed cable length vs. time derived from CORRTEX satellite-hole data collected during an underground nuclear explosion. The cable length remains constant until the shock front arrives at the satellite hole at about 1.7 ms, at which time the cable is crushed about 30 m from its original end. The cable length then decreases steadily as the crushing point moves along the cable, except for discontinuous downward jumps at the point labeled 1, 2, and 3, which are produced by fiducial loops in the cable (see text). The feature in the curve at about 2.7 ms is not expected for a spherically symmetric shock front; its cause is not known to the present authors. The curve was kindly supplied by the Los Alamos CORRTEX group.

cal pulse corresponding to the time of detonation, with an accuracy of $\pm 1 \mu\text{s}$, for each explosion. If this electrical pulse is not received, the time of detonation can still be estimated from the time at which the electromagnetic pulse (EMP) caused by the nuclear explosion arrives at the CORRTX recorder. The CORRTX technique is less affected by electromagnetic signals produced by the explosion than were earlier techniques. In order to prevent the pick-up and recording of electromagnetic signals that could reveal sensitive nuclear design information to the verifying party, the TTBT protocol provides for installation of "anti-intrusiveness" devices in each cable running from a satellite hole to any recording facility of the verifying party.

As discussed in §4, an error of 1 m in the measured radius of the shock front will cause an error of about 50 kt in the yield estimate, for yields near 150 kt. Thus, accurate knowledge of the path of the sensing cable relative to the center of the explosion is required in order to make an accurate yield estimate. The paths of the emplacement and satellite holes can be determined by directional surveys, geodetic measurements, depth measurements, and distance measurements. The paths of sensing cables within the satellite hole must also be known accurately. If, for example, the cable wanders within the hole and this is not taken into account, the length of the cable crushed by the shock wave will be greater than the distance along the satellite hole traveled by the shock front, causing the speed of the shock wave and therefore the yield of the explosion to be overestimated. The path of a cable within the satellite hole can be fixed by creating fiducial loops in the cable at predetermined points; such loops will cause the length of uncrushed cable to decrease discontinuously as the shock front passes over them (see Fig. 4). Using these jumps, the cable length measurements can be adjusted for systematic errors.

Although the paths of the satellite and emplacement holes can be determined relatively accurately, the position of the center of the explosion within the explosive canister usually will not be accurately known to the verifying party in advance of the test. In principle, the center of the explosion could be offset from the axis of the explosive canister by a substantial fraction of the 1-1.5 m canister radius and could be located either near the top or near the bottom of a 12 m-long canister. Such a large uncertainty in the position of the center of the explosion would lead to a very large uncertainty in the estimated yield of the explosion.

In practice, the position of the center of the explosion relative to the axis of the explosive canister can often be determined from the shock front position data, if the explosion is spherically symmetric. Furthermore, if the satellite hole is essentially straight and parallel to the emplacement hole and extends well past the nuclear charge emplacement point, the position of the center of the explosion along the axis of the explosive canister can be determined from cable length measurements, since its position is the same as the position of first crush on the sensing cable (see Fig. 4). In part to make sure that the location of first crush can be determined, the TTBT protocol requires that for a test configuration to be standard, each satellite hole must extend beyond the end of the associated emplacement hole by at least 30 and 15 m, respectively, for vertical and horizontal emplacement geometries.

The discrete character of CORRTX cable-length measurements can lead to a significant uncertainty in determining the point of first crush, since the cable crushing point moves along the cable at very high speed just after the shock front first reaches the cable. For example, if the satellite hole is 10 m away from the emplacement hole and the yield of the explosion is 100 kt, the shock front will be moving at about 10 km s^{-1} when it reaches the sensing cable. Hence, even if the CORRTX equipment is set to make measurements every $10 \mu\text{s}$, the radius of the shock front will increase by 0.1 m between one CORRTX pulse and the next. However, in the most unfavorable case the shock front will have moved 1.4 m away from the point of first

crush by the time the crushing is detected. An error of this magnitude in determining the point of first crush could introduce an error of 50 kt in estimating the yield of a 150 kt explosion. This uncertainty can be reduced by using the SLIFER technique to determine the point of first crush, or by placing many CORRTX cables in each satellite hole and staggering the times at which pulses are transmitted down the cables.

If the explosion is not spherically symmetric, due to the test geometry or the presence of natural or man-made inhomogeneities in the surrounding medium, reconstruction of the evolving shape of the shock front becomes more complicated and can be quite difficult, especially if there is only one satellite hole, since there will then be data only about the motion of the crushing point nearest the recording equipment along a single path in three-dimensional space (no data can be collected from the cable beyond the point of first crush, where the behavior of the shock wave may be significantly different). The reconstruction problem is particularly difficult for nuclear explosions in vertical shaft or tunnel complexes or in cavities, which may be accompanied by complicated (and unanticipated) energy flows and complex shock wave patterns.

In the context of treaty-monitoring, problems of this kind can be reduced by cooperative agreements. Thus, for example, the TTBT verification protocol [U. S. Arms Control and Disarmament Agency, 1990b] allows the verifying party to use up to six sensing cables in each of three satellite holes drilled or excavated at different azimuths, in order to monitor a nonstandard test. In addition, the verifying party may use transducers to measure the peak pressure or other properties of the shock front, in addition to its position as a function of time. The verifying party may also request a reference test carried out in accordance with a variety of yield, canister, and placement requirements, in order to calibrate seismic yield estimation methods. Finally, an explosion with a planned aggregate yield greater than 35 kt can be carried out in a cavity only if both parties agree on verification measures.

4. Yield Estimation Algorithms

Once measurements of the length of the sensing cable have been converted to estimates of the position of the shock front as a function of time, the yield of the explosion can be estimated by applying an algorithm, by which we mean a particular procedure for comparing the shock front position data with a particular model of the motion of the shock front. Because shock wave yield estimation methods are evolving as research continues, the description of yield estimation algorithms given here should be viewed as a status report.

We first describe the components of a yield-estimation algorithm and then discuss the weighting of shock-front-position data, including heavier weighting of data in the so-called "insensitive interval". Next we summarize the conditions under which explosions satisfy "cube-root scaling" and describe yield estimation algorithms that are based on this scaling. These include the power-law algorithm, similar-explosion scaling, algorithms based on analytical models, and simulated-explosion scaling. All assume that the explosion is spherically symmetric and that the ambient medium is uniform. When this is the case, the shock wave is spherically symmetric and the propagation of the shock front can be described by a radius vs. time curve. If the explosion is aspherical or the ambient medium is nonuniform, the evolution is more complicated and detailed numerical modeling may be required, as discussed at the end of this section.

General Features

A yield estimation algorithm consists of (1) a model of the motion of the shock front that depends on the yield and (2) a procedure

for comparing the model with shock-front-position data to derive a yield estimate. The procedure normally includes a prescription for weighting the data when comparing it with the model. For example, if the model describes the shock wave evolution more accurately at some times than at others, data taken during the time when it is more accurate should be weighted higher than data taken at other times. A simple weighting procedure would be to assign unit weight to data collected during a certain interval and zero weight to data collected outside it. A more sophisticated procedure would be to assign weights that gradually increase and then decrease with time in an optimal way. At a minimum, weights should be chosen to eliminate data corrupted by non-hydrodynamic effects of the kind discussed in §3.

Given the uncertainties in the ambient medium of nuclear weapon tests that are typically encountered, it is usually appropriate to give a higher weight to data collected during the so-called "insensitive interval" (see Lamb [1988]). This interval is so-named because observations have shown that the radius of the shock front produced by a nuclear explosion of given yield is relatively insensitive to the medium in which the explosion occurs during a certain interval in time and radius toward the end of the transition interval, for explosions in the particular geologic media for which the United States has good experimental data or theoretical models [Bass and Larsen, 1977; Lamb, 1988; Lamb, Callen, and Sullivan, 1989, and in preparation; Callen, Lamb, and Sullivan, 1990]. These media include the dry alluvium, partially saturated tuff, saturated tuff, granite, basalt, and rhyolite at the nuclear test sites the United States has used. These media are mostly silicates and almost all are located at the Nevada Test Site. For explosions in these media, the radius of the shock front appears to depend only weakly on the medium during the insensitive interval, despite the fact that phase transitions and shock wave splitting occur in some of these media within the insensitive interval. As shown in Figure 5, the radius of the shock front in one rock gradually approaches, crosses, and then gradually deviates from that in

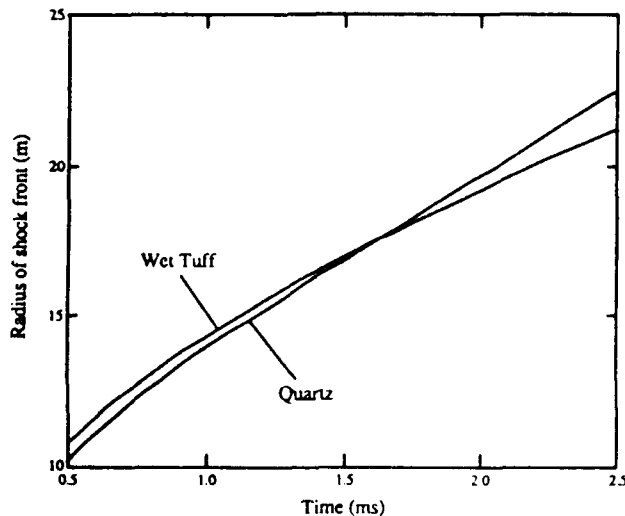


Fig. 5. Typical shock front radius vs. time curves for 100 kt explosions in two different silicate rocks found at the Nevada Test Site. Note the "insensitive interval" near 1.6 ms during which the two curves lie close to one another. Experience has shown that radius vs. time curves for other silicate media found at U.S. test sites also lie close to these curves near 1.6 ms. Because the curves gradually approach each other, cross, and then gradually deviate from one another, the insensitive interval is not sharply defined.

another similar rock, so that the insensitive interval is not sharply defined.

The existence of an insensitive interval for this collection of media is not well understood from a fundamental physical point of view. However, work by Lamb, Callen, and Sullivan [1989, and in preparation, see also Callen, Lamb, and Sullivan, 1990] indicates that the existence of an insensitive interval for this collection of silicates is a consequence of a particular correlation among the physical properties of these rocks. Lamb et al. have also described a procedure for determining in advance whether an insensitive interval exists for a given collection of media. Previously, whether such an interval exists could be determined only from nuclear test experience or numerical simulations of the evolution of shock waves in all the media in the collection.

Knowledge of whether an insensitive interval exists and, if so, its position and extent is especially important when attempting to use the power-law algorithm, since this algorithm gives relatively accurate yields only if such an interval exists and only if the data used come from this interval. However, exploitation of any insensitive interval is also important for optimal use of other algorithms. Given typical uncertainties about the physical properties of the geologic medium surrounding the nuclear explosive, assigning more weight to data taken during the insensitive interval will improve the precision of any yield-estimation algorithm, even if the model employed in the algorithm provides a relatively good description of the evolution of a shock wave in rock outside as well as within the insensitive interval.

Scaling Algorithms

All scaling algorithms assume that the explosion is spherically symmetric and that the ambient medium is uniform. As noted above, the shock front is then spherical and its evolution can be described by a shock-front radius vs. time (RVT) curve. Scaling algorithms assume further that the RVT curve scales with the cube root of the yield. In addition to the central role of cube-root scaling in scaling algorithms, most of the very limited quantity of RVT data from underground nuclear explosions that have been made publicly available have been scaled so that the apparent yield is 1 kt, on the assumption that cube-root scaling is valid, in order to protect the confidentiality of the original data. We therefore begin our description of yield-estimation algorithms with a brief discussion of cube-root scaling.

Cube-root scaling.—In its usual form, cube-root scaling assumes that if $R = g(t)$ is the RVT curve produced by a 1 kt explosion in a given medium during the hydrodynamic phase, the curve produced by an explosion with a yield of W kt in the same medium is given by

$$R = W^{1/3} g(t/W^{1/3}) \quad (15)$$

It is frequently assumed, incorrectly, that this scaling follows from the hydrodynamic equations alone. Actually, in order to determine whether the RVT curves of two nuclear explosions scale with the cube-root of the yield, one must examine not only the hydrodynamic equations, but also the jump conditions across the shock front, the equation of state of the ambient medium, and the initial data (that is, the pressure, density, and internal energy profiles at the time the explosion becomes purely hydrodynamic). Previous analyses [Brode, 1968; King et al., 1989] have neglected one or more of these considerations.

The RVT curves produced by different point explosions in the same medium are congruent during the hydrodynamic interval, once they have been scaled using equation (15) [King et al., 1989; Callen, Fiedler, Lamb, and Sullivan, in preparation]. However, the RVT curves produced by different hydrodynamic sources of finite size—such as the effective sources produced by underground nuclear

explosions—scale exactly only if the sources have the same equation of state and their masses, radii, and initial pressures scale appropriately with their yields [Callen, Fiedler, Lamb, and Sullivan, in preparation]. These requirements usually are not satisfied by nuclear weapon tests. Thus, for most nuclear weapon tests, cube-root scaling is at best only approximately valid, even during the hydrodynamic interval. The numerical simulations of Moran and Goldwire [1990] show that cube-root scaling may be in error by 20–30% in yield during the hydrodynamic interval for hydrodynamic sources that they present as models of the hydrodynamic sources produced by different nuclear explosives and test geometries. Callen, Fiedler, Lamb, and Sullivan [in preparation] reach similar conclusions, based on their numerical simulations of underground explosions. Despite the approximate nature of cube-root scaling for underground nuclear tests, yield estimation algorithms that assume this scaling often work quite well (see Lamb, Callen, and Sullivan [1990]). Further investigation of the domain of validity of cube-root scaling is needed.

Power-law algorithm—This is the simplest yield-estimation algorithm currently in use. The power-law algorithm assumes that the expansion of the shock wave produced by an underground nuclear explosion can be accurately modeled by a simple power-law formula that does not depend on the medium in which the explosion occurs (see Bass and Larsen [1977]). The power-law formula is

$$R(t) = a W^{1/3} (t/W^{1/3})^b, \quad (16)$$

where R is the radius of the shock front in meters, W is the yield of the explosion in kilotons, t is the elapsed time since the beginning of the explosion in milliseconds, and a and b are constants. Formula (16) has no theoretical basis, in contrast to the power-law formula for the radius of a strong, self-similar shock wave; it is instead a purely empirical, approximate relation based on the observation that in many cases RVT data from cables in the emplacement holes of U. S. nuclear tests fall close to relation (16) for a short time after they are no longer disturbed by non-hydrodynamic signals. The fact that formula (16) only approximates the actual RVT curve for a brief time is demonstrated by Figure 6, which compares it with a detailed model of the evolution of the shock wave produced in granite by a spherically-symmetric point explosion with a yield of 62 kt.

According to the assumption on which the power-law algorithm is based, the values of a and b in equation (16) do not depend on the medium (because of this and the fact that it has frequently been used at Los Alamos National Laboratory, eq. [16] is sometimes referred to as the "Los Alamos Universal Formula"; see Heusinkveld [1982]). The values of the constants a and b are typically determined by fitting equation (16) to a selected interval of RVT data from a collection of nuclear explosions. If only data from the insensitive interval for the particular collection of media being considered are used, the data can be approximated by a single curve, as explained above. However, different individuals and groups have found different best-fit values of a and b for different collections of data. Even the values used by a single group have changed with time by amounts that have caused yield estimates to change by tens of percent. For illustration in this article, we use the values of a and b suggested by Bass and Larsen [1977] and Heusinkveld [1979, 1982], namely 6.29 and 0.475, respectively.

In the usual form of the power-law algorithm, formula (16) is used to derive a yield estimate W , from each of the shock-front radius and time measurements R_s and t , over a broad interval that is thought to include the insensitive interval. Due to the departure of the power-law formula from the actual RVT curve at both early and late times (see Fig. 6), the sequence of yield estimates W , typically forms a U-shaped distribution, as illustrated by the yield estimates for the *Piledriver* explosion in granite, which are shown in Figure 7. If there

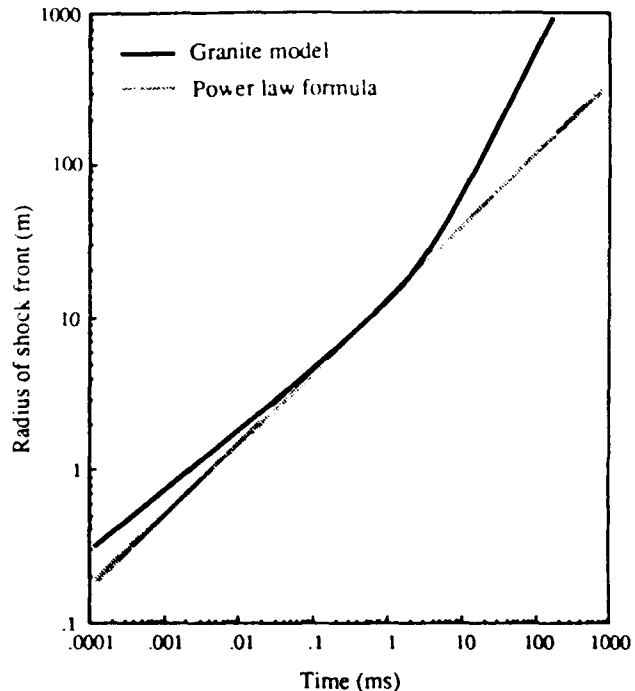


Fig. 6. Comparison of the power-law formula (16) with a model of the evolution of a shock wave in granite produced by a spherically-symmetric point explosion with a yield of 62 kt, showing the agreement of the formula with the model during a portion of the transition interval and the deviation of the formula from the model at earlier and later times. The effect of the phase transformation at 30 GPa is included in the model. From Lamb [1988].

is an insensitive interval for the collection of rocks being considered and if the constants in the formula have been chosen appropriately, the yield estimates near the bottom of the distribution should approximate the actual yield of the explosion. This is the case for the *Piledriver* estimates, which lie near the 62 kt official yield near the bottom of the "U".

In making the final yield estimate, only RVT data that fall within a certain narrower interval (sometimes called the "algorithmic interval") are used. The procedure used to select this interval varies tremendously from group to group. Often there is no set protocol. Instead, the data to be used are selected by eye, on the basis of experience. Heusinkveld [1979, p. 13] says that investigators at Los Alamos found that the power-law formula (with the a and b values cited above) agrees best with RVT field data during the interval $0.16 W^{1/3}$ ms to $0.6 W^{1/3}$ ms after the beginning of the explosion, where W is the yield of the explosion in kilotons. More recently, the interval of best agreement has been cited as 0.1 to 0.5 scaled ms [U. S. Congress, 1988]. Indeed, these intervals roughly correspond to the insensitive interval identified by Lamb, Callen, and Sullivan [1989, and in preparation; see also Callen, Lamb, and Sullivan, 1990]. One possible protocol would be to use only radius vs. time data from a prescribed interval of scaled time in the final yield estimate (see Lamb [1988]). Because the beginning and ending clock times of any prescribed interval in scaled time depend on the yield, use of such a protocol requires that an iterative procedure be followed to estimate the yield of an explosion of unknown yield. For definiteness, we take the algorithmic interval to be 0.1 to 0.5 scaled ms throughout the present article. Table 3 lists the time and radius intervals that

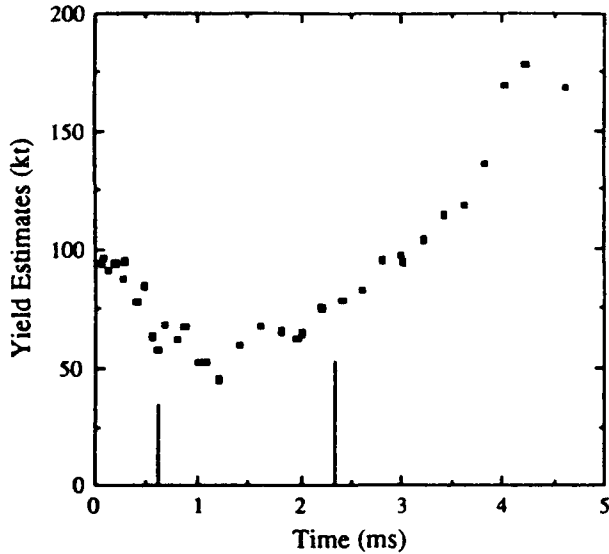


Fig. 7. The sequence of yield estimates obtained by applying the power-law formula to SLIFER data from the Piledriver explosion in granite. Note the U-shaped distribution of the yield estimates, which is due to the failure of the power-law formula to describe accurately the actual radius of the shock front as a function of time over any extended interval. The yield estimates near the bottom of the "U" are close to the official yield, which is 62 kt. The interval between the two vertical bars is the algorithmic interval defined in the text, for a yield of 62 kt. From Lamb [1988].

TABLE 3. Measurement Intervals for the Power-Law Algorithm*

Yield (kt)	Time Interval (ms)	Radius Interval (m)
1	0.10 — 0.5	2.1 — 4.5
10	0.21 — 1.1	4.5 — 9.7
50	0.37 — 1.8	7.7 — 17
100	0.46 — 2.3	9.8 — 21
150	0.53 — 2.7	11 — 24

*Corresponding to 0.1 to 0.5 scaled ms after the beginning of the explosion (see text). From Lamb [1988].

correspond to this interval in scaled time, for several yields.

Proper use of the power-law algorithm requires that shock-wave sensing cables be placed close enough to the center of the explosion that they sample the insensitive interval and that only data from this interval be used in the final analysis, since the shock wave evolution model used in the algorithm approximates the actual evolution of the shock wave only during this interval, if at all.

It has sometimes been argued incorrectly that the interval in scaled time used in the power-law algorithm lies in the strong shock interval and that the relative insensitivity of yield estimates to the properties of the medium during the algorithmic interval stems from this. (For example, according to the U. S. Department of State [1986a, 1986b], "The accuracy of the method is believed to be relatively, but not wholly, independent of the geologic medium, provided the satellite hole measurements are made in the 'strong shock' region...") This misconception apparently has arisen at least in part because the interval formerly used to estimate the yields of nuclear explosions in the atmosphere using hydrodynamic methods is within the strong shock region.

The relative insensitivity of the radius of the shock front to the medium during the intervals used in the power-law algorithm would

indeed be explained in part if these intervals were within the strong shock region and if the motion were self-similar. The formula for the radius of the shock front would then be a power-law function of time and the exponent of t would be exactly 0.4 (see eq. [13]). In reality, however, the shock-wave motion is not self-similar during the intervals used in the power-law algorithm for current test geometries and the yields permitted by the TTBT. In fact, the shock wave is not even strong during this interval, since the shock speed is only a few times the low-pressure plastic wave speed while the peak pressure is much less than the pressure required to achieve the limiting density ratio. Indeed, the exponent of time usually used in the power-law algorithm, 0.475, is significantly greater than the exponent 0.4 that characterizes a strong, self-similar shock wave [Heusinkveld, 1979, p. 13; Lamb, 1988]. As explained above, the relative insensitivity of the radius of the shock front to the medium during the algorithmic interval appears to be due to a particular correlation among the physical properties of the rocks in the collection being considered [Lamb, Callen, and Sullivan, 1989, and in preparation; Callen, Lamb, and Sullivan, 1990].

The sensitivity of an individual yield estimate to an error in the inferred location of the shock front depends on the position of the data point within the algorithmic interval and the yield of the explosion. For example, the sensitivity dW/dR , as determined from equation (16), varies from 13 kt m^{-1} at the beginning of the interval to 5.9 kt m^{-1} at the end of the interval, for a 10 kt explosion, and from 58 to 27 kt m^{-1} , for a 150 kt explosion.

The power-law algorithm does not work well for all test geometries and all media. This is illustrated in Figure 8, which shows the yield estimates obtained by fitting equation (16) to good-quality SLIFER data from a typical low-yield explosion in alluvium. The shock-front radius and time measurements for this event were multiplied by $W^{-1/3}$ before being made publicly available. As a result, the apparent yield should be 1 kt, if cube-root scaling is valid. (The name of this event and its official yield remain classified.) The yield

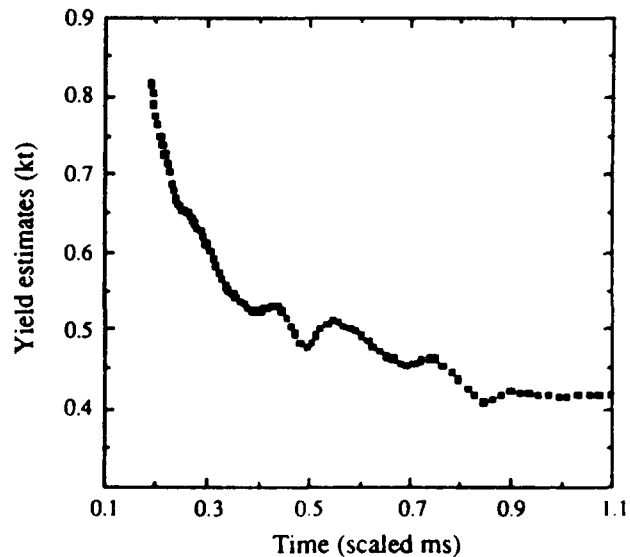


Fig. 8. Yield estimates derived by applying the power-law formula (16) to SLIFER data from a low-yield explosion in alluvium (note the offset of the vertical axis from zero). If the power-law algorithm and cube-root scaling were valid, the yield estimates would form a U-shaped distribution with a minimum near 1 kt. Difficulties in applying the power-law algorithm to low-yield explosions in alluvium are not uncommon. From Lamb [1988].

estimates given by the power-law algorithm range from 0.30 to 0.82 kt and do not form a U-shaped distribution. The average of the yield estimates that lie within the algorithmic interval is about 0.6 kt. The overall appearance of the yield vs. time curve shows that the assumptions of the algorithm are not satisfied.

Similar-explosion scaling—As noted in the discussion of cube-root scaling, the RVT curves of shock waves produced by point explosions with different yields but in the same uniform medium will coincide during the hydrodynamic interval, once they have been scaled using equation (15) (see, for example, Fig. 10 of Holzer [1965]). Even for nuclear tests—which certainly are not point explosions—the scaled RVT curves frequently agree closely for events in similar media. This is the basis of the “similar-explosion” scaling algorithm. In this algorithm, the yield of an explosion of interest is estimated by scaling RVT measurements from a reference explosion of known yield in a similar medium so that they agree with the RVT measurements made during the explosion of interest. Unlike the power-law algorithm, the similar-explosion-scaling algorithm can make good use of data taken outside the insensitive interval, since the ambient media of the explosion of interest and the reference explosion are assumed to be identical.

Similar-explosion scaling generally works well if the ambient media of the two explosions are very similar. Occasionally, application of this algorithm has led to an unexpectedly large error in the derived yield, presumably because the ambient media were not as similar as had been thought (see Holzer [1965]). Usually, however, similar-explosion scaling provides an accurate yield estimate. Its main disadvantage from a treaty-monitoring viewpoint is that the verifying party may not have access to data from nuclear explosions in a medium similar to that in which the test in question is being conducted.

Analytical modeling—Another possible approach to yield estimation uses analytical models of the shock wave evolution, such as those proposed by Heusinkveld [1979, 1982], Lamb [1987, 1988] and Moss [1988], and Axford and Holm [1987].

The analytical model of Lamb and Moss (see §2) treats the properties of the ambient medium and the motion of the shock front in a simplified way that nevertheless includes the most important effects. The result is a relatively simple analytical expression for the radius of the shock front as a function of time. The model also gives simple expressions for the post-shock pressure, particle speed, and density. Such a model is a useful tool for studying the evolution of shock waves in geologic media and the dependence of the evolution on the ambient medium.

The model of §2 can also be used to derive relatively accurate yield estimates from RVT data, if the required physical properties of the ambient medium are known. For example, Lamb, Callen, and Sullivan [1990] have shown that the model gives yield estimates for U.S. underground nuclear tests conducted in granite, basalt, and saturated wet tuff that are within 10% of the official yields of these events, when realistic Hugoniot and RVT data from only the hydrodynamic interval are used.

Like the similar-explosion-scaling algorithm but unlike the power-law algorithm, yield-estimation algorithms based on the model of §2 can make use of data taken outside as well as inside the insensitive interval, since the model describes the evolution of the shock wave throughout the hydrodynamic phase. The model can also be used to estimate the uncertainty in the yield caused by lack of knowledge of the properties of the ambient medium, and is more convenient than numerical simulations for analyzing how shock wave evolution is affected by changes in the physical properties of the ambient medium. For this reason, the model was used by Lamb, Callen, and Sullivan [1989, and in preparation, see also Callen, Lamb, and Sullivan, 1990] in their investigation of the physical origins of the insensitive interval.

Simulated-explosion scaling—The basis of so-called simulated-explosion scaling is the same as that of similar-explosion scaling, namely, the fact that the RVT curves of shock waves produced by different nuclear tests in the same medium frequently are quite similar during the hydrodynamic interval, once they have been scaled using equation (15).

In simulated-explosion scaling, the yield of an explosion of unknown yield is estimated by scaling the RVT curve from a numerical simulation of an explosion in a similar medium so that it follows the RVT data measured during the explosion of interest (see, for example, Figs. 10, 11, and 13 of Holzer [1965]). Thus, the simulated explosion scaling algorithm is identical to the similar explosion scaling algorithm, except that data from a computer simulation is used in place of data from a reference explosion. This has the advantage, from a treaty-monitoring viewpoint, of allowing the verifying party to construct a reference explosion via numerical simulation if it does not have access to field data from a similar explosion but does have a good model of the equation of state of the ambient medium.

A potential difficulty with simulated-explosion scaling is that the equation of state of the ambient medium constructed from laboratory measurements made on small samples may not accurately reflect the equation of state of the rock in the field. In part for this reason, computer simulations that generate reference explosions for use in simulated-explosion scaling algorithms often make use of “generic” equations of state, which are based both on laboratory measurements and shock wave data from actual underground nuclear explosions. For example, a “quartz” equation of state may be used to simulate explosions in hard silicate rocks, such as granites, while a “wet tuff” equation of state may be used to simulate explosions conducted below the water table in a variety of tuffs.

Like the similar-explosion scaling algorithm, the simulated-explosion scaling algorithm can make use of data taken outside the insensitive interval.

Detailed numerical modeling

All the algorithms discussed up to this point assume that cube root scaling is accurate. However, as we have previously noted, nuclear tests typically violate the conditions required for cube-root scaling to hold exactly. This is particularly true for those tests defined as non-standard by the TTBT protocol. Such tests may have large explosive canisters or lines of sight without choke sections, may be conducted in vertical shaft or tunnel complexes or in large cavities, and may lead to significant transport of energy via radiation even at relatively large distances from the center of the explosion (see, for example, King et al. [1989]). Even if a test has a standard vertical or horizontal geometry, the presence of a geological or geophysical discontinuity in the hydrodynamic measurement zone may cause a deviation of the shock wave from spherical symmetry (see Lamb [1988]); violations of the other conditions that are required for cube-root scaling to be an accurate approximation may occur as well.

At present, detailed numerical simulations using two- and three-dimensional finite-difference or finite-element hydrodynamic codes are the only way one can model nuclear tests in which transport of energy via radiation is important in the shock-front measurement zone, in which shock wave evolution in this zone is significantly affected by the physical properties of the hydrodynamic source, or in which the ambient medium is significantly inhomogeneous. Numerical simulations are also the only way one can model shock wave evolution beyond the hydrodynamic zone, although in this zone the predictive power of present constitutive relations for geologic media and present computer codes is limited.

In addition to the difficulties sometimes encountered in modeling accurately the equation of state of the ambient medium, which have already been discussed, numerical simulations of explosions in shaft

or tunnel complexes, in media with voids or geophysical discontinuities, or in cavities also have to confront the difficulties involved in treating accurately the interaction of a shock wave with sharp boundaries between different rocks or between rocks and air.

In algorithms based on detailed numerical modeling, a new simulation must be run for each yield considered. Hence, estimating the yield of even a single nuclear test can be computationally intensive.

It may be possible to use data taken within a shaft or tunnel complex or cavity, if radiation transport and shock wave propagation within the complex or cavity can be accurately simulated. It may also be possible to use data from beyond the hydrodynamic zone, if reliable constitutive relations are available for the ambient medium. Obviously, algorithms that make use of such data are not purely hydrodynamic.

Low-Yield Explosions

Tamped underground nuclear explosions as small as a few kilotons produce shock waves that evolve in the same way as those produced by larger-yield explosions. However, because the hydrodynamic zone for such low-yield explosions ends much closer to the explosive canister than it does for tests with yields ≥ 50 kt, the effects of the canister, cableways, and open lines of sight on the evolution of the shock front are generally more important. Moreover, low-yield tests can be and often are set off at shallow depths in softer material, such as alluvium, or in tunnels or cavities. The shock waves produced by such explosions can differ markedly from the models of spherically-symmetric shock waves in hard rock that are used in most hydrodynamic yield estimation algorithms. Moreover, the shock waves produced by such explosions have been observed to differ from test to test. These differences are potential sources of error in the yield estimate.

Serious practical, operational, and engineering problems also arise in trying to use hydrodynamic methods to estimate the yields of explosions with yields of a few kilotons. For one thing, the sensing cable must be placed very close to the nuclear charge in order to sample the hydrodynamic zone. Drilling emplacement and satellite holes 4 meters from one another to the depth at which the explosive canister is emplaced (≥ 200 m), which would be required in order to use hydrodynamic methods to monitor a 10 kt test in a standard vertical geometry, is at or beyond the capabilities of current drilling techniques.⁶ In horizontal tunnel geometries, the need to take data so close to the center of the explosion would force placement of the sensing cable so close to the tunnel wall that the motion of the shock front along the sensing cable would probably be significantly distorted by the tunnel.

The need to make measurements close to the center of the explosion would also necessitate more stringent restrictions on the dimensions of explosive canisters, cableways, and open lines of sight, in order to assure accuracy. Such restrictions might be deemed an unacceptable interference with test programs. Finally, because the shock front must be measured at much smaller radii, any errors in surveying the emplacement and satellite holes or in determining the time of the explosion and the point of first crush are more important than for larger-yield explosions.

It is possible that some of these difficulties could be alleviated by developing models and algorithms that would allow routine use of shock wave position data taken at distances beyond the hydrodynamic interval, although current experience with such data is not very encouraging. In any case, these and other potential solutions to the problems that would be encountered in monitoring low-yield tests using hydrodynamic methods have not yet been carefully and thoroughly studied. Thus, at the present time hydrodynamic yield estimation methods could not be used with confidence to monitor compliance with threshold test bans in which the threshold is less than several tens of kilotons.

Accuracy of Shock Wave Methods

What accuracy can be expected from routine monitoring of the yields of underground nuclear tests using shock-wave methods? In our judgment, shock-wave methods have not yet been studied in the United States as widely or as thoroughly as seismic methods. Furthermore, very few of the studies that have been carried out have been published in the open literature. For example, the results of the 1988 Joint Verification Experiment carried out by the United States and the Soviet Union have still not been made available to the public, even though they are fully available to both governments. The status of shock-wave methods in the Soviet Union is even less clear, with essentially no information available in the open literature. Given the very limited information available in the open literature, it is all but impossible to present here a meaningful assessment of the probable accuracy of shock-wave methods when used as a treaty-monitoring tool. Nevertheless, the most likely sources of systematic and random error can be identified.

Variations in the contents of the explosive canister can cause systematic errors in yield estimates based on shock-wave methods. For example, Moran and Goldwire [1990] have shown, as noted earlier, that the yields of spherically-symmetric explosions inferred from data taken in the hydrodynamic measurement zone may differ from the actual yields by 20%, for the hydrodynamic sources they present as models of the sources produced by different nuclear explosives and test geometries. The conclusions of Moran and Goldwire [1990] are supported by the numerical simulations of Callen, Fiedler, Lamb, and Sullivan [in preparation], who also find that the characteristics of the source can affect yield estimates based on hydrodynamic algorithms. Since the contents of the explosive canister are unlikely to be known to the verifying party, such differences are a source of uncertainty for hydrodynamic yield estimates made under treaty-monitoring conditions.

In addition to systematic errors caused by differences between the assumed and actual properties of the hydrodynamic source, any differences between the actual and assumed geological and geophysical properties of the surrounding medium will cause systematic or random errors in the yield estimate. For example, incorrect assumptions about the average properties of the ambient medium, including the equation of state of the rock, would bias the yield estimate, decreasing its accuracy, whereas variations in the properties of the medium on small scales would cause scatter in shock-front position measurements, decreasing the precision of the yield estimate [Lamb, 1988].

Large-scale geological or geophysical structures within the hydrodynamic measurement zone can also affect the yield estimate. For example, the alluvial deposits at the Nevada Test Site are weakly consolidated erosion products of the surrounding mountains with physical properties that vary widely. Layers of gravel, the residues of ancient stream beds, are often encountered in drilled holes. While most shock-front position measurements at NTS behave as expected, an occasional test has produced irregular data that defy simple explanation. Such results have been attributed to spatial variations in the ambient medium [Holzer, 1965]. As another example, dissolution cavities may be present in the carbonate rocks of the Soviet Northern Test Site on the island of Novaya Zemlya. Such cavities, if located within the hydrodynamic measurement zone and unrecognized or unfilled, could significantly distort the shock front, thereby biasing the yield estimate.

Man-made structures within the hydrodynamic measurement zone can also cause systematic errors in the yield estimate, if they are not adequately filled or modeled. Such structures may include vertical shafts or horizontal tunnels as well as cavities. Other potential sources of bias include errors in determining the time of detonation and the position of the center of the explosion and in determining the paths of the sensing cables relative to the center of the explosion.

SLIFER data have been collected from sensing cables positioned in the nuclear explosive emplacement hole for many tens of underground nuclear tests, and from sensing cables positioned in satellite holes for several tens of tests [U. S. Congress, 1988]. CORRTEX data has reportedly been collected from sensing cables positioned in the emplacement hole for ~100 nuclear tests, and from sensing cables positioned in one or more satellite holes for a dozen or so tests [U. S. Department of State, 1986a, 1986b, U. S. Congress, 1988]. A very small fraction of the SLIFER data has been released publicly, most of it only after having been scaled (assuming the validity of cube-root scaling) so that the apparent yield is 1 kt (see Heusinkveld [1979] and Heusinkveld [1982]). At present, all CORRTEX data remain classified.

According to the U. S. Department of State [1986a, 1986b], hydrodynamic yield estimates have fallen within 15% of radiochemical yield estimates (at the 95% confidence level), for historic tests with yields greater than 50 kt conducted in the geologic media of the Nevada Test Site. According to these same reports, hydrodynamic methods are expected to have an uncertainty of a factor of 1.3 at the 95% confidence level when used under treaty-monitoring conditions at the Soviet test sites near Shagan River to monitor explosions with yields greater than 50 kt. However, some scientists familiar with hydrodynamic methods believe that the uncertainty could be somewhat larger (see U. S. Congress [1988], appendix on CORRTEX).

While one may hope that the uncertainties will turn out to be as small as 30%, only time and experience will show what the uncertainties actually are. This is especially so because the U. S. nuclear community does not yet have experience with monitoring tests in geologic media such as the frozen carbonate and silicate rocks at the Soviet Northern Test Site on Novaya Zemlya Island, or in monitoring nuclear tests involving complex geometries, substantial cavities, or multiple explosions at Soviet test sites.

It has been claimed in Congressional hearings on TTBT and PNET verification and elsewhere⁷ that hydrodynamic methods are "direct" whereas seismic methods are not. In fact, both hydrodynamic and seismic methods estimate the yield indirectly, by measuring the ground motion produced by the explosion. In both methods, the important events are: (1) production of a signal by the exploding nuclear charge, (2) propagation of the signal to points more or less remote from the detonation point, and (3) detection of the signal by sensors at the remote points. Relevant questions for both methods include how the size of the signal varies with yield, how well the propagation of the signal is understood, and how accurately and precisely the signal can be measured.

It has also been asserted that use of hydrodynamic methods in and of itself eliminates the possibility of systematic error or "bias" (see, for example, the testimony of J. H. McNally in U. S. Senate [1987], pp. 27 and 99-101). If what was meant is that hydrodynamic methods do not suffer from "regional seismic bias", the statement is true but trivial, since regional seismic bias obviously is not relevant to non-seismic yield-estimation methods. On the other hand, if what was meant is that hydrodynamic methods do not suffer from bias in the sense of systematic error, the statement is obviously false. Both hydrodynamic and seismic yield estimation methods are subject to systematic as well as random errors. Relevant questions are the expected sizes of the errors, and whether they are so large as to be of concern.

5. Conclusions

Shock-wave yield estimation methods were developed by the United States and the Soviet Union primarily as tools for estimating the yields of their respective nuclear tests. These methods make use of the fact that the strength of the expanding shock wave

produced by an underground explosion increases with the yield of the explosion. At present, the most accurate yields are given by algorithms that use only data collected within the hydrodynamic zone, which extends $\sim 5(W/1\text{kt})^{1/3}$ meters from the center of the explosion.

The evolution of the shock wave within the hydrodynamic zone depends on the properties of the source and the nature of the surrounding geologic medium. When hydrodynamic methods are used under treaty monitoring conditions, the verifying party's lack of information about the contents of the explosive canister introduces an uncertainty in the derived yield that may be about 20% for tests conducted in standard geometries. Any errors or uncertainties in determining the time of the explosion or the position of the shock front relative to the center of the explosion or in modeling the equation of state of the ambient medium and the effects of any natural or man-made geological or geophysical structures will increase the uncertainty of the yield estimate. For standard tests with yields greater than several tens of kilotons conducted in ambient geologic media for which the verifying party has direct experience or good theoretical models, the uncertainty in yield estimates may be as small as 30%. Nuclear tests conducted in cavities or in vertical shaft or horizontal tunnel complexes typically produce more complicated shock waves. Hence the uncertainty in the estimated yield of such a nonstandard test is likely to be greater than for a test conducted in a standard vertical or horizontal geometry.

The algorithms that have been used to extract yield estimates from shock-wave measurements within the hydrodynamic zone vary in accuracy and reliability. Even the best hydrodynamic algorithms may not always be more precise than seismic algorithms, especially if regional as well as teleseismic phases are used in constructing the seismic yield estimate [Hansen, Ringdal, and Richards, 1990]. Shock-wave yield estimation algorithms are not affected by the large-scale features of the test site or the geophysical properties of the earth beneath it, as seismic algorithms are, but shock-wave algorithms are more affected than seismic algorithms by local structures that disturb the evolution of the shock wave, such as tunnels, shafts, and voids, and geological and geophysical discontinuities. Thus, for explosions with yields greater than several tens of kilotons, shock-wave methods can complement seismic methods. The yields of such underground nuclear explosions can therefore be estimated more accurately by combining the two methods than by using either method alone.

Acknowledgements.—It is a pleasure to thank T. Ahrens, D. Eilers, R. Geil, M. Heusinkveld, R. Hill, B. Leith, and G. Miller for helpful discussions of shock wave propagation and yield estimation. The authors are also grateful to T. Ahrens and W. Moss for carefully reading a draft of this review and suggesting numerous improvements. This work was supported in part by DARPA through the Geophysics Laboratory under contract F-19628-88-K-0040.

Notes

¹The motion of the shock wave changes only gradually and so the point at which it is said to enter the transition interval is purely conventional. Throughout the present article we use the convention that the transition interval begins when the peak density ratio falls to 80% of its limiting value.

²Again, the motion of the shock wave changes only gradually and so the point at which it is said to enter the low-pressure plastic wave interval is purely conventional. Throughout the present article we use the convention that the low-pressure plastic wave interval begins when the shock speed falls to 1.2 times the low-pressure plastic wave speed.

³In order to prevent seepage of radioactive gases to the surface, the

depth of burial (DOB) of U. S. tests is at least $(20(W/1\text{kt})^{1/3})\text{ m}$. This requires a DOB of at least 650 m for a 150 kt explosion. When the DOB given by this relation would be relatively small, or in media with a substantial water content, the actual DOB is increased in order to assure containment of radioactive gases. The actual DOB of an explosion at the Nevada Test Site is normally not less than 200 m. See U. S. Congress [1989], pp. 35-37.

⁴SLIFER is an acronym for Shorted Location Indicator by Frequency of Electrical Resonance.

⁵CORTEX is an acronym for Continuous Reflectometry for Radius versus Time Experiments. It is a misnomer, since the sampling in time is discrete.

⁶During preparations for the 1988 U. S.-Soviet Joint Verification Experiment (see U. S. Department of State [1988]), the Soviets stated that they did not have the technology to drill satellite and emplacement holes to the required depth (presumably ~ 650 m) while maintaining a horizontal displacement within the tolerance (presumably ~ 10 m) required by the United States. As a result, the United States flew its drill rig and crew to the Soviet test site. See C. P. Robinson, Testimony before the Subcommittee on Arms Control, International Security, and Science, House Committee on Foreign Affairs, June 28, 1988.

⁷See U. S. Senate [1987]; R. B. Barker, at pp. 8, 19, and 89-90; D. A. Vesser, at p. 94; S. R. Foley, at p. 11; J. H. McNally, at pp. 27 and 99-101; H. A. Holmes, at pp. 5 and 108. See also Robinson [1990].

References

- Al'tshuler, L. V., N. N. Kalinin, L. V. Kuz'mina, and B. S. Chekin, Shock adiabats for ultrahigh pressures, *Sov. Phys.—JETP* 45, 161-171, 1977.
- Axford, R. A. and D. D. Holm, in *Proc. Nuclear Explosion Design Conference*, Los Alamos National Laboratory, October 1987.
- Barenblatt, G. I., *Similarity, Self-similarity, and Intermediate Asymptotics*, Consultants Bureau, New York, 1979 [English Translation].
- Bass, R. C., and Larsen, G. E., *Shock propagation in several geologic materials of interest in hydrodynamic yield determinations*, Sandia Laboratory, Rep. SAND77-0402, 1977.
- Brode, H. L., Review of nuclear weapons effects, *Ann. Rev. Nuclear Sci.*, 18, 153-202, 1968.
- Butkovich, T. R., Calculation of the shock wave from an underground nuclear explosion in granite, *J. Geophys. Res.*, 70, 885-892, 1965.
- Callen, B. W., F. K. Lamb, and J. D. Sullivan, Insensitive interval in the evolution of shock waves from explosions, in *Shock Compression of Condensed Matter—1989*, S. C. Schmidt, J. N. Johnson, and L. W. Davison, eds., pp. 241-244, Elsevier Science Pubs., Amsterdam, 1990.
- Chung, D. H., and G. Simmons, Pressure derivatives of the elastic properties of polycrystalline quartz and rutile, *Earth Planet. Sci. Lett.*, 6, 134-138, 1969.
- Deupree, R. G., D. D. Eilers, T. O. McKown, and W. H. Storey, *CORTEX: a compact and versatile system for time domain reflectometry*, Los Alamos National Laboratory, Rep. LA-UR-80-3382, 1980.
- Germain, L. S., and Kahn, J. S., *Phenomenology and containment of underground nuclear explosions*, Lawrence Radiation Laboratory, Rep. UCRL-50482, November 1968.
- Glasstone, S., and P. Dolan, *Effects of Nuclear Weapons*, U. S. Government Printing Office, Washington, 1977.
- Glenn, H. D., T. F. Stubbs, J. A. Kalinowski, and E. C. Woodward, *Containment analysis for the Queso event*, Lawrence Livermore National Laboratory, Rep. UCRL-89410, August 1983.
- Glenn, H. D., T. F. Stubbs, and J. A. Kalinowski, in *Shock Waves in Condensed Matter*, Y. M. Gupta, ed., pp. 639-644, Plenum, New York, 1986.
- Hansen, R. A., F. Ringdal, and P. G. Richards, *The stability of rms L_2 measurements, and their potential for accurate estimation of the yields of soviet underground nuclear explosions*, Geophysics Laboratory (Hanscom Air Force Base, Mass.), Rep. GL-TR 90-0061, February 1990.
- Heusinkveld, M., and F. Holzer, Method of continuous shock front position measurement, *Rev. Sci. Instr.*, 35, 1105-1107, 1964.
- Heusinkveld, M., *Analysis of SLIFER data from underground nuclear explosions*, Lawrence Livermore National Laboratory, Rep. UCRL-52648, 1979.
- Heusinkveld, M., *Analysis of shock wave arrival time from underground explosions*, *J. Geophys. Res.*, 87, 1891-1898, 1982.
- Holzer, F., Measurements and calculations of peak shock-wave parameters from underground nuclear detonations, *J. Geophys. Res.*, 70, 893-905, 1965.
- Johnson, G. W., G. H. Higgins, and C. E. Violet, Underground nuclear detonations, *J. Geophys. Res.*, 64, 1457-1470, 1959.
- King, D. S., B. E. Freeman, D. D. Eilers, and J. D. Johnson, The effective yield of a nuclear explosion in a small cavity in geologic material, *J. Geophys. Res.*, 94, 12375-12385, 1989.
- Lamb, F. K., *An approximate solution for ground shock propagation*, University of Illinois Program in Arms Control, Disarmament, and International Security, Rep. WP-2-87-2, February 1987.
- Lamb, F. K., Monitoring yields of underground nuclear tests using hydrodynamic methods, in *Nuclear Arms Technologies in the 1990s*, D. Schroerer and D. Hafemeister, eds., pp. 109-148, American Institute of Physics, New York, 1988.
- Lamb, F. K., B. W. Callen, and J. D. Sullivan, Insensitive interval in the evolution of shock waves from underground nuclear explosions, Rep. prepared for 11th Annual AFGL/DARPA Seismic Research Symposium, San Antonio, Tex., May 1989; University of Illinois Physics Dept. Rep. P-89-5-77, May 1989.
- Lamb, F. K., B. W. Callen, and J. D. Sullivan, An approximate analytical model of shock waves from underground nuclear explosions, submitted to *J. Geophys. Res.*, December 1990.
- Los Alamos National Laboratory, Public information sheet on CORTEX, April 1986.
- McQueen, R., J. N. Fritz, and J. W. Hopson, *High-pressure equation of state of SiO₂*, M-6 Prog. Rep. M-6-200, pp. 78-136, Los Alamos National Laboratory, Los Alamos, N. M., Jan.-March 1977.
- Moran, B., and H. C. Goldwire, Jr., Effect of source modelling on the inferred yield from an underground nuclear explosion, in *Shock Compression of Condensed Matter—1989*, S. C. Schmidt, J. N. Johnson, and L. W. Davison, eds., pp. 645-648, Elsevier Science Pubs., Amsterdam, 1990.
- Murri, W. J., D. R. Curran, C. F. Petersen, and R. C. Crewdson, Response of solids to shock waves, in *Advances in High-Pressure Research*, Vol. 4, R. H. Hentorf, Jr., ed., 1-163, Academic Press, London, 1974.
- Moss, W. C., A method to estimate the yield of an underground nuclear explosion, *J. Appl. Phys.*, 63, 4771-4773, 1988.
- Nuckolls, J. H., A computer calculation of Rainier (the first 100 milliseconds), in *Proc. Second Plowshare Symposium, May 13-15, 1959, San Francisco, California Part I. Phenomenology of Underground Nuclear Explosions*, University of California Radiation Laboratory, Rep. UCRL-5675, pp. 120-134, 1959.
- Ragan, C. E., III, Shock wave experiments at three-fold compression, *Phys. Rev. A* 29, 1391-1402, 1984.
- Robinson, C. P., Verifying testing treaties—old and new (interview), *Arms Control Today*, 20, 3-7, 1990.
- Schmitt, G. G., and R. D. Dick, Use of CORTEX to measure explosive performance and stem behavior in oil shale fragmentation

- tests. Los Alamos National Laboratory, Rep. LA-UR-85-231, 1985.
- Sedov, L. I., The motion of air in a strong explosion [in Russian], *Akademiya nauk SSSR, Doklady*, 52, 17-20, 1946.
- Sedov, L. I., *Similarity and Dimensional Methods in Mechanics*, Academic Press, New York, 1959 [English translation].
- Storey, W. H., Jr., D. D. Eilers, T. O. McKown, D. M. Holt, and G. E. Conrad, *CORRTEX II: a dual micro-processor controlled instrument for dynamic shock position measurements*, Los Alamos National Laboratory, Rep. LA-UR-82-558, 1982.
- Taylor, G. I., The formation of a blast wave by a very intense explosion I Theoretical discussion, *Proc. Roy. Soc. (London)*, A201, 159-174, 1950 (a).
- Taylor, G. I., The formation of a blast wave by a very intense explosion II The atomic explosion of 1945, *Proc. Roy. Soc. (London)*, A201, 175-186, 1950 (b).
- Terhune, R. W., H. D. Glenn, D. E. Burton, H. L. McKague, and J. T. Rambo, Numerical simulation of the Baneberry event, *Nucl. Tech.*, 46, 159-169, 1979.
- U. S. Arms Control and Disarmament Agency, *Arms Control Agreements*, 1990 (a).
- U. S. Arms Control and Disarmament Agency, *Treaty Between the United States of America and the Union of Soviet Socialist Republics on the Limitation of Underground Nuclear Weapons Tests and Treaty Between the United States of America and the Union of Soviet Socialist Republics on Underground Nuclear Explosions for Peaceful Purposes: Text of Treaties and Protocols*, 1990 (b).
- U. S. Congress, Office of Technology Assessment, *The Containment of Underground Nuclear Explosions*, OTA-ISC-414, U. S. Government Printing Office, Washington, D. C., October 1989.
- U. S. Congress, Office of Technology Assessment, *Seismic Verification of Nuclear Testing Treaties*, OTA-ISC-361, U. S. Government Printing Office, Washington, D. C., May 1988.
- U. S. Department of State, Bureau of Public Affairs, U. S. policy regarding limitations on nuclear testing, *Special Report No. 150*, August 1986 (a).
- U. S. Department of State, Bureau of Public Affairs, Verifying nuclear testing limitations possible U. S.-Soviet cooperation, *Special Report No. 152*, August 1986 (b).
- U. S. Department of State, *Agreement Between the United States of America and the Union of Soviet Socialist Republics on the Conduct of a Joint Verification Experiment*, May 1988.
- U. S. Senate, *Threshold Test Ban Treaty and Peaceful Nuclear Explosions Treaty, Hearings Before the Committee on Foreign Relations*, U. S. Government Printing Office, Washington, D. C., 1987.
- Virchow, C. F., G. E. Conrad, D. M. Holt, and E. K. Hodson, Microprocessor-controlled time domain reflectometer for dynamic shock position measurements, *Rev. Sci. Instr.*, 51, 642-646, 1980.
- Wackerle, J., Shock wave compression of quartz, *J. Appl. Phys.*, 33, 922-937, 1962.
- Zel'dovich, Ya. B., and Yu. P. Raizer, *Physics of Shock Waves and High-Temperature Hydrodynamic Phenomena*, Academic Press, New York, 1967 [English translation].

An Approximate Analytical Model of Shock Waves From Underground Nuclear Explosions

F. K. LAMB,¹ B. W. CALLEN,² AND J. D. SULLIVAN

*Department of Physics and Program in Arms Control, Disarmament, and International Security
University of Illinois, Urbana-Champaign*

We discuss an approximate analytical model for the hydrodynamic evolution of the shock front produced by a spherically symmetric explosion in a homogeneous medium. The model assumes a particular relation between the energy of the explosion, the density of the medium into which the shock wave is expanding, and the particle speed immediately behind the shock front. The assumed relation is exact for shock waves that are strong and self-similar. Comparison with numerical simulations indicates that the relation is also approximately valid for shock waves that are neither strong nor self-similar. Using the assumed relation and the Hugoniot of the ambient medium expressed as a relation between the shock speed and the postshock particle speed, one can calculate the radius and other properties of the shock front as a function of time. The model also allows one to investigate how the evolution of the shock wave is influenced by the properties of the ambient medium and how these properties affect the characteristic radius at which the shock wave becomes a low-pressure plastic wave. The shock front radius versus time curves predicted by the model agree well with numerical simulations of explosions in quartz and wet tuff and with data from four underground nuclear tests conducted in granite, basalt, and wet tuff when the official yields are assumed. When the model is used instead to fit radius versus time data from the hydrodynamic phases of these tests, it gives yields that are within 8% of the official yields when piecewise-linear approximations to the Hugoniot are used. This accuracy is comparable to the accuracy of other models.

1. INTRODUCTION

Shock wave methods have long been used to estimate the yields of nuclear explosions, both in the atmosphere (see, for example, *Sedov* [1946] and *Taylor* [1950*b*]) and underground (see, for example, *Johnson et al.* [1959] and *Nuckolls* [1959]). All such methods are based on the fact that the strength of the shock wave produced by an explosion increases with the yield, all other things being equal. As a result, the peak pressure, peak density, and shock speed at a given radius all increase monotonically with the yield. Hence, by comparing measurements of these quantities with the values predicted by a model of the evolution of the shock wave in the relevant ambient medium, the explosive yield can be estimated. Shock wave methods for determining the yields of underground nuclear explosions are of increasing interest as one means of monitoring limitations on underground nuclear testing. These methods were first introduced as a treaty-monitoring tool in the original Protocol of the Peaceful Nuclear Explosions Treaty of 1976 [*U.S. Arms Control and Disarmament Agency*, 1990*a*]. Hydrodynamic methods were explored further in a joint U.S.-USSR verification experiment [*U.S. Department of State*, 1988] and have now been incorporated in new protocols to the Threshold Test Ban and Peaceful Nuclear Explosions Treaties [*U.S. Arms Control and Disarmament Agency*, 1990*b*].

Most shock wave algorithms for estimating the yields of underground nuclear explosions have focused on the so-

called hydrodynamic phase [see *Lamb*, 1988], because the evolution of the shock wave during this phase is relatively simple. The energy released by a nuclear explosion initially emerges from the nuclear device as nuclear radiation, fission fragments, and thermal electromagnetic radiation [see *Glavstone and Dolan*, 1977, pp. 12-25 and 61-63]. At the very earliest times, energy is carried outward by the expanding weapon debris and radiation. As this debris and radiation interact with the surrounding medium, a strong shock wave forms and begins to expand. The evolution of the explosion during this phase can be followed using the equations of hydrodynamics and radiation transport. However, within ~ 10 - $100 \mu\text{s}$, depending on the yield and the composition and distribution of matter surrounding the nuclear charge, the outward flow of energy via radiation becomes unimportant, and the explosion can be described using the equations of hydrodynamics alone. At this point the explosion enters the (purely) hydrodynamic phase. The radial stress produced by the shock wave at the beginning of this phase greatly exceeds the critical stress at which the surrounding rock becomes plastic, so that to a good approximation the shocked medium can be treated as a fluid. As the shock wave expands, it weakens. Eventually, the strength of the rock can no longer be neglected, the fluid approximation fails, and the hydrodynamic phase ends. Yield estimation methods that use measurements made during the hydrodynamic phase are called hydrodynamic methods.

All hydrodynamic methods require a model of the evolution of the shock wave. Models in recent or current use range in sophistication from an empirical power law formula that supposes the evolution is completely independent of the medium [*Bass and Larsen*, 1977] (see also *Heusinkveld* [1982] and *Lamb* [1988]) to multidimensional numerical simulations based on detailed equations of state (for recent examples of one-dimensional simulations, see *Moss* [1988], *King et al.* [1989], and *Moran and Goldwire* [1990]). When

¹Also at Department of Astronomy, University of Illinois, Urbana-Champaign.

²Now at Department of Physics, Drury College, Springfield, Missouri.

Copyright 1992 by the American Geophysical Union

Paper number 91JB02348
0148-0227/92/91JB-02348\$05.00

detailed equations of state data are available, state-of-the-art numerical simulations are expected to be highly accurate, at least for spherically symmetric, tamped explosions in homogeneous media. Nevertheless, a simple analytical model of the shock wave produced by such explosions that allows one to determine how the evolution depends on the Hugoniot and the yield is useful for several reasons. First, detailed equations of state are available only for a few geologic media. Second, large codes can be run for only a limited number of cases. Third and most importantly, an analytical model is more convenient than numerical simulations for analyzing how the evolution is affected by the properties of the ambient medium.

This is the first of several papers in which we investigate the evolution of the shock wave produced by a spherically symmetric explosion in a homogeneous medium during the hydrodynamic phase. Such a shock wave is necessarily spherically symmetric. Here we investigate a simple analytical model. In this model the compression of the medium at the shock front is treated exactly, using the Rankine-Hugoniot jump conditions and the Hugoniot of the ambient medium. The rarefaction of the shocked fluid that occurs as the shock front advances is treated approximately, via an ansatz relating the specific kinetic energy of the fluid just behind the shock front to the mean specific energy within the shocked volume. This model was proposed by Lamb [1987], who showed that it is exact for strong, self-similar shock waves. Lamb [1987] also made a preliminary comparison of the shock front radius versus time curves predicted by the model with data from several underground nuclear explosions and numerical simulations. The model was proposed independently by Moss [1988], who compared its predictions with particle speed data from underground nuclear explosions and numerical simulations. Their results showed that the model provides a useful approximate description of the shock wave evolution throughout the hydrodynamic phase. The model is similar in spirit to one proposed earlier by Heusinkveld [1979, 1982] but is more satisfactory theoretically and appears to provide a more accurate description of underground nuclear explosions, as shown in our appendix.

In section 2 we first discuss the assumptions on which the model is based, including the ansatz relating the specific kinetic energy of the fluid just behind the shock front to the mean specific energy within the shocked volume. Next, we combine the ansatz with the Hugoniot of the ambient medium expressed as a relation between the shock speed D and the postshock particle speed u_1 to obtain a first-order ordinary differential equation that describes the motion of the shock front. We show that solutions of this equation of motion can be expressed in terms of simple analytical functions when the D versus u_1 relation is piecewise linear. Since an arbitrary D versus u_1 relation can be represented to any desired accuracy by an appropriate piecewise-linear relation, the radius versus time predictions of the model for an arbitrary Hugoniot can always be expressed as a sum of simple analytical functions. Alternatively, the equation of motion can be integrated numerically to find the model predictions for any prescribed Hugoniot. In practice, the latter approach is often more convenient. The model also gives the shock speed, postshock density, postshock particle speed, and postshock pressure as functions of the shock front radius or the elapsed time, the yield of the explosion, and the Hugoniot of the ambient medium.

In section 3 we assess the accuracy of the model. We first show that the ansatz is exact for a shock wave that is strong and self-similar. We then compare this ansatz with results from numerical simulations and find that it is also remarkably accurate for spherical shock waves that are neither strong nor self-similar. Finally, we compare the radius versus time and particle velocity versus radius curves predicted by the model with the corresponding curves obtained from numerical simulations of underground nuclear explosions. We conclude that the model with point source boundary conditions provides a remarkably good description of the spherically symmetric shock waves produced by such explosions.

In section 4 we show that the radius versus time curves given by the analytical model of section 2 provide an excellent description of the field data from four underground nuclear tests conducted by the United States, despite the fact that these tests are not point explosions and that the ambient media may be nonuniform. In fact, the model sometimes describes the data accurately even well beyond the hydrodynamic phase of the explosion. When the model and the Hugoniot of sections 3 and 4 are used to estimate yields using data from the hydrodynamic phase of these four nuclear explosions, the resulting estimates are within 8% of the official yields. For comparison, when the numerical simulations described in section 3 are fitted to the same data, the resulting yield estimates are within 9% of the official yields. Our lack of knowledge of the geometry of these tests, of the way in which the data was gathered, and, in the case of one explosion, of the medium in which the explosion occurred makes it difficult to assess whether the relatively small differences between the various yield estimates are due to errors in the radius versus time data, departures from spherical symmetry due to asphericity of the source and/or inhomogeneity of the ambient medium, uncertainties in the yield standard, or inadequacies of the models. The U.S. Department of State [1986a, b] has claimed that hydrodynamic methods are accurate to within 15% (at the 95% confidence level) of radiochemical yield estimates for tests with yields greater than 50 kt in the geologic media found at the Nevada Test Site (see also U.S. Congress, Office of Technology Assessment [1988, pp. 129-139] and Lamb [1988]). Thus the analytical model of section 2 appears to be competitive with other models for purposes of yield estimation. A preliminary account of this work has been given by Callen et al. [1990b].

2 MODEL

In this section we first present the fundamental assumptions of the model and derive the resulting equation of motion for the shock front. We then solve this equation of motion and discuss the scalings allowed by the shock front radius versus time curve predicted by the model.

Assumptions

The model assumes that the shock wave is purely hydrodynamic, that is, that transport of energy via radiation is negligible and that the stress produced by the shock wave is much larger than the critical stress at which the medium becomes plastic. The model assumes further that the medium in which the shock wave is propagating is homogeneous and that the shock wave is spherically symmetric at

the time the model first applies. The shock wave therefore remains spherically symmetric. As the shock wave expands and weakens, the strength of the ambient medium eventually becomes important. At this point the model is no longer applicable.

Part of the energy released in any nuclear explosion escapes without contributing to the energy of the shock wave [see *Glasstone and Dolan*, 1977, pp. 12–13]. Thus the yield measured by hydrodynamic methods is less than the total energy released in the explosion. Here we are concerned exclusively with the hydrodynamic phase of the explosion, and hence the yield W to which we refer is the so-called hydrodynamic yield, namely, the energy that contributes to the formation and evolution of the shock wave. The model assumes that W is constant in time. This is expected to be an excellent approximation during the hydrodynamic phase.

The Rankine-Hugoniot jump conditions express conservation of mass, momentum, and energy across the shock front (see, for example, *Zel'dovich and Raizer* [1967, chapter I]). The model is based on approximate forms of the jump conditions, which are nevertheless extremely accurate under the conditions of interest. The model neglects the pressure p_0 of the unshocked ambient medium in comparison with the pressure p_1 of the fluid just behind the shock front. Since p_1 is ≥ 1 GPa for the times and shock radii of interest, whereas p_0 is ~ 20 MPa, neglecting p_0 is an excellent approximation. The model also neglects the specific internal energy ϵ_0 of the unshocked medium in comparison with the specific internal energy ϵ_1 of the fluid just behind the shock front. This approximation is also highly accurate, since ϵ_1 is greater than ϵ_0 for postshock particle speeds u_1 greater than about 100 m/s, and u_1 is ≥ 1 km/s for the times and shock front radii of interest.

With these approximations, the Rankine-Hugoniot equations, written in the frame in which the unshocked material is at rest, become

$$\rho_1(D - u_1) = \rho_0 D, \quad (1)$$

$$\rho_0 D u_1 = p_1, \quad (2)$$

and

$$\frac{1}{2} p_1 \left(\frac{1}{\rho_0} - \frac{1}{\rho_1} \right) = \frac{1}{2} u_1^2 - \epsilon_1, \quad (3)$$

where $D = dR/dt$ is the speed of the shock front and ρ_0 and ρ_1 are the densities just ahead of and just behind the front. Equation (3) shows that the energy $p_1(1/\rho_0 - 1/\rho_1)$ acquired by a unit mass of the medium as a result of shock compression is divided equally between kinetic energy of bulk motion and the increase in the specific internal energy. The shock speed D is related to the postshock particle speed u_1 by the Hugoniot

$$D = D(u_1), \quad (4)$$

which depends on the medium.

Without loss of generality, the specific kinetic energy of the fluid just behind the shock front can be related to the mean specific energy within the shocked volume via the expression

$$u_1 = f(3W/4\pi R^3 \rho_0), \quad (5)$$

where f is a dimensionless factor that generally depends on the equation of state of the ambient medium and the radius of the shock front. A key assumption of the model is that f is independent of the shock front radius R for all shock front radii of interest. We assess the validity of this ansatz in the next section, where we show that it is exact when the shock wave is strong and is approximately valid throughout the hydrodynamic phase of the explosion.

The model treats the compression of the ambient medium at the shock front exactly, since the jump conditions and the Hugoniot are correctly incorporated. On the other hand, the rarefaction that occurs as a shocked fluid element is left behind by the advancing shock front is treated only indirectly, and approximately, via the parameter f . The value of this parameter depends on the density, velocity, and specific internal energy distributions within the shocked volume, distributions that would be determined in a full hydrodynamic calculation of the structure and evolution of the shock wave. In order to carry out such a calculation, knowledge of the equation of state off the Hugoniot (i.e., along the release adiabat) is required. This requirement is sidestepped in the model by assuming that f is independent of R . The parameter f is then the only free parameter in the model.

The best value of f to use for explosions in a given rock can be determined by fitting the postshock particle speed relation (5) (or the relations for the shock speed, shock front radius, and postshock pressure that follow from it) to data from numerical simulations or data from actual underground explosions in that rock. Once f is determined, the model provides a description of the properties and evolution of the shock wave produced by an explosion of any yield in the same medium.

Predicted Radius Versus Time

With the assumption that f is independent of R , the right side of equation (4) becomes a known function of R , and hence equation (4) becomes a first-order ordinary differential equation for R . This equation can be integrated directly to determine the radius of the shock front as a function of time. Solutions of the shock front equation of motion can be expressed in terms of simple analytical functions when the shock speed is a linear or piecewise-linear function of the postshock particle speed, as we now show.

Linear Hugoniot. Experimental studies of shock waves in solids (see, for example, *Zel'dovich and Raizer* [1967, chapter XI]) have shown that for many materials the relation between the speed D of a shock front and the particle speed u_1 just behind it is approximately linear for large u_1 , that is,

$$D(u_1) = A + B u_1, \quad (6)$$

for some constants A and B . In general, the $D(u_1)$ relation deviates from this high-speed relation as the postshock particle speed falls. If we assume for the moment that $D(u_1)$ can be adequately represented by a single linear relation of the form (6) over the full range of u_1 that is of interest, we can obtain an interesting and useful analytical solution for the motion of the shock front.

First, for convenience, we introduce the dimensionless variables

$$x = R/L = \tau/(fT), \quad (7)$$

where

$$L = (3fWB^2/4\pi\rho_0A^2)^{1/3}, \quad T = L/A. \quad (8)$$

The characteristic length L and the characteristic time T depend on the medium through the constants ρ_0 , A , B , and f and scale as the cube root of the yield W . Making use of relation (5) and the characteristic length L , equation (6) becomes

$$D = dR/dt = A[1 + (L/R)^{3/2}]. \quad (9)$$

This equation shows that the length L is the radius that separates the strong shock regime, where $D \propto R^{-3/2}$, from the low-pressure plastic wave regime, where $D = \text{const}$. In nondimensional form, equation (9) is

$$dx/d\tau = 1 + (1/x)^{3/2}. \quad (10)$$

The general solution of equation (10) is

$$\tau - \tau_0 = h(x) - h(x_0), \quad (11)$$

where $\tau_0 = t_0/T$ and $x_0 = R_0/L$. Here R_0 is the radius of the shock front at t_0 , the time at which the evolution of the shock wave is first described by the model. The function $h(x)$ in equation (11) is given by

$$h(x) \equiv x - \frac{1}{3} \ln \left(\frac{x - 2x^{3/2} + 1}{x - x^{3/2} + 1} \right) - \frac{2}{3^{1/2}} \left[\frac{\pi}{6} - \tan^{-1} \left(\frac{2x^{3/2} - 1}{3^{1/2}} \right) \right]. \quad (12)$$

For a point explosion, $x_0 = 0$ at $\tau_0 = 0$. For such explosions the function $x(x_0, \tau_0, \tau)$ defined implicitly by equation (11) becomes, at small radii ($x \ll 1$),

$$x(\tau) \approx (5/2)^{2/5} \tau^{2/5}, \quad (13)$$

which is the well-known temporal behavior of a strong, self-similar shock wave produced by a point explosion [Sedov, 1959]. At large radii ($x \gg 1$) this function becomes

$$x(\tau) \approx \text{const} + \tau, \quad (14)$$

which describes a constant-speed plastic wave (this is sometimes referred to as a bulk wave). Equation (11) thus provides an interpolation between the strong shock wave and the low-pressure plastic wave regimes.

Within the assumptions of the model an explosion is completely defined by its yield W and the ambient medium, which in turn is completely defined by the quantities ρ_0 , A , B , and f . The shock front radius versus time curve for an explosion of any yield in any medium can be generated from the function $x(x_0, \tau_0, \tau)$ by using the relation

$$R(t) = L x(t/T), \quad (15)$$

For a point explosion, this simplifies to

$$R(t) = L x(t/T), \quad (16)$$

The radius versus time curve (15) satisfies a scaling involving the yield W and the properties A , B , and ρ_0 of the ambient medium. In particular, relation (15) implies that if

the radius versus time curve for explosion i is known, then the radius versus time curve for a second explosion j can be generated, provided that ρ_0 , A , B , f , and W are known for both explosions and the initial radii and times R_{0i} , t_{0i} , R_{0j} , and t_{0j} satisfy

$$R_{0j} = (L_j/L_i)R_{0i}, \quad t_{0j} = (T_j/T_i)t_{0i}. \quad (17)$$

Under these conditions, the radius versus time curve $R_j(t)$ for explosion j is given in terms of the curve $R_i(t)$ for explosion i by the similarity transformation

$$R_j(t) = (L_j/L_i)R_i(t/T_j). \quad (18)$$

The required scaling (17) is satisfied trivially if both explosions are point explosions. The similarity transformation (18) can be used to shed light on the physical origin of the so-called "insensitive interval" and to develop optimal weighting schemes for radius versus time data (F. K. Lamb et al. (manuscript in preparation, 1991), for preliminary accounts, see Lamb et al. [1989] or Callen et al. [1990a]).

A special case of (18) that we use in the next sections is the case of explosions in identical ambient media. According to (18), the radius versus time curves of two such explosions satisfy

$$R_j(t) = (W_j/W_i)^{1/3} R_i(W_i^{1/3}t/W_j^{1/3}), \quad (19)$$

provided that

$$R_{0j} = (W_j/W_i)^{1/3} R_{0i}, \quad t_{0j} = (W_j/W_i)^{1/3} t_{0i}. \quad (20)$$

In other words, the radius versus time curves scale with the cube root of the yield if the initial radii and times scale with the cube root of the yield. This result illustrates the more general point that cube root scaling does not follow from the hydrodynamic equations and the jump conditions alone; in addition, the relevant properties of the hydrodynamic source must scale [Lamb et al., 1991]. The required scaling of the source is again satisfied trivially if both explosions are point explosions. This is consistent with the known validity of cube root scaling during the hydrodynamic phase for point explosions in uniform media [King et al., 1989; B. W. Callen et al., manuscript in preparation, 1991].

So far, we have discussed the predictions of the model for the postshock particle speed u_1 as a function of R (equation (5)), shock speed D as a function of R (equation (9)), and shock front radius R as a function of time (equation (15)). The model also predicts the evolution of other quantities of interest, including the mass density, specific internal energy, and pressure immediately behind the shock front. Expressions for these quantities can be obtained from the jump conditions (1), (2), and (3) by substituting expressions (5) and (9) for u_1 and D .

The predicted postshock mass density is

$$\rho_1 = \left(\frac{x^{3/2} + 1}{x^{3/2} + 1 - B^{-1}} \right) \rho_0, \quad (21)$$

where $x = R/L$ is the dimensionless shock front radius. For $x \ll 1$, $\rho_1 \approx [B/(B-1)]\rho_0$, which is the limiting value for a strong shock wave. For large radii, ρ_1 approaches ρ_0 , as it must. The predicted postshock specific internal energy is

$$\epsilon_1 = \frac{A^2}{2B^2 x^3}. \quad (22)$$

while the predicted postshock pressure p_1 is

$$p_1 = \rho_0(A^2/B)(\alpha^{-3/2} + \alpha^{-3}). \quad (23)$$

For small radii ($\alpha \ll 1$), $p_1 \approx \rho_0(A^2/B)\alpha^{-3}$, whereas for large radii, $p_1 \approx \rho_0(A^2/B)\alpha^{-3/2}$.

Arbitrary Hugoniot. Although for many materials the Hugoniot at high particle speeds (or, equivalently, at high pressures) is well described by a single linear relation of the form (6), the Hugoniot at lower particle speeds usually deviates from the high-speed relation. If the linear relation that is valid at high particle speeds could be extrapolated to small u_1 , the constant A would correspond to the low-pressure plastic wave speed c_0 . However, such an extrapolation usually is not valid. In granite, for example, A is about 3 km/s, whereas c_0 is about 4 km/s.

Even if the Hugoniot is not linear over the range of u_1 of interest, it can still be represented to any desired accuracy by a sequence of piecewise-linear segments. In this case, equation (10) still describes the motion of the shock front within each segment of the Hugoniot, but at each break in $D(u_1)$, new Hugoniot parameters A and B must be introduced. While it is possible to write the radius versus time curve for a piecewise-linear Hugoniot with an arbitrary number of segments as a sum of standard functions, in practice it is more convenient to treat this case by integrating the shock front equation of motion (9) numerically.

In integrating equation (9), we handled the transitions between different linear segments of the Hugoniot as follows. The transitions occur at a sequence of fixed points in u_1 , which, for a given yield, are related to a sequence of radii by equation (5). After each time step, we computed the new value of the particle speed from equation (5) and compared it with the particle speed u_1^j at the junction of the $(i-1)$ st segment of the Hugoniot and the i th segment. When the newly computed value of u_1 dropped below u_1^j , in the next integration step, we replaced the constants A_{i-1} and B_{i-1} that described the previous segment of the Hugoniot with the constants A_i and B_i that described the current segment. The transition points between the different linear segments of the Hugoniot are not readily apparent in the resulting radius versus time curve, because steps occur only in the second derivative of the shock front radius with respect to time; both $R(t)$ and its first derivative are continuous.

The radius versus time curve predicted by the model for an arbitrary Hugoniot satisfies the cube root scaling relation (19), provided that the initial conditions satisfy equation (20).

3. COMPARISONS WITH ANALYTICAL MODELS AND NUMERICAL SIMULATIONS

In this section we assess the accuracy of the model. We first derive a general expression for the dimensionless factor f and show that the constancy of f is exact for a point explosion in a homogeneous medium when the shock wave is strong. (A strong shock wave is one in which the speed of the shock front is much larger than the speed of sound in the undisturbed rock, the pressure behind the shock front is predominantly thermal, and the ratio of the density immediately behind the shock front to the density ahead of the front is close to its limiting value. Such shock waves have special properties. In particular, the shock wave produced by a point explosion is self-similar while it remains strong [see *Zel'dovich and Raizer*, 1967, chapters I and XII]. The

condition that a shock wave be strong is not the same as the condition that the shock produce a radial stress greater than the critical stress at which the rock becomes plastic. The latter is the hydrodynamic condition, which is usually satisfied for some time after the shock wave is no longer strong (see section 4).) Having shown f to be constant when the shock wave is strong, we then explore the validity of relation (5) with f constant when the shock is no longer strong, by comparing predictions of the model with numerical simulations of underground nuclear explosions in quartz and wet tuff.

Expression for f

In order to evaluate the accuracy of the ansatz that f is constant, we make use of the assumption that the hydrodynamic energy of the matter interior to the shock front is constant, that is,

$$W \equiv 4\pi \int_0^{R(t)} \rho(r, t) \left[\frac{1}{2} u^2(r, t) + \epsilon(r, t) \right] r^2 dr = \text{const.} \quad (24)$$

To turn (24) into a relationship between u_1 and W , we first introduce the time-dependent dimensionless radius $\xi = r/R(t)$. Then, the distributions $\rho(r, t)$, $u(r, t)$, and $\epsilon(r, t)$ inside the shocked volume may be rewritten, without loss of generality, as

$$\begin{aligned} \rho(r, t) &= g(\xi, t)\rho_1(t), & u(r, t) &= w(\xi, t)u_1(t), \\ \epsilon(r, t) &= e(\xi, t)\epsilon_1(t), \end{aligned} \quad (25)$$

where $\rho_1(t)$, $u_1(t)$, and $\epsilon_1(t)$ are the mass density, particle speed, and specific internal energy just behind the shock front (where $\xi = 1$). It will be convenient to express the postshock mass density ρ_1 in terms of the preshock density ρ_0 via the dimensionless factor

$$\kappa(t) \equiv \rho_1/\rho_0. \quad (26)$$

Using (25) and (26), equation (24) can be rewritten as

$$\begin{aligned} \frac{W}{4\pi R^3 \rho_0} &= \kappa(t) \int_0^1 g(\xi, t) \left[\frac{1}{2} u_1^2(t) w^2(\xi, t) \right. \\ &\quad \left. + \epsilon_1(t) e(\xi, t) \right] \xi^2 d\xi \\ &= \frac{1}{2} u_1^2(t) \kappa(t) \int_0^1 g(\xi, t) \{ w^2(\xi, t) \\ &\quad + e(\xi, t) \} \xi^2 d\xi, \end{aligned} \quad (27)$$

where in the final expression we have used (3). Comparison of (27) with the ansatz (5) gives a useful expression for the dimensionless factor f , namely,

$$\frac{1}{f(t)} = \frac{1}{2} \kappa(t) \int_0^1 g(\xi, t) \{ w^2(\xi, t) + e(\xi, t) \} \xi^2 d\xi \quad (28)$$

Equation (28) is merely a reexpression of (24) and therefore is completely general. It shows that $f(t)$ depends on the density, velocity, and specific internal energy distributions

within the shocked volume at time t . We now investigate the value of $f(t)$ and its variation with time.

Strong Shock Interval

Consider for simplicity a point explosion during the interval when the shock wave is strong. As noted above, during this interval the ratio of the density ρ_1 behind the shock front to the density ρ_0 ahead of the shock front approaches a limiting value [see *Zel'dovich and Raizer*, 1967, p. 708]. Thus κ is independent of time and independent of W in this interval. Moreover, during the strong shock interval the shock wave produced by a point explosion is self-similar. Therefore the profiles g , w , and e are also independent of time and independent of W . Thus f is independent of time and independent of W in the strong shock interval.

For a medium that is adequately described by a Mie-Grüneisen equation of state with a constant Grüneisen coefficient, the value of f in the strong shock interval can be calculated by comparison with the solution for a self-similar shock wave produced by a strong point explosion [Sedov, 1946, 1959; Taylor, 1950a] as follows.

The Mie-Grüneisen equation of state assumes that the total pressure p is the sum of two parts: a thermal pressure p_T , which depends on the temperature and density, and a cold pressure p_c , which depends only on the density, that is,

$$p = p_T(\rho, T) + p_c(\rho) = \rho[\epsilon_T + p_c(\rho)], \quad (29)$$

where ϵ_T is the thermal component of the internal energy and Γ is the Grüneisen coefficient (see, for example, *Zel'dovich and Raizer* [1967, p. 697]). The thermal pressure p_T increases with the strength of the shock, whereas the cold pressure p_c is bounded, since ρ approaches a limiting value. Thus, in the strong shock interval the cold pressure term in (29) can be neglected [see *Zel'dovich and Raizer*, 1967, pp. 708–709]. If in addition the Grüneisen coefficient is constant, this equation of state has the form considered by Sedov and Taylor in their solutions.

The dependence of f on Γ in the strong shock interval can be calculated from (28) using Sedov's solution for the functions κ , $g(\xi)$, $w(\xi)$, and $e(\xi)$ (see, for example, *Landau and Lifshitz* [1987, pp. 403–406] for explicit expressions for κ , g , w , and e). The result is shown in Figure 1. When the shock wave is no longer strong, or when it never was strong, a value of f different from that given by Figure 1 may give a more accurate description of the shock wave evolution.

Actual nuclear tests are not point explosions but are generated by aspherical sources of finite size. In part to give the shock wave time to become more spherically symmetric, radius versus time measurements are usually made at scaled radii $\sim 2\text{--}5 \text{ m/kt}^{1/3}$ for tests with yields $\sim 150 \text{ kt}$ (at larger radii, the hydrodynamic approximation is no longer valid). At these scaled radii, the strong shock expression for f shown in Figure 1 is no longer accurate. As we now show, $f \approx 0.53$ appears to give a relatively accurate description of the evolution of shock waves in granite and wet tuff over the interval in radius where measurements are usually made.

Assessment of Particle Speed Predictions

The behavior of f when the shock wave is not strong can be investigated by comparing the predictions of the ansatz

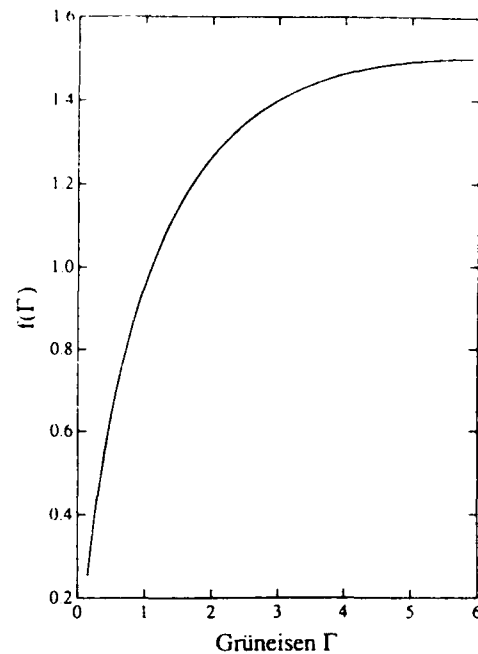


Fig. 1. Dimensionless energy partition factor f as a function of Grüneisen coefficient Γ for a strong point explosion in a medium obeying a Mie-Grüneisen equation of state.

(5) with shock wave data from actual and simulated nuclear explosions.

Lamb [1987] showed that the radius versus time curves predicted by (4) and (5) agree fairly well with radius versus time data from a numerical simulation of a nuclear explosion in wet tuff by the P-15 CORTEX Group at Los Alamos National Laboratory and with field data from the Piledriver and Cannikin nuclear tests, which were conducted in granite and basalt, respectively. A more detailed comparison of the radius versus time curves predicted by the model with data from numerical simulations is presented at the end of this section. The predictions of the model are compared with field data from underground nuclear tests in section 4.

A more direct test of the ansatz (5) can be made by comparing the postshock particle speed that it predicts with postshock particle speed data from nuclear tests and numerical simulations. *Perret and Bass* [1975] have summarized a large collection of particle speed data obtained from underground nuclear explosions. *Moss* [1988] has shown that these data agree fairly well with the scaling $u_1 \propto R^{-3/2}$ predicted by relation (5), for particle speeds $\geq 1 \text{ km/s}$. These data appear roughly consistent with this scaling even for particle speeds as low as $\sim 10^{-4} \text{ km/s}$. *Moss* [1988] also compared the ansatz (5) with postshock particle speeds from his numerical simulations of 125-kt nuclear explosions in quartz and wet tuff. He found that for particle speeds between 1 and 30 km/s, both the radius and the density dependence of his granite and wet tuff data are accurately described by relation (5) with $f = 0.53$.

To assess the ansatz (5) further, we compare it with postshock particle speed data obtained from simulations of 100-kt nuclear explosions in quartz and wet tuff. These simulations were performed by the Los Alamos CORTEX

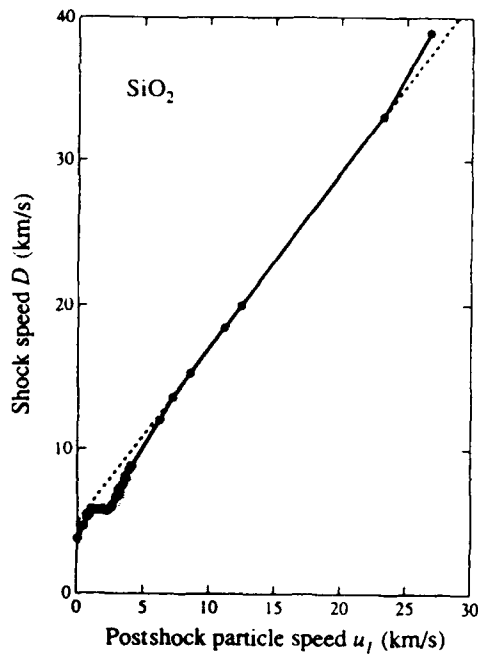


Fig. 2. Hugoniot data for SiO_2 (dots) and two of the representations used in calculations described in the text. The solid line shows the piecewise-linear approximation to the full Hugoniot, while the dashed line shows a simple linear approximation to the high-pressure portion of the Hugoniot.

group using the radiation hydrocode described by Cox *et al.* [1966]. In order to compare relation (5) with the simulations, we have had to reconstruct the postshock particle speeds using appropriate Hugoniot and the radius versus time curves obtained from the simulations. The radius versus time curves were kindly provided to us by D. Eilers (private communication, 1987).

The reconstruction process can distort the particle speed curve if the Hugoniot used in the reconstruction differs from the Hugoniot used in the simulation. Throughout this paper, when modeling shock waves in quartz we use the Hugoniot data compiled by King *et al.* [1989] from several sources [Chung and Simmons, 1969; Al'tshuler *et al.*, 1977; Wacklerle, 1962; McQueen *et al.*, 1977; Ragan, 1984]. These data are shown in Figure 2. An expanded view of the low- u_1 section of the data is shown in Figure 3. When comparing with the quartz simulations of the Los Alamos CORTEX group, we use a piecewise-linear representation of the data compiled by King *et al.*, using their interpolation at low postshock particle speeds (indicated by the dash-dotted line in Figure 3). In modeling shock waves in wet tuff, we use the piecewise-linear Hugoniot given by King *et al.* [1989], which is shown in Figure 4. The light solid curves in Figures 3 and 4 show where the postshock pressure calculated from the jump condition (2) is 15 GPa. For the reasons discussed in section 4, we adopt this pressure as marking the end of the hydrodynamic phase. We believe these Hugoniot are very close to the Hugoniot used in the numerical simulations, but we cannot rule out the possibility of some distortion.

Figure 5 shows that relation (5) with $f = 0.53$ provides an excellent description of the postshock particle speed data from the simulated explosion in quartz, for particle speeds

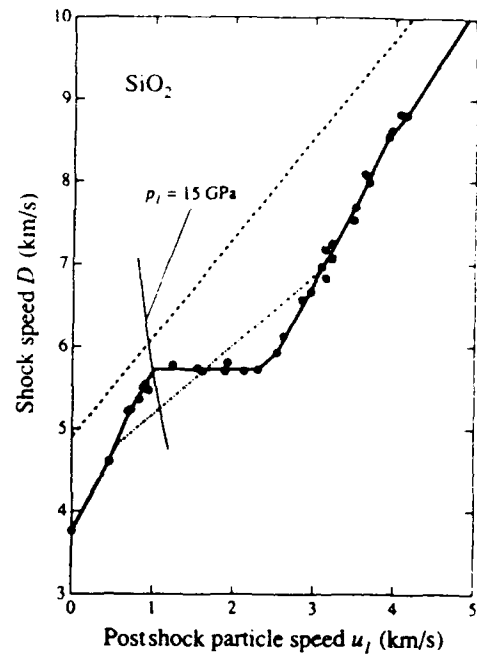


Fig. 3. Expanded view of SiO_2 Hugoniot data at low pressures (dots) and three representations used in calculations described in the text. The solid line shows the piecewise-linear approximation to the full Hugoniot while the dashed line shows a simple linear approximation to the high-pressure portion of the Hugoniot. The latter is clearly inaccurate at low particle speeds. The dash-dotted segment at low u_1 is similar to the approximate Hugoniot used by King *et al.* [1989] and replaces the corresponding section of the piecewise-linear Hugoniot when comparisons are made with the numerical simulations of D. Eilers *et al.* (private communication, 1987). Also shown is the isobar at 15 GPa, the pressure we have adopted as marking the end of the hydrodynamic phase.

from ~ 30 down to ~ 0.6 km/s. Figure 6 shows that relation (5) with $f = 0.53$ also provides an excellent description of the postshock particle speed data from the simulated explosion in wet tuff, for particle speeds from ~ 40 down to ~ 1 km/s.

On the basis of these comparisons, we conclude that relation (5) with $f = 0.53$ provides a good description of the relation between the yield, the mass density of the ambient medium, the radius of the shock front, and the postshock particle speed during the hydrodynamic phase of the explosion, including times when the shock wave is no longer strong.

Assessment of Radius Versus Time Predictions

In order to assess further the accuracy of the model, we compare the radius versus time curves that it predicts with the corresponding curves predicted by numerical simulations of underground nuclear explosions in quartz and wet tuff. We set f equal to 0.53 and use point source boundary conditions when solving equation (10) here and throughout this paper.

Quartz. We compared the present model with the simulation of a 100-kt nuclear explosion in quartz by the Los Alamos CORTEX Group, using both a linear description of the quartz Hugoniot and the more complete piecewise-linear

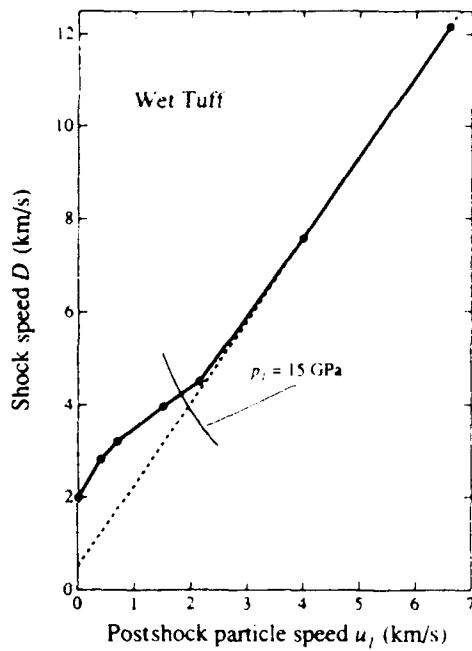


Fig. 4. Hugoniot data (dots) for wet tuff from King *et al.* [1989] and two representations used in calculations described in the text. The solid line shows our piecewise-linear approximation to the full Hugoniot, while the dashed line shows the simple linear approximation to the high-pressure portion of the Hugoniot. Also shown is the isobar at 15 GPa, the pressure we have adopted as marking the end of the hydrodynamic phase.

description discussed above. These Hugoniot are indicated by the dashed and dash-dotted lines, respectively, in Figures 2 and 3. The mass density used in the model was the same as that used in the simulation, namely, 2650 kg/m^3 .

Figure 7 compares the radii predicted by the model with the radii predicted by the simulation. The left-hand side of Figure 7 shows these radii as functions of time, whereas the right-hand side displays the relative difference

$$\delta \equiv \left(\frac{R_{\text{sim}}(t) - R_{\text{model}}(t)}{R_{\text{sim}}(t)} \right) \quad (30)$$

between these radii. The dashed curve is the value of δ that results from using the linear description of the Hugoniot in the analytical model, whereas the dash-dotted curve is the result given by using the piecewise-linear Hugoniot. When the linear approximation to the Hugoniot is used, the absolute value of δ is less than 5% before 0.7 ms but rises to ~12% by ~5 ms. As expected from the behavior of the actual Hugoniot, the radii predicted by the linear approximation are systematically too large at late times. When the more accurate piecewise-linear Hugoniot is used, δ is never more than 1.8%.

Wet tuff. We compared the present model with the simulation of a 100-kt nuclear explosion in saturated wet tuff by the Los Alamos CORTEX Group, again using both a linear description of the wet tuff Hugoniot and the more complete piecewise-linear description of King *et al.* [1989]. These Hugoniot are indicated respectively by the dashed and solid lines in Figure 4. The mass density used in the

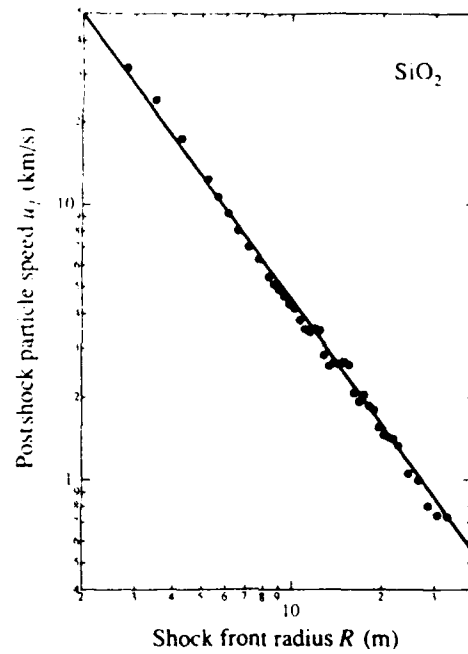


Fig. 5. Peak particle speed u_1 versus shock front radius R for a 100-kt explosion in SiO_2 (dots), from a numerical simulation by D. Eilers *et al.* (private communication, 1987), compared with the peak particle speed predicted by the analytical model (solid line). The analytical model describes the data quite well over two decades of particle speed, showing that the energy partition ansatz (equation (5)) is relatively accurate.

model was the same as that used in the simulation, namely, 1950 kg/m^3 .

Figure 8 compares the radii predicted by the analytical model with the radii predicted by the simulation. When the linear approximation to the Hugoniot is used, the absolute value of δ is always less than 9%. Again, as expected from the behavior of the actual Hugoniot, the radii predicted by the linear approximation are systematically too small at late times. When the more accurate piecewise-linear Hugoniot is used, the relative difference is never more than 6% and is less than 2% after 0.6 ms.

Discussion. These comparisons of the radius versus time curves predicted by the model with the radius versus time curves predicted by numerical simulations confirm the earlier assessment, which was based on comparison of peak particle velocities, that the model with f set equal to 0.53 provides an excellent description of spherically symmetric shock waves from underground nuclear explosions in granite and wet tuff, during much of the hydrodynamic phase. Therefore we shall adopt this value for f when comparing the model with field data from underground nuclear explosions.

4. COMPARISONS WITH FIELD DATA

In this section we use radius versus time data from four underground nuclear tests conducted by the United States to assess the usefulness of the analytical model. The four data sets we consider are from the nuclear tests code-named Piledriver, Cannikin, and Chiberta, and from a test that we call NTS-X, since its official name remains classified. The radius versus time data from the first three tests were

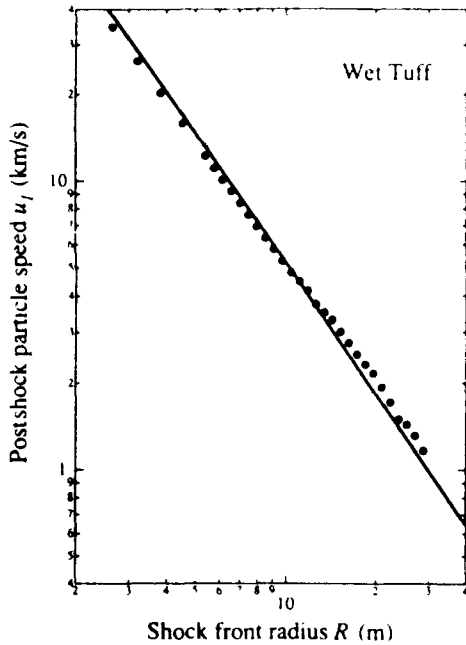


Fig. 6. Peak particle speed u_1 versus shock front radius R for a 100-kt explosion in wet tuff (dots), from a numerical simulation by D. Eilers et al. (private communication, 1987), compared with the peak particle speed predicted by the analytical model (solid line). Again, the analytical model describes the data quite well over two decades of particle speed, showing that the energy partition ansatz (equation (5)) is relatively accurate

obtained using the SLIFER technique [Heusinkveld and Holzer, 1964]. These data were kindly provided to us by Heusinkveld [1986; also private communication, 1987]. The radius versus time data from NTS-X were taken from

Heusinkveld [1979], the measurement technique used to obtain these data was not reported. To our knowledge, no radius versus time measurements made using the more recently developed CORTEX technique [Vatnow et al., 1980] are publicly available.

Any attempt to compare models or simulations of spherically symmetric explosions in uniform media with data from underground nuclear tests must confront at the outset the fact that the shock wave produced by such a test evolves from an aspherical source of finite size into a medium that is at least somewhat inhomogeneous [see Lamb, 1988; Lamb et al., 1991]. In comparing the predictions of the model of section 2 with data from nuclear tests, we adopt the particular solution that corresponds to a point explosion. For this solution, cube root scaling is exact. We also assume cube root scaling is valid when comparing the results of the numerical simulations with data from nuclear tests. Since these simulations follow the shock wave produced by an initial source of finite size, cube root scaling is at best only approximately valid for these simulations.

In using cube root scaling, we are tacitly assuming that the finite size of the source, the asphericity of the explosion, and any inhomogeneities in the ambient medium have a negligible effect, both in the simulations and in the actual test, by the time the shock front has expanded to the radii at which the comparison is made. Although shock waves produced by underground explosions in uniform media do tend to become more spherical with time, the properties of the source can sometimes have a significant effect during the hydrodynamic phase [Moran and Goldwire, 1990; R. A. Fiedler et al., manuscript in preparation, 1991]. Unfortunately, we are unable to assess directly the validity of our assumptions, because we lack detailed knowledge of the sources used in the numerical simulations, the conditions under which the nuclear tests were conducted, and the way in which the field data were collected.

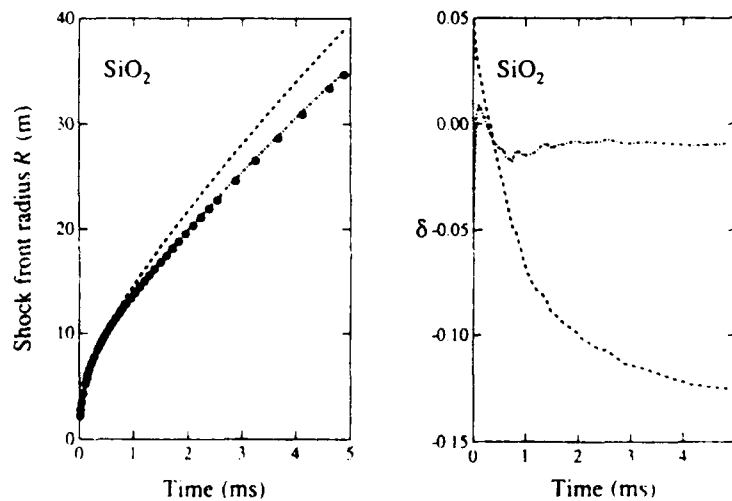


Fig. 7. Comparison of shock front radius versus time curves predicted by the analytical model with radius versus time data from the numerical simulation of a 100-kt explosion in SiO_2 by D. Eilers et al. (private communication, 1987). (Left) Predicted radii as functions of time. (Right) Relative difference between radii predicted from the SiO_2 simulation and from the analytical model. The dots in the left panel show the results of the simulation, the dash-dotted lines show the results when the piecewise-linear representation of the full Hugoniot (see Figures 2 and 3) is used in the analytical model, the dashed lines show the results when the simple linear approximation to the high-pressure portion of the Hugoniot (again see Figures 2 and 3) is used.

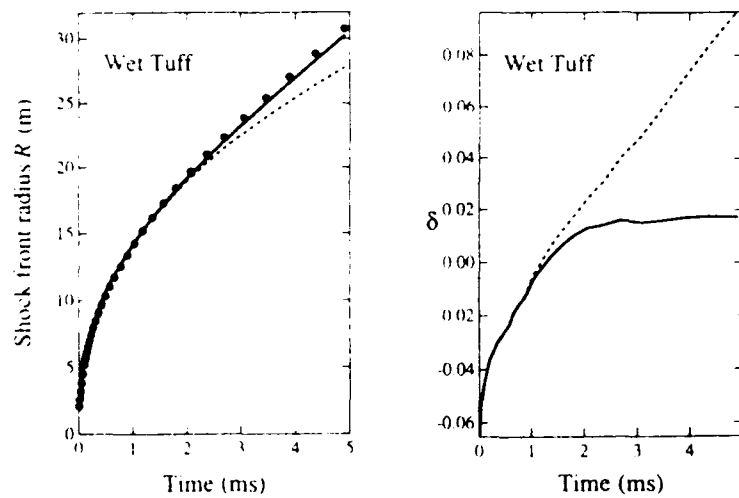


Fig. 8. Comparison of shock front radius versus time curves predicted by the analytical model with radius versus time data from the numerical simulation of a 100-kt explosion in wet tuff by D. Eilers et al. (private communication, 1987). (Left) Predicted radii as functions of time. (Right) Relative difference between radii predicted from the SiO_2 simulation and from the analytical model. The dots in the left panel show the results from the simulation; the solid lines show the results when the piecewise-linear representation of the full Hugoniot (see Figure 4) is used in the analytical model; the dashed lines show the results when the simple linear approximation to the high-pressure portion of the Hugoniot (again see Figure 4) is used.

We also lack detailed knowledge of how the official yields were determined for these four events. In using the official yields to assess hydrodynamic methods, we are implicitly assuming that they are accurate and independent of hydrodynamic methods. However, the procedure by which official yields are determined is known to be complex and is not publicly available. It is possible in some cases that the official yield is actually less accurate than the hydrodynamic yield estimate. Moreover, the official yield determination procedure may make use of information derived from hydrodynamic methods, as well as radiochemical and other methods. If so, the official yield obviously is not independent of the hydrodynamic yield. Furthermore, in some cases the material properties used to obtain hydrodynamic yield estimates may have been adjusted to give better agreement with estimates obtained using other methods. The comparisons in this section show that despite the complexity of underground nuclear explosions, both the analytical model and the numerical simulations accurately describe the shock waves produced by the nuclear tests considered here, when the official yields are used.

A solution of the analytical model is determined by specifying the Hugoniot, the value of the parameter f , and the yield. The Hugoniot can in principle be determined from laboratory measurements made on samples taken from the emplacement and satellite holes. Unfortunately, if such measurements were made for the four events analyzed here, they are not publicly available. Therefore we used generic Hugoniot data characteristic of the ambient medium of each explosion. For the reasons discussed in section 3, we used $f = 0.53$ throughout the present analysis.

We first assess the accuracy of the analytical model in predicting the radius of the shock front by comparing the radius versus time curves it gives with radius versus time data from the four nuclear tests cited above. We then investigate the usefulness of the model for yield estimation

by fitting it to radius versus time data from these tests, treating the yield as the only adjustable parameter.

Radius Versus Time Curves

In comparing the radius versus time predictions with field data, we generally used either the subset of the available data that fell within the hydrodynamic interval defined below, or, where stated, certain larger data sets. However, for NTS-X we followed the recommendation of Heusinkveld [1979] and omitted the first nine data points from our analysis. For Chiberta the first seven points were inconsistent with each other and with the remaining points, and hence these seven points were also omitted from our analysis. We now discuss the analysis of each event in turn.

Piledriver. The Piledriver event was an explosion conducted in granite at the Nevada Test Site on June 2, 1966, and had an announced yield of 62 kt [U.S. Department of Energy, 1987]. In modeling this explosion we considered the simple linear and piecewise-linear approximations to the quartz Hugoniot shown by the dashed and solid lines in Figures 2 and 3, respectively. We assumed that the granite surrounding the nuclear device had a density equal to the standard density of quartz, namely, 2650 kg/m^3 , and that the yield of the explosion was 62 kt. We then integrated the differential equation (10) as described in section 2.

Figure 9 compares the predictions of the analytical model with the data from Piledriver. The left-hand side of Figure 9 shows the radius as a function of time, whereas the right-hand side displays the relative difference

$$\delta = \left(\frac{R_{\text{data}}(t) - R_{\text{model}}(t)}{R_{\text{data}}(t)} \right), \quad (31)$$

between the measured and predicted radii to allow a more detailed assessment of the accuracy of the model. The

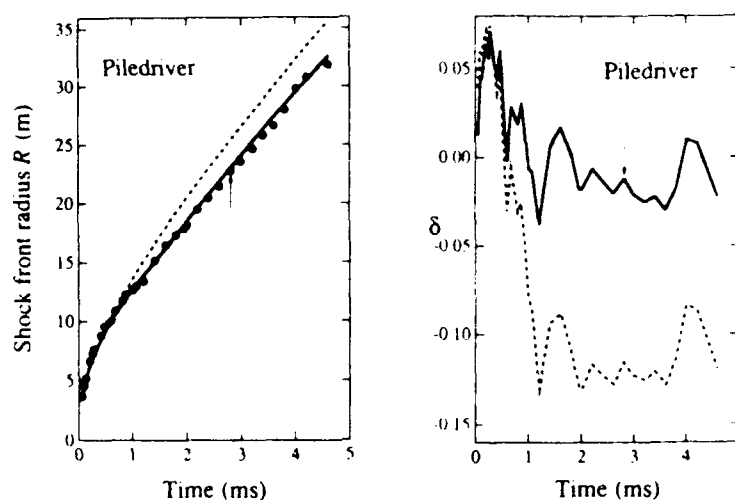


Fig. 9. Comparison of shock front radius versus time curves predicted by the analytical model with radius versus time data from Piledriver, a 62-kt explosion in granite. The arrow in each panel marks the radius at which the peak pressure drops to 15 GPa, which we have adopted as the end of the hydrodynamic phase. (Left) Predicted and measured radii as functions of time. (Right) Relative difference between measured and predicted radii. The dots in the left panel show the field data, the solid lines show the results when the piecewise-linear representation of the full Hugoniot (see Figures 2 and 3) is used in the analytical model, the dashed lines show the results when the simple linear approximation to the high-pressure portion of the Hugoniot (again see Figures 2 and 3) is used. When the piecewise-linear Hugoniot is used, the radii predicted by the analytical model differ from the measured radii by no more than 7% over the whole range of the data.

dashed curve is the result given by the simple linear approximation to the Hugoniot, whereas the solid curve is the result given by the piecewise-linear description of the full Hugoniot.

As expected, the radii given by the simple linear and the piecewise-linear Hugoniot are very similar at early times but deviate significantly from one another at later times. When the full Hugoniot is used, the relative difference δ between the measured and predicted radii is never more than 7% and is less than 4% after 0.6 ms. When the simple linear Hugoniot is used for all particle speeds, the absolute value of δ is less than 7% before 0.6 ms but rises to $\sim 11\%$ after 1.2 ms. The radii predicted by the simple linear Hugoniot are systematically too large after 0.6 ms because this approximation gives shock speeds that are systematically too high when the particle speed is low (see Figure 3). For reference, the peak pressure drops to 15 GPa at about 2.8 ms. As discussed below, we adopted this pressure as marking the end of the hydrodynamic phase.

Cannikin. The Cannikin event was an explosion conducted in basalt at Amchitka Island, Alaska, on November 6, 1971. The official yield of this event remains classified; the U.S. Department of Energy [1987] has said only that it was less than 5 Mt. The data from Cannikin that were given to us had been scaled by dividing both the radius and the time measurements by the cube root of the official yield in kilotons. If cube root scaling were exact, this would make the radius versus time curve appear identical to the curve that would result from detonation of a 1-kt device in the same medium. As noted above, cube root scaling may not always be accurate for underground nuclear explosions. However, since the analytical model we are exploring exhibits exact cube root scaling, comparisons of this model with scaled and unscaled data will give the same result. We

therefore treated the data from Cannikin as though it had been produced by a 1-kt explosion.

To construct a Hugoniot for Cannikin, we used the data on Vacaville basalt obtained by Jones *et al.* [1968] and Ahrens and Gregson [1964]. These data and the piecewise-linear and simple linear Hugoniot that we constructed from them are shown in Figure 10. We assumed the rock surrounding the explosion had a density of 2860 kg/m^3 , equal to the density of the samples measured by Jones *et al.*

Figure 11 compares the radii predicted by the analytical model with the radii measured during Cannikin. Again, the left-hand side shows the radius as a function of time, whereas the right-hand side displays the relative difference between the predicted and measured radii. When the piecewise-linear approximation to the full Hugoniot is used, the magnitude of the relative difference between the radii is always less than 3%. When the simple linear Hugoniot is used for all particle speeds, the magnitude of δ is also less than 3% for the entire data set. As in Piledriver, the radii predicted by the simple linear Hugoniot are systematically too large after 0.4 ms because this approximation gives shock speeds that are systematically too high when the particle speed is low. For reference, the peak pressure falls to 15 GPa at about 0.7 scaled ms. Thus all the radius versus time data from Cannikin lie within the hydrodynamic region.

Chiberta. The Chiberta explosion was conducted in wet tuff at the Nevada Test Site on December 20, 1975. The official yield of this test remains classified; the U.S. Department of Energy [1987] has said only that it was between 20 and 200 kt. Using seismic data, Dahlman and Israelson [1977, p. 398] estimated that the yield of Chiberta was 160 kt. Like the data from Cannikin, the radius versus time data from Chiberta available to us were scaled by the cube root of the official yield. For the reason explained above in connec-

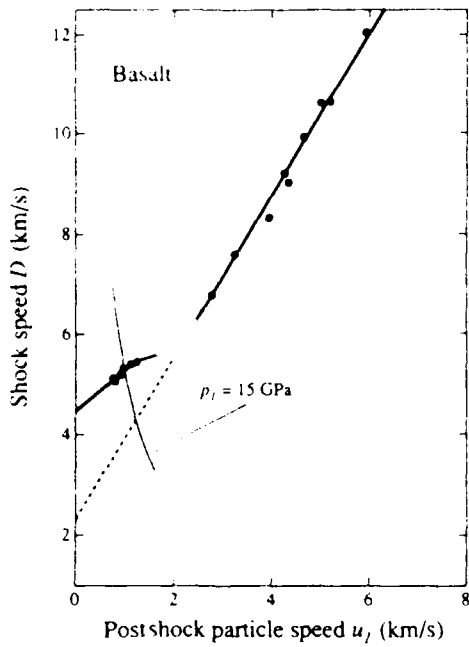


Fig. 10. Hugoniot data (dots) for basalt from Jones *et al.* [1968] and Ahrens and Gregson [1964] and two representations used in calculations described in the text. The solid line shows the piecewise-linear representation of the full Hugoniot, while the dashed line shows the simple linear approximation to the high-pressure portion of the Hugoniot. Also shown is the isobar at 15 GPa, the pressure we have adopted as marking the end of the hydrodynamic phase.

tion with Cannikin, we treated the data from Chiberta as though it had been produced by a 1-kt explosion.

In modeling Chiberta, we used the linear and piecewise-linear approximations to the wet tuff Hugoniot shown by the

dashed and solid lines, respectively, in Figure 4. We assumed that the rock surrounding the device emplacement had a density of 1950 kg m^{-3} .

Figure 12 compares the predictions of the analytical model with the data from Chiberta. Again, the dashed curve is the result given by the simple linear Hugoniot, whereas the solid curve is the result given by the piecewise-linear approximation to the full Hugoniot. As before, the radii given by the two approximations are very similar at early times, but deviate significantly from one another at late times. When the piecewise-linear Hugoniot is used, the magnitude of the relative difference δ between the measured and predicted radii is never more than $\sim 4\%$ and is $\sim 1\%$ between 0.35 and 1.6 ms. When the simple linear Hugoniot is used for all particle speeds, the absolute value of δ is less than 3% before 0.6 ms but increases after this time, reaching 14% at 1.6 ms, near the end of the data set. The radii predicted by the simple linear Hugoniot are systematically too small after 0.4 ms because this approximation gives shock speeds that are systematically too low for low particle speeds (see Figure 4). For this event, the peak pressure falls below 15 GPa at about 0.5 scaled ms. Thus a large fraction of the radius measurements were made outside the hydrodynamic region.

NTS-X. The event we call NTS-X was an explosion conducted at the Nevada Test Site. Radius versus time data from this explosion were reported by Heusinkveld [1979], who stated that the official yield was 54.2 kt. Heusinkveld surmised that the ambient medium was saturated wet tuff, the ambient medium of most tests conducted at the Nevada Test Site.

In modeling NTS-X we assumed that the explosion did occur in wet tuff. We followed the same procedure used in modeling Chiberta, except that we assumed the yield was 54.2 kt. Figure 13 compares the predictions of the analytical model with the data from NTS-X. As before, the radii given

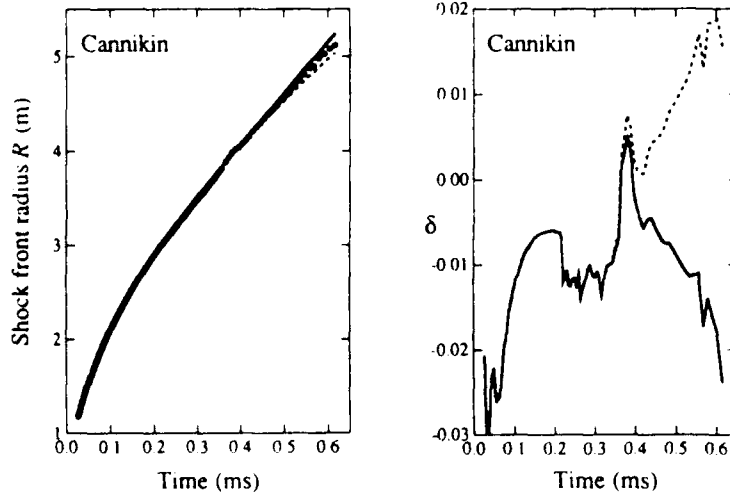


Fig. 11. Comparison of shock front radius versus time curves predicted by the analytical model with radius versus time data from Cannikin, an explosion in basalt with a yield of several megatons. The measurements have been scaled to show an apparent yield of 1 kt (see text). (Left) Predicted and measured radii as functions of time. (Right) Relative difference between measured and predicted radii. The dots in the left panel show the field data; the solid lines show the results when the piecewise-linear representation of the full Hugoniot (see Figure 10) is used in the analytical model, the dashed lines show the results when the simple linear approximation to the high-pressure portion of the Hugoniot (again see Figure 10) is used. The analytical model with the piecewise-linear Hugoniot predicts shock front radii that are within 3% of the measured radii over the full range of the data.

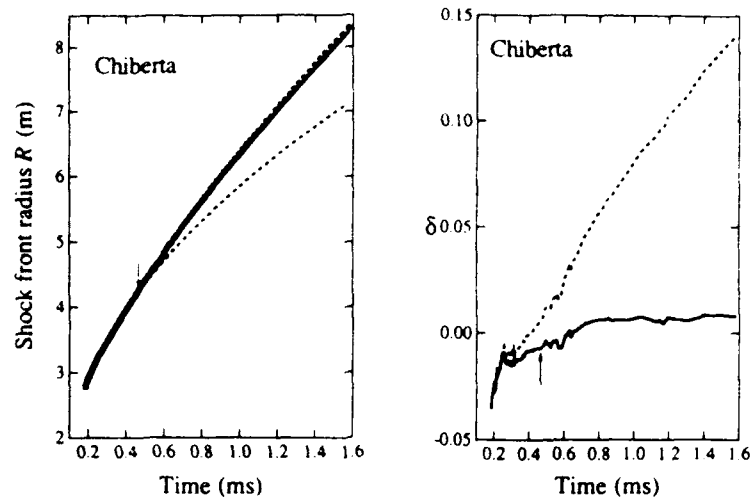


Fig. 12. Comparison of shock front radius versus time curves predicted by the analytical model with radius versus time data from Chiberta, an explosion in wet tuff with a yield in the range 20–200 kt. The measurements have been scaled to show an apparent yield of 1 kt (see text). The arrow in each panel marks the radius at which the peak pressure drops to 15 GPa, which we have adopted as the end of the hydrodynamic phase. (Left) Predicted and measured radii as functions of time. (Right) Relative difference between measured and predicted radii. The dots in the left panel show the field data; the solid lines show the results when the piecewise-linear representation of the full Hugoniot (see Figure 4) is used in the analytical model; the dashed lines show the results when the simple linear approximation to the high-pressure portion of the Hugoniot (again see Figure 4) is used. The analytical model with the piecewise-linear Hugoniot predicts shock front radii that are within 3% of the measured radii over the full range of the data.

by the simple linear Hugoniot and by the piecewise-linear approximation to the full Hugoniot are very similar at early times but deviate significantly from one another at later times. The relative difference δ is never more than 5% when the piecewise-linear Hugoniot is used. When the simple

linear Hugoniot is used for all particle speeds, δ is less than 5% before 2 ms but increases after this time, reaching 17% at 6 ms, near the end of the data set. As in Chiberta, the radii predicted by the simple linear Hugoniot are systematically too small after 0.1 ms because this approximation gives

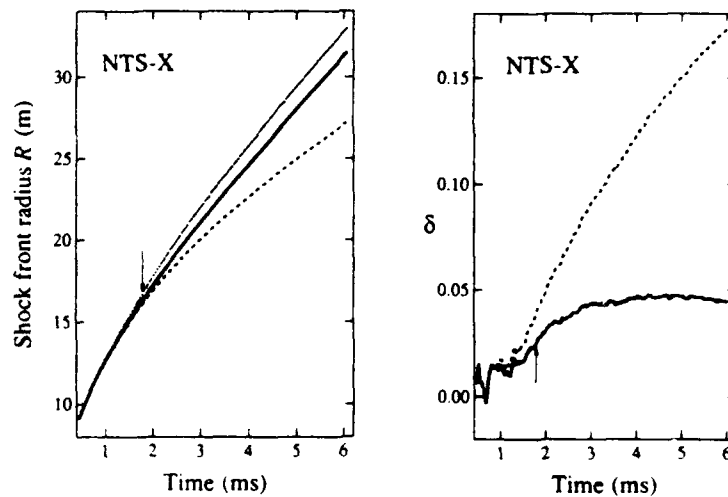


Fig. 13. Comparison of shock front radius versus time curves predicted by the analytical model with radius versus time data from NTS-X, assumed to be an explosion in wet tuff with a yield of 54.2 kt. The measurements have been scaled to show an apparent yield of 1 kt (see text). The arrow in each panel marks the radius at which the peak pressure drops to 15 GPa, which we have adopted as the end of the hydrodynamic phase. (Left) Predicted and measured radii as functions of time. (Right) Relative difference between measured and predicted radii. The dots in the left panel show the field data; the solid lines show the results when the piecewise-linear representation of the full Hugoniot (see Figure 4) is used in the analytical model; the dashed lines show the results when the simple linear approximation to the high-pressure portion of the Hugoniot (again see Figure 4) is used. The analytical model with the piecewise-linear Hugoniot predicts shock front radii that are within 5% of the measured radii over the full range of the data.

TABLE 1. Yield Estimates for Piledriver

Model	Hugoniot	W_{est} , kt	N	ΔR_{rms} , m	$\Delta R_{rms}/W_{est}^{1/3}$
Analytical model	linear SiO_2	37.6	22	0.785	0.234
Analytical model	full SiO_2	62.5	28	0.312	0.079
Numerical simulation	King <i>et al.</i> [1989] SiO_2	63.4	24	0.349	0.088

Yield estimates obtained by fitting the model or simulation to measurements made during the hydrodynamic phase of the explosion. W_{est} is the estimated yield, N is the number of data points used in the yield estimate, and ΔR_{rms} is the root-mean-square difference between the measured and predicted shock front radii. The quantity $\Delta R_{rms}/W_{est}^{1/3}$ can be used to compare the quality of the fits for different explosions. The official yield of Piledriver was 62 kt [U.S. Department of Energy, 1987].

shock speeds that are systematically too low for low particle speeds (see Figure 4). For reference, the peak pressure falls below 15 GPa at about 2.0 ms. As in Chiberta, a large fraction of the radius measurements were made outside the hydrodynamic region.

Yield Estimation

Having shown that the analytical model of section 2 provides a relatively accurate description of the evolution of the shock waves produced by underground nuclear explosions for several of the geologic media found at U.S. test sites, we now consider its usefulness in yield estimation. We do this by adjusting the assumed yield to give the best fit of the model to radius versus time data from the four U.S. nuclear tests discussed previously.

In order to determine the best fit of the analytical model to a given set of radius versus time data, we need a measure of the goodness of the fit. This should be a function of the difference between the predicted and measured shock front radii, weighted in an appropriate way. Unfortunately, the radius data that we were furnished came without any information on the random and systematic errors. In fact, no error information is available for any of the currently declassified radius versus time data, a large fraction of which is analyzed here.

The absence of error information made it impossible to develop a proper measure of the goodness of the fits and to determine the uncertainties of the yield estimates. We therefore adopted a very simple fitting procedure that allowed us to determine a best fit yield and to compare fits to field data made with the analytical model and with the numerical simulations of the Los Alamos CORRTEX group. We assess the accuracy of the yield estimates made with the analytical model by comparing them with the estimates obtained by fitting numerical simulations to the same data, an approach called simulated explosion scaling, and by comparing them with the official yields. The precise algorithm used in determining official yields is unknown but presumably makes use

of radiochemical and seismic as well as shock wave measurements, when these are available [see Lamb, 1988].

Procedure. For simplicity, we assumed that all yields are equally likely a priori and that the measurement errors follow a Gaussian distribution. Then the maximum of the likelihood function can be found by minimizing the properly weighted sum of the mean square differences between the predicted and measured shock front radii (see, for example, Mathews and Walker [1970, section 14-7]). Since we had no information on the errors of the individual measurements, we assumed that the measurements are unbiased and assigned them unit weight if they met our selection criteria (see below) or zero weight if they did not. The maximum of the likelihood function is then given by the minimum of the measure

$$\frac{1}{N} \sum_i [R(t_i) - R_{\text{model}}(t_i)]^2, \quad (32)$$

where the sum runs over the measurements used in the particular yield estimate.

The analytical model and the numerical simulations discussed in sections 2 and 3 are valid only during the hydrodynamic phase, when the strength of the ambient medium can be neglected. However, the influence of the strength of the medium increases gradually as the shock wave weakens, so there is no well-defined peak pressure at which the hydrodynamic phase ends. Wackerle [1962] found that in quartz, strength effects can be ignored above the critical stress, which is about 4 GPa. Studies by Grady *et al.* [1974] of quartz at pressures above 15 GPa demonstrated that strength effects are negligible in this pressure regime. Basalt becomes plastic at a critical stress of about 4 GPa [Ahrens and Gregson, 1964]. The critical stress for saturated wet tuff is estimated to be ~ 1 GPa [Holzer, 1965]. In the present work we have adopted the convention that the hydrodynamic phase ends in all these materials when the peak pressure falls below 15 GPa. This is a conservative criterion.

TABLE 2. Yield Estimates for Cannikin

Model	Hugoniot	W_{est} , kt	N	ΔR_{rms} , m	$\Delta R_{rms}/W_{est}^{1/3}$
Analytical model	linear basalt	0.980	154	0.030	0.031
Analytical model	full basalt	0.925	158	0.020	0.021
Numerical simulation	King <i>et al.</i> [1989] SiO_2	0.990	158	0.037	0.037

Yield estimates obtained by fitting the model or simulation to measurements made during the hydrodynamic phase of the explosion. W_{est} , N , ΔR_{rms} , and $\Delta R_{rms}/W_{est}^{1/3}$ have the same meanings as in Table 1. The data for Cannikin have been scaled so that the apparent yield is 1 kt (see text).

TABLE 3. Yield Estimates for NTS-X

Model	Hugoniot	W_{est} , kt	N	ΔR_{rms} , m	$\Delta R_{rms}/W_{est}^{1/3}$
Analytical model	linear wet tuff	59.2	30	0.061	0.022
Analytical model	full wet tuff	58.5	34	0.057	0.022
Numerical simulation	full wet tuff	57.9	34	0.084	0.022

Yield estimates obtained by fitting the model or simulation to measurements made during the hydrodynamic phase of the explosion. W_{est} , N , ΔR_{rms} and $\Delta R_{rms}/W_{est}^{1/3}$ have the same meanings as in Table 1. The yield of NTS-X is given as 54.2 kt by *Heusinkveld* (1979).

in the sense that the hydrodynamic approximation most likely extends to lower peak pressures.

When fitting the analytical model or the simulated explosion in wet tuff (D. Eilens et al., private communication, 1987) to field data, we determined the point at which the peak pressure fell below 15 GPa using the analytical model with the piecewise-linear representations of the full Hugoniot of section 3. When fitting the simulated explosion in SiO₂ (D. Eilens et al., private communication, 1987) to field data, we determined the point at which the peak pressure fell below 15 GPa using the analytical model with the approximate Hugoniot adopted by *King et al.* [1989] to this model. Plots of the peak pressure predicted by the analytical model are given in the appendix.

We are interested in the accuracy of the analytical model when it is used with simple linear Hugoniot, since we use this approximation in a companion study of how the evolution of the shock wave is influenced by the properties of the ambient medium and how these properties affect the characteristic radius at which the shock wave becomes a low-pressure plastic wave (F. K. Lamb et al., manuscript in preparation, 1991); for a preliminary account, see *Lamb et al.* [1989] and *Callen et al.* [1990a]. We therefore compare the yields obtained by fitting the analytical model to the field data using simple linear approximations to the Hugoniot with the yields obtained using the full, piecewise-linear Hugoniot.

Although the analytical model and the numerical simulations we consider are valid only during the hydrodynamic phase, in some cases they may describe the evolution of the shock wave adequately even beyond the region where the peak stress is large compared with the critical stress of the medium. Knowing how rapidly these models become inaccurate when used outside the hydrodynamic region is important for assessing whether they can be used for yield estimation when the shock wave within the hydrodynamic region is disturbed, either because the yield is low, causing the hydrodynamic region to be close to the device canister, or because the geometry of the test is complex [see *Lamb*, 1988]. In order to investigate the accuracy of the analytical model when fit to data taken at relatively large radii, we first

estimated yields using only data taken during the hydrodynamic phase as defined above and then using two successively larger sets of data, defined by successively lower cutoff pressures. The radius at which the peak pressure predicted by the analytical model falls below a given pressure depends on the assumed yield. Thus the number of data points used in evaluating expression (32) varies with the assumed yield.

Results. The results obtained by fitting the analytical model and numerical simulations to field data from the hydrodynamic interval are summarized in Tables 1-4. The first column in each table shows which model was used: the analytical model or one of the numerical simulations discussed in section 3. The second column shows which Hugoniot was used: the simple linear approximation to the generic Hugoniot, the piecewise-linear representation of the full generic Hugoniot, or the approximate SiO₂ Hugoniot used by *King et al.* [1989]. The next four columns list results obtained by fitting the models with the specified Hugoniot to field data from the hydrodynamic phase. Shown are the yield estimate W_{est} , the number N of data points used in the estimate, the root-mean-square difference in radius

$$\Delta R_{rms} = \left[\frac{1}{N} \sum_i (R(t_i) - R_{model}(t_i))^2 \right]^{1/2} \quad (33)$$

and the quantity $\Delta R_{rms}/W_{est}^{1/3}$ for each fit. The last quantity can be used to compare the quality of the fits achieved for the four events. For Piledriver and NTS-X, the yield estimates are given to the nearest 0.1 kt, whereas for Cannikin and Chiberta, the estimates are given to the nearest 0.005 kt. Table 5 compares the results obtained by fitting the analytical model to data from the hydrodynamic interval with the results obtained by fitting to data sets that include data from beyond the hydrodynamic interval.

Not surprisingly, the best agreement between the official yield and the yield estimated by fitting the analytical model to the radius versus time data is achieved when a piecewise-linear representation of the full Hugoniot is used and the model is fit only to data from the hydrodynamic phase. In this case, the difference between the official yield and the

TABLE 4. Yield Estimates for Chiberta

Model	Hugoniot	W_{est} , kt	N	ΔR_{rms} , m	$\Delta R_{rms}/W_{est}^{1/3}$
Analytical model	linear wet tuff	0.950	42	0.028	0.028
Analytical model	full wet tuff	0.930	47	0.021	0.021
Numerical simulation	full wet tuff	0.910	45	0.013	0.014

Yield estimates obtained by fitting the model or simulation to measurements made during the hydrodynamic phase of the explosion. W_{est} , N , ΔR_{rms} and $\Delta R_{rms}/W_{est}^{1/3}$ have the same meanings as in Table 1. The data for Chiberta were scaled so that the apparent yield is 1 kt (see text).

TABLE 5. Effect on Yield Estimates of Including Data From Outside the Hydrodynamic Phase

Cutoff (GPa)	NTS-X				Chiberta			
	W_{off} (kt)	N	ΔR_{lim} (m)	$\Delta R_{\text{lim}}/W_{\text{off}}$	W_{off} (kt)	N	ΔR_{lim} (m)	$\Delta R_{\text{lim}}/W_{\text{off}}$
15	58.5	34	0.087	0.022	0.930	47	0.021	0.021
7.5	66.4	83	0.271	0.067	0.970	81	0.037	0.037
4.6	71.5	141	0.320	0.077	0.995	104	0.044	0.044

The results shown are for fits of the analytical model to data out to the radius at which the peak pressure predicted by the analytical model falls below the indicated cutoff value. According to the convention used in this work, the hydrodynamic phase ends when the peak pressure falls below 15 GPa. Thus the fits with cutoff pressures below this value include data from beyond the hydrodynamic phase. W_{off} , N, ΔR_{lim} , and $\Delta R_{\text{lim}}/W_{\text{off}}$ have the same meanings as in Table 1. The yield of NTS-X is given as 54.2 kt by Heinskyvel [1979]. The data from Chiberta have been scaled so that the apparent yield is 1 kt (see text).

yield obtained by fitting the analytical model is 17% for Piledriver, 8% for Cannikin, and 7% for Chiberta. The difference between the yield quoted by Heinskyvel [1979] for NTS-X and the yield obtained by fitting the analytical model is 8%. For comparison, the differences between the official or quoted yields of these events and the yields obtained by fitting the numerical simulations to data from the hydrodynamic phase are 2%, 1%, 7%, and 9%, respectively. Thus the yield estimates obtained by fitting the analytical model with piecewise-linear representations of the Hugoniot to data from the hydrodynamic phases are nearly as accurate as the yield estimates obtained by fitting the numerical simulations to these same data.

The agreement between the official yield and the yield estimated by fitting the analytical model with simple linear Hugoniot to data from the hydrodynamic phases is not as close but is still remarkably good. For the events in wet tuff, the estimated yields differ from the official or quoted yields by only 9% for NTS-X and 5% for Chiberta. This is not surprising, since the simple linear approximation to the Hugoniot is nearly identical to the full, piecewise-linear representation of the Hugoniot for the particle speeds encountered during the hydrodynamic phase in this medium (see Figure 4). For the same reason, the yield of the Cannikin event obtained by using the analytical model with the simple linear approximation to the basalt Hugoniot differs from the official yield by only 2%. Although the relative difference $\Delta W/W$ obtained using this approximation to the Hugoniot is smaller than the relative difference obtained using the piecewise-linear representation of the full Hugoniot, the quality of the fit is somewhat poorer, as shown by the size of ΔR_{lim} (see Table 2). However, for the Piledriver event the difference between the official yield and the yield obtained using the simple linear Hugoniot is ~40%, much greater than the difference when the piecewise-linear Hugoniot is used. This is not surprising, since the simple linear approximation to the SiO_2 Hugoniot is inaccurate for the particle speeds encountered during most of the hydrodynamic phase (see Figures 2 and 3).

Consider now the effect on the yield estimates when data from outside the hydrodynamic phase are included. A meaningful study of this effect is only possible for Chiberta and NTS-X, since all or almost all of the available data from Cannikin and Piledriver lie within the hydrodynamic region. As shown in Table 5, the estimated yield of NTS-X obtained using the analytical model increases from 58.5 to 66.4 and 71.5 kt when data out to peak pressures of 7.5 and 4.6 GPa are included. The differences between the latter yields and the quoted yield of 54.2 kt are 23% and 32%, respectively.

For Chiberta, on the other hand, including data out to peak pressures of 7.5 and 4.6 GPa increases the estimated yield only slightly, from 0.930 to 0.970 and 0.995 kt. The differences between the latter yields and the official yield of 1.00 kt are 3% and 0.5%, respectively.

The large difference in the sensitivity of the Chiberta and NTS-X yield estimates to inclusion of data from outside the hydrodynamic interval is somewhat surprising, since both events supposedly took place in wet tuff and the data from both events extend to approximately the same scaled time ($\sim 0.6 \text{ ms kt}^{1/3}$). However, as explained above, we do not know either the medium or the yield of NTS-X for certain. Furthermore, we have no knowledge of any special conditions that may have affected the explosion or the shock wave radius measurements. There does appear to be a systematic difference between the fits of the analytical model to these two events at late times. Without more information, we are unable to determine whether this difference is due to some difference in the events themselves, to systematic error in one of the sets of radius measurements, to systematic error in the Hugoniot we have used, or to inaccuracy of the analytical model when it is used so far outside the hydrodynamic region.

5. SUMMARY AND CONCLUSIONS

We have explored an approximate analytical model of the evolution, during the hydrodynamic phase, of the shock wave produced by a spherically symmetric explosion in a homogeneous medium. The equation of motion for the shock front treats the compression of material at the front exactly, using the Rankine-Hugoniot jump conditions and the Hugoniot of the ambient medium. The rarefaction behind the shock front is treated only approximately through a parameter f that describes the distribution of the fluid variables within the shocked volume. A key assumption of the model is that f remains constant throughout the evolution of the shock wave. The model predicts the evolution of the particle speed, shock speed, mass density, pressure, and specific internal energy immediately behind the shock front, as well as the shock front radius as a function of time. For a point explosion the model exhibits cube root scaling, in accordance with the conservation laws for spherically symmetric point explosions in uniform media [see King *et al.*, 1989; B. W. Callen *et al.*, manuscript in preparation, 1991].

We have shown that the parameter f , which relates the specific kinetic energy of the fluid just behind the shock front to the mean specific energy within the shocked volume, is constant when the shock wave is strong and self-similar. By

comparing the relation involving f with results from numerical simulations of underground nuclear explosions in quartz and wet tuff, we have shown that it is also remarkably constant even when the shock wave is no longer strong, for explosions in these media. Furthermore, we find that the value of f is relatively independent of the ambient medium and that $f = 0.53$ adequately reproduces the particle speed curve extracted from the numerical simulations, in agreement with the previous results of *Moss* [1988].

The radius versus time curves predicted by the model for a point explosion are in excellent agreement with the shock front radii measured during underground nuclear tests in granite, wet tuff, and basalt, when the official yields are assumed and f is set equal to 0.53. If the model is used with a piecewise-linear approximation to the Hugoniot, the largest differences between the predicted and measured radii range from 3% to 7% for the different events. Even when the model is used with a simple linear approximation to the Hugoniot, the shock front radii that it predicts agree extremely well with the measured radii for the events in wet tuff (Chiberta and NTS-X), where the differences are less than 3% and 6%, respectively, during the hydrodynamic phase. For the events in basalt (Cannikin) and granite (Piledriver) the high-pressure approximation works less well, but the differences in the predicted and measured radii are still less than 14% during the hydrodynamic phase. The average differences are substantially less in all cases.

We have shown that the model can also be used to estimate the yields of underground nuclear explosions, with good results. When the analytical model is used with point source boundary conditions and a piecewise-linear representation of the Hugoniot, the yields obtained by fitting the radius versus time data from the hydrodynamic phase of the explosions are within 8% of the official yields. For comparison, the yields obtained by fitting numerical simulations carried out by the Los Alamos CORRTX group to the same data are within 9% of the official yields. Thus the yield estimates obtained using the analytical model are nearly as accurate as the yield estimates obtained using the numerical simulations.

More generally, the U.S. Department of State has claimed that hydrodynamic methods are accurate to within 15% (at the 95% confidence level) of radiochemical yield estimates for tests with yields greater than 50 kt in the geologic media in which tests have been conducted at the Nevada Test Site (*U.S. Department of State* [1986a, b]; see also *U.S. Congress, Office of Technology Assessment* [1988] and *Lamb* [1988]). Thus the analytical model appears to be competitive with existing models for estimating the yields of underground nuclear tests conducted in relatively uniform media.

In a future paper (*F. K. Lamb et al.*, manuscript in preparation, 1991), we will use the analytical model studied here to investigate hydrodynamic yield estimation algorithms more fully, including optimal weighting of radius versus time data (a preliminary account of this work has been given by *Lamb et al.* [1989] and *Callen et al.* [1990a]). In a subsequent paper (*B. W. Callen et al.*, manuscript in preparation, 1991), we will analyze the validity of cube-root scaling for spherically symmetric underground nuclear explosions, using similarity transformation methods and numerical simulations to explore the effects of source size and composition.

APPENDIX: COMPARISON WITH HEUSINKVELD'S MODEL

In this appendix, we compare the approximate analytical model of section 2 with the approximate model proposed by *Heusinkveld* [1979, 1982]. Both models neglect the specific internal energy and pressure of the ambient medium. Both also predict radius versus time curves that exhibit the temporal behavior characteristic of a strong, self-similar shock wave at early times, then enter a gradual transition period, and finally exhibit the temporal behavior of a low-pressure plastic wave. However, Heusinkveld's model differs from the model of section 2 in several important respects.

First, Heusinkveld assumed that the internal energy per unit volume just behind the shock front, namely $e_1 = \rho_1 \epsilon_1$, is a constant fraction f_H of the total energy per unit volume within the shock front, that is,

$$e_1 = 3f_H W / 4\pi R^3. \quad (A1)$$

In contrast, the model of section 2 assumes that the specific kinetic energy of the fluid just behind the shock front is a constant fraction f of the total specific energy within the shock front (see equation (5)); the specific internal energy just behind the shock front is equal to the specific kinetic energy there (see equation (3)).

Second, Heusinkveld's model satisfies only the momentum jump condition (2), whereas the model of section 2 satisfies all three jump conditions (1), (2), and (3). In place of the specific internal energy jump condition (3), Heusinkveld assumed that the pressure just behind the shock front is proportional to a constant coefficient Γ times the energy per unit volume there, that is,

$$p_1 = \Gamma e_1. \quad (A2)$$

As noted in section 3, this is the strong shock limit of the Mie-Grüneisen equation of state when the Grüneisen Γ does not depend on the density. It may be an adequate description of the equation of state of the shocked medium, provided that the Grüneisen Γ is independent of density and the shock wave is strong. However, the shock waves produced by underground nuclear explosions are relatively weak during much of their hydrodynamic phase [see *Lamb*, 1988; *Lamb et al.*, 1991].

Heusinkveld also assumed a simple linear relation between D and u_1 of the form (6). However, the jump conditions (1), (2), and (3), the equation of state (A2), and the D versus u_1 relation (6) are mutually inconsistent. For example, if one accepts the mass flux jump condition (1), the momentum jump condition (2), and the ansatz (A1), one finds that the energy jump condition (3) is inconsistent with a linear D versus u_1 relation. Alternatively, if one accepts the D versus u_1 relation (6), one is led to the Hugoniot [see *Zel'dovich and Raizer*, 1967, p. 710]

$$\rho_H (V_1)^2 = \frac{A^2 (V_0 - V)}{[BV - (B-1)V_0]^2}, \quad (A3)$$

which is inconsistent with the jump conditions (1), (2), and (3) and the equation of state (A2).

Heusinkveld's model gives expressions for the shock speed, the radius versus time curve, and the postshock pressure, postshock particle speed, and postshock internal energy that are qualitatively different from the expressions

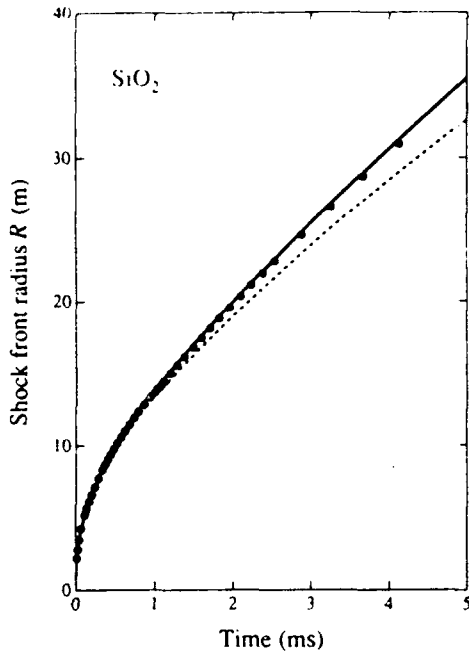


Fig. A1. Comparison of the shock front radii predicted by the analytical model of section 2 (solid line) and the model of Heusinkveld [1982] (dashed line) with radius data (dots) from a numerical simulation of a 100-kt explosion in SiO_2 by D. Eilers et al. (private communication, 1987). The piecewise-linear representation of the SiO_2 Hugoniot shown in Figures 2 and 3 was used in both models.

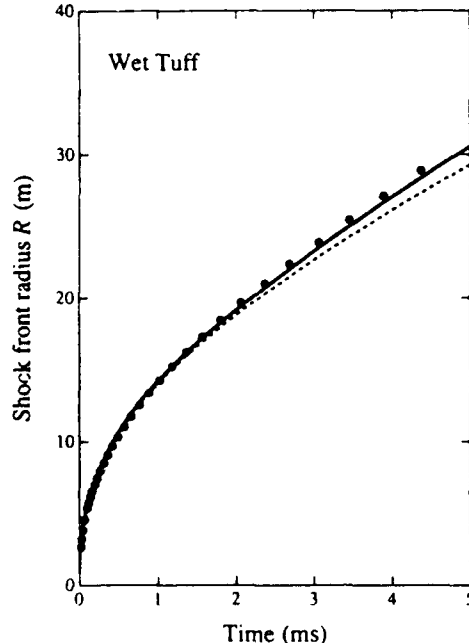


Fig. A2. Comparison of the shock front radii predicted by the analytical model of section 2 (solid line) and the model of Heusinkveld [1982] (dashed line) with radius data (dots) from a numerical simulation of a 100-kt explosion in wet tuff by D. Eilers et al. (private communication, 1987). The piecewise-linear representation of the wet tuff Hugoniot shown in Figure 4 was used in both models.

given by the model of section 2. For example, by equating the pressure given by expression (A2) with the postshock pressure given by the momentum jump condition (2) and making use of the ansatz (A1), Heusinkveld obtained a quadratic equation involving the shock speed. The solution of this equation is

$$D_H = \frac{A}{2} \left[1 + \left(1 + \frac{g^3}{R^3} \right)^{1/2} \right], \quad (\text{A4})$$

where

$$g = (3\Gamma_H BW / \pi \rho_0 A^2)^{1/3} \quad (\text{A5})$$

is a characteristic length, analogous to the characteristic length l , defined in equation (8). Expression (A4) is qualitatively different from equation (9), the relationship predicted by the model of section 2. The radius versus time curve predicted by Heusinkveld's model can be obtained by numerically integrating equation (A4). (Although Heusinkveld assumed a simple linear D versus u_1 relation, an arbitrary D versus u_1 relation can be treated to any desired accuracy by using a piecewise-linear approximation, as described in section 2.)

Even though the model of section 2 is self-consistent, whereas Heusinkveld's model is not, both are approximate. Thus their usefulness is best evaluated by comparing their predictions with data from nuclear tests and/or numerical simulations. We show here comparisons of the predictions of

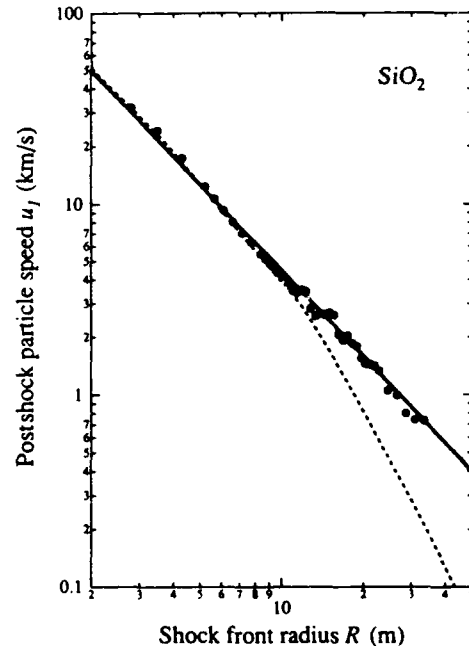


Fig. A3. Comparison of the peak particle speed predicted by the analytical model of section 2 (solid line) and the model of Heusinkveld [1982] (dashed line) with peak particle speeds (dots) from a numerical simulation of a 100-kt explosion in SiO_2 by D. Eilers et al. (private communication, 1987). The piecewise-linear representation of the SiO_2 Hugoniot shown in Figures 2 and 3 was used in the model of Heusinkveld. The peak particle speed predicted by the analytical model of section 2 is independent of the Hugoniot and scales as $R^{-3/2}$.

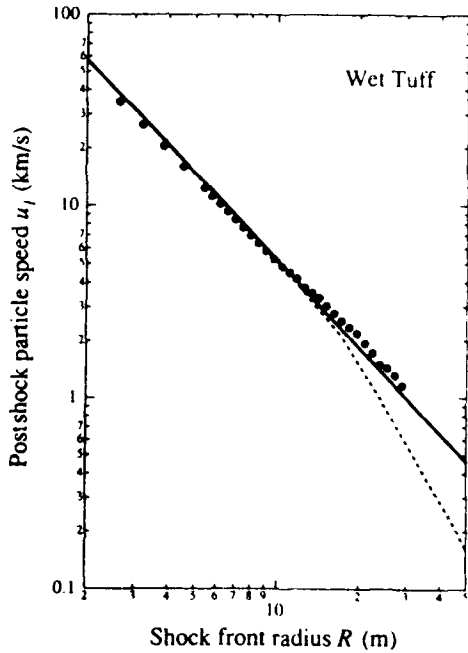


Fig. A4. Comparison of the peak particle speed predicted by the analytical model of section 2 (solid line) and the model of Heusinkveld [1982] (dashed line) with peak particle speeds (dots) from a numerical simulation of a 100-kt explosion in wet tuff by D. Eilers et al. (private communication, 1987). The piecewise-linear representation of the wet tuff Hugoniot shown in Figure 4 was used in the model of Heusinkveld. The peak particle speed predicted by the analytical model of section 2 is independent of the Hugoniot.

the two models with data from numerical simulations for three reasons. First, the initial conditions of these simulations approach that of point explosions, a simple case that the two models each describe. Second, we lack detailed knowledge of the conditions under which the nuclear test data were obtained (see section 4). Third, the simulations have reportedly been validated by extensive comparison with data from underground nuclear tests.

In comparing the two models with the results of simulations, we wish to make a consistent choice of model parameters. We do this by forcing agreement between the two models at the beginning of the explosion, as follows. At early times, the radius versus time curve given by Heusinkveld's model displays the $t^{2/5}$ dependence characteristic of a strong, self-similar shock wave, that is,

$$R_H(t) = (75\Gamma_H BW/16\pi\rho_0)^{1/5} t^{2/5}. \quad (\text{A6})$$

On comparing this curve with the early time curve given by the model of section 2, namely,

$$R(t) = (75fB^2W/16\pi\rho_0)^{1/5} t^{2/5}. \quad (\text{A7})$$

we see that if Γ_H is set equal to fB , the two models will give identical results at the beginning of the explosion. In the comparisons that follow, we do this.

Figures A1 and A2 compare the radius versus time curves predicted by the two models for explosions in quartz and wet tuff with the data from the simulated explosions in these media that were described in section 2. For the explosion in quartz, we used $\Gamma_H = 0.325$, whereas for wet tuff we used

$\Gamma_H = 0.299$. For comparison, Heusinkveld obtained $\Gamma_H = 0.78$ for explosions in alluvium and wet tuff and 1.03 for explosions in granite by fitting his model to the particle speed data of Perret and Bass [1975] at relatively late times. Had we used these values in the comparisons, the discrepancies between Heusinkveld's model and the simulations would have been much greater. Although the radius versus time curves are integrals of the shock speeds predicted by the models and hence tend to smooth out differences, the curve predicted by the analytical model of section 2 agrees better with the simulations than does the curve predicted by Heusinkveld's model.

Additional and more decisive comparisons can be made between the postshock pressures and particle speeds given by the models. On substituting equation (A4) into the D versus u_1 relation (6), one finds that Heusinkveld's model predicts the postshock particle speed

$$u_1^H = \frac{A}{2B} \left[\left(1 + \frac{3\Gamma_H BW}{\pi\rho_0 A^2 R^3} \right)^{1/2} - 1 \right]. \quad (\text{A8})$$

At small radii, (A8) becomes

$$u_1^H \approx (3\Gamma_H W/4\pi\rho_0 BR^3)^{1/2}, \quad R \ll g. \quad (\text{A9})$$

Thus, u_1^H has the same R dependence at small radii as that given by the ansatz (5) of section 2, once Γ_H has been set equal to fB . However, at large radii the postshock particle speed predicted by Heusinkveld's model scales with radius according to

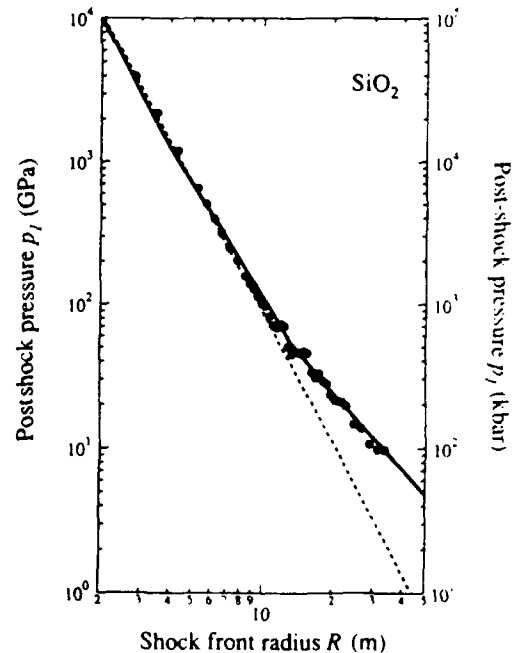


Fig. A5. Comparison of the peak pressure predicted by the analytical model of section 2 (solid line) and the model of Heusinkveld [1982] (dashed line) with peak pressures (dots) from a numerical simulation of a 100-kt explosion in SiO_2 by D. Eilers et al. (private communication, 1987). The numerical results are more consistent with the $R^{-3/2}$ variation at large R predicted by the model of section 2 than with the R^{-3} variation predicted by the model of Heusinkveld.

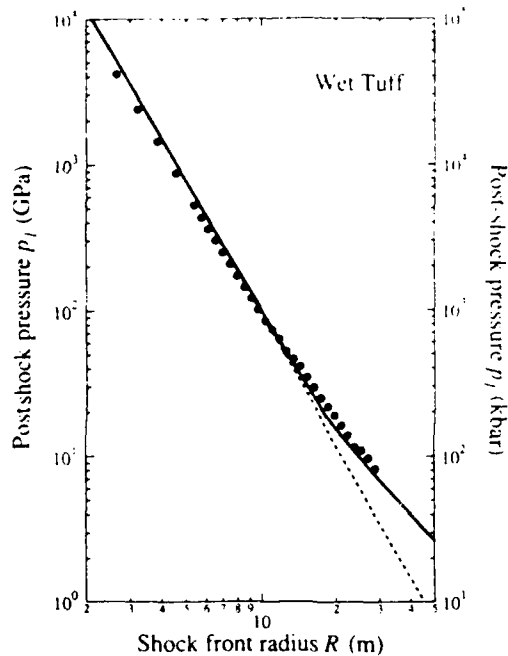


Fig. A6. Comparison of the peak pressure predicted by the analytical model of section 2 (solid line) and the model of Heusinkveld [1982] (dashed line) with peak pressures (dots) from a numerical simulation of a 100-kt explosion in wet tuff by D. Eilers et al. (private communication, 1987). Again, the numerical results are more consistent with the $R^{-3.2}$ variation at large R predicted by the model of section 2 than with the R^{-3} variation predicted by the model of Heusinkveld.

$$u_1^H \approx 3\Gamma_H W / \pi \rho_0 A R^3, \quad R \gg q. \quad (\text{A10})$$

Figures A3 and A4 compare the postshock particle speeds predicted by the two models with those derived from the simulated explosions in quartz and wet tuff. The $R^{-3.2}$ dependence predicted by the model of section 2 agrees much better with the particle speed data at late times than does the R^{-3} dependence predicted by Heusinkveld's model. In particular, there is no evidence of the break in the slope of the u_1 versus R curve at $R \approx q$ that is predicted by Heusinkveld's model.

The postshock pressure predicted by Heusinkveld's model is given by (A1) and (A2) and is

$$p_1 = 3\Gamma_H W / 4\pi R^3. \quad (\text{A11})$$

In contrast, the model of section 2 predicts that the postshock pressure falls off as R^{-3} for $R \ll L$ but is proportional to $R^{-3.2}$ for $R \gg L$ (see equation (23)). Figures A5 and A6 show that the pressure data derived from the simulations show such a break at about the right radius, demonstrating that the model of section 2 is in better agreement with the simulations than is Heusinkveld's model.

Perret and Bass [1975] show that pressure data from explosions in several geologic media are well fit by $R^{-2.96}$ out to distances of $8 \text{ m W}^{1/3}$, at which point a clear break occurs. At distances beyond this break, the data are better described by $R^{-3.2}$. This large R behavior is more in keeping with the analytical model of section 2 than the R^{-3}

dependence at all distances predicted by Heusinkveld's model.

The predictions of the two models differ significantly well before the assumptions of the model discussed in section 2 become invalid. As discussed in section 4, the hydrodynamic phase extends at least out to the radius at which the postshock pressure has fallen to 15 GPa. Obviously, the ambient pressure of 20 MPa can be neglected throughout the hydrodynamic phase. As noted in section 2, the ambient specific internal energy can be neglected for particle speeds greater than 0.1 km/s. Figures A3 and A4 show that the postshock particle speed is actually 1 km/s or greater throughout the hydrodynamic phase. Figures A1–A6 show that the differences between the two models are already significant at 10 m and increase dramatically at larger radii, whereas the postshock pressure falls to 15 GPa at 25 m in quartz and 22 m in wet tuff. At 25 m in quartz, the peak particle speed predicted by the model we discuss falls right on the curve predicted by the numerical simulation and is 2.5 times larger than the peak particle speed predicted by Heusinkveld's model, which is far below the curve predicted by the simulation.

These comparisons show that the model of section 2, which fully incorporates the Rankine-Hugoniot jump conditions and does not assume any particular equation of state, also agrees better with the radius versus time curves and the postshock particle speed and pressure data derived from the simulated explosions than does the model proposed by Heusinkveld.

Acknowledgments. We are especially grateful to M. Heusinkveld for discussions of shock wave propagation in geologic media and for providing SLIFER data from a variety of underground nuclear explosions. We wish to thank W. Moss for detailed discussions of the analytical model investigated here and D. D. Eilers and the other members of the P-15 CORTEX group at Los Alamos National Laboratory for kindly providing us with copies of the SESAME equations of state for quartz and wet tuff and for sharing with us the results of their numerical simulations of nuclear explosions in quartz and wet tuff. It is a pleasure to thank T. J. Ahrens, D. D. Eilers, R. G. Geil, R. E. Hill, W. S. Leith, and G. S. Miller for helpful discussions of shock wave propagation in geologic media. This research was supported in part by DARPA through the Phillips Laboratory under contract F-19628-88-K-0040.

REFERENCES

- Ahrens, T. J., and V. G. Gregson, Jr., Shock compression of crustal rocks: Data for quartz, calcite, and plagioclase rocks, *J. Geophys. Res.*, **69**, 4839–4874, 1964.
- Al'tshuler, L. V., N. N. Kalitkin, L. V. Kuz'mina, and B. S. Chekin, Shock adiabats for ultrahigh pressures, *Sov. Phys. JETP*, Engl. Transl., **45**, 167–171, 1977.
- Bass, R. C., and G. E. Larsen, Shock propagation in several geologic materials of interest in hydrodynamic yield determinations, *Sandia Natl. Lab. Tech. Rep. SAND77-0402*, March 1977.
- Callen, B. W., F. K. Lamb, and J. D. Sullivan, Insensitive interval in the evolution of shock waves from explosions, in *Shock Compression of Condensed Matter—1989*, edited by S. C. Schmidt, J. N. Johnson, and L. W. Davison, pp. 241–244, Elsevier Science, New York, 1990a.
- Callen, B. W., F. K. Lamb, and J. D. Sullivan, Hydrodynamic determination of the yield of underground nuclear explosions, in *Proceedings of the 12th Annual DARPA-GL Seismic Research Symposium*, pp. 241–250, Air Force Geophysics Laboratory, Hanscom Air Force Base, Mass., 1990b. (Also Rep. P 90/9 116, Dep. of Phys., Univ. of Ill., Urbana, Sept. 1990.)
- Chung, D. H., and G. Simmons, Pressure derivatives of the elastic

- properties of polycrystalline quartz and rutile, *Earth Planet. Sci. Lett.*, **6**, 134-138, 1969.
- Cox, A. N., R. R. Brownlee, and D. D. Eilers, Time-dependent method for computation of radiation diffusion and hydrodynamics, *Astrophys. J.*, **144**, 1024-1037, 1966.
- Dahlman, O., and H. Israelson, *Monitoring Underground Nuclear Explosions*, Elsevier, New York, 1977.
- Glasstone, S., and P. J. Dolan, *Effects of Nuclear Weapons*, 3rd ed., U.S. Government Printing Office, Washington, D. C., 1977.
- Grady, D. E., W. J. Murri, and G. R. Fowles, Quartz to stishovite: Wave propagation in the mixed phase region, *J. Geophys. Res.*, **79**, 332-338, 1974.
- Heusinkveld, M., Analysis of SLIFER data from underground nuclear explosions, *Lawrence Livermore Natl. Lab. Rep. UCRL-52648*, 1979.
- Heusinkveld, M., Analysis of shock wave arrival times from underground explosions, *J. Geophys. Res.*, **87**, 1891-1898, 1982.
- Heusinkveld, M., Shock arrival times in granite, *Mem. 0004A*, Lawrence Livermore Natl. Lab., Earth Sci. Dep., Oct. 30, Livermore, Calif., 1986.
- Heusinkveld, M., and F. Holzer, Method of continuous shock front position measurement, *Rev. Sci. Instrum.*, **35**, 1105-1107, 1964.
- Holzer, F., Measurements and calculations of peak shock wave parameters from underground nuclear detonations, *J. Geophys. Res.*, **70**, 893-905, 1965.
- Johnson, G. W., G. H. Higgins, and C. E. Violet, Underground nuclear detonations, *J. Geophys. Res.*, **64**, 1457-1470, 1959.
- Jones, A. H., W. M. Isbell, F. H. Shipman, R. D. Perkins, S. J. Green, and C. J. Maiden, Material properties measurements for selected materials, interim report, contract NAS2-3427, Gen. Motors Tech. Cent., Warren, Mich., April 1968.
- King, D. S., B. E. Freeman, D. D. Eilers, and J. D. Johnson, The effective yield of a nuclear explosion in a small cavity in geologic material, *J. Geophys. Res.*, **94**, 12,375-12,385, 1989.
- Lamb, F. K., An approximate solution for ground shock propagation, *Rep. WP-2-87-2*, Univ. of Ill., Program in Arms Control, Disarmament, and Int. Secur., Urbana, Feb. 1987.
- Lamb, F. K., Monitoring yields of underground nuclear tests using hydrodynamic methods, in *Nuclear Arms Technologies in the 1990s*, edited by D. Schroerer and D. Hafemeister, pp. 109-148, American Institute of Physics, New York, 1988.
- Lamb, F. K., B. W. Callen, and J. D. Sullivan, Insensitive interval in the evolution of shock waves from underground nuclear explosions, in *Proceedings of the 11th Annual DARPA/AFGL Seismic Research Symposium*, Air Force Geophysics Laboratory, Hanscom Air Force Base, Mass., 1989. (Also *Rep. P18915177*, Dep. of Phys., Univ. of Ill., Urbana, May 1989.)
- Lamb, F. K., B. W. Callen, and J. D. Sullivan, Yield estimation using shock wave methods, in *Explosion Source Phenomenology*, *Geophys. Monogr. Ser.*, vol. 65, edited by S. R. Taylor, P. G. Richards, and H. J. Patton, pp. 73-89, AGU, Washington, D. C., 1991.
- Landau, L. D., and E. M. Lifshitz, *Fluid Mechanics*, 2nd ed., Pergamon, New York, 1987.
- Mathews, J., and R. L. Walker, *Mathematical Methods of Physics*, 2nd ed., W. A. Benjamin, New York, 1970.
- McQueen, R., J. N. Fritz, and J. W. Hopson, High-pressure equation of state of SiO₂, *M-6 Prog. Rep. M-6-200*, pp. 78-136, Los Alamos Natl. Lab., Los Alamos, N. M., Jan.-March 1977.
- Moran, B., and H. C. Goldwire, Jr., Effect of source modelling on the inferred yield from an underground nuclear explosion, in *Shock Compression of Condensed Matter-1989*, edited by S. C. Schmidt, J. N. Johnson, and L. W. Davison, pp. 645-648, North-Holland, New York, 1990.
- Moss, W. C., A method to estimate the yield of an underground nuclear explosion, *J. Appl. Phys.*, **63**, 4771-4773, 1988.
- Nuckolls, J. H., A computer calculation of Rainier (the first 100 milliseconds), in *Proceedings of Second Plowshare Symposium*, May 13-15, 1959, San Francisco, California, part I, Phenomenology of Underground Nuclear Explosions, *Lawrence Livermore Natl. Lab. Rep. UCRL-5675*, 120-134, 1959.
- Perret, W. R., and R. C. Bass, Free-field ground motion induced by underground explosions, *Sandia Natl. Lab. Tech. Rep. SAND74-0252*, Feb. 1975.
- Ragan, C. E., III, Shock-wave experiments at threefold compression, *Phys. Rev. A Gen. Phys.*, **29**, 1391-1402, 1984.
- Sedov, L. I., The motion of air in a strong explosion (in Russian), *Dokl. Akad. Nauk SSSR*, **52**, 17-20, 1946.
- Sedov, L. I., *Similarity and Dimensional Methods in Mechanics*, Academic, San Diego, Calif., 1959.
- Taylor, G. I., The formation of a blast wave by a very intense explosion. I. Theoretical discussion, *Proc. R. Soc. London, Ser. A*, **201**, 159-174, 1950a.
- Taylor, G. I., The formation of a blast wave by a very intense explosion. II. The atomic explosion of 1945, *Proc. R. Soc. London, Ser. A*, **201**, 175-186, 1950b.
- U.S. Arms Control and Disarmament Agency, *Arms Control and Disarmament Agreements*, Washington, D. C., 1990a.
- U.S. Arms Control and Disarmament Agency, *Treaty Between the United States of America and the Union of Soviet Socialist Republics on the Limitation of Underground Nuclear Weapons Tests and Treaty Between the United States of America and the Union of Soviet Socialist Republics on Underground Nuclear Explosions for Peaceful Purposes: Text of Treaties and Protocols*, Washington, D. C., 1990b.
- U.S. Congress, Office of Technology Assessment, *Seismic Verification of Nuclear Testing Treaties*, OTA-ISC-361, U.S. Government Printing Office, Washington, D. C., May 1988.
- U.S. Department of Energy, *Announced United States Nuclear Tests, July 1945 through December 1986*, NVO-209 (Rev. 7), Nevada Operations Office, Las Vegas, Jan. 1987.
- U.S. Department of State, Bureau of Public Affairs, U.S. policy regarding limitations on nuclear testing, *Spec. Rep. 150*, Washington, D. C., Aug. 1986a.
- U.S. Department of State, Bureau of Public Affairs, Verifying nuclear testing limitations: possible U.S.-Soviet cooperation, *Spec. Rep. 152*, Washington, D. C., Aug. 1986b.
- U.S. Department of State, *Agreement Between the United States of America and the Union of Soviet Socialist Republics on the Conduct of a Joint Verification Experiment*, Washington, D. C., May 1988.
- Virchow, C. F., G. E. Conrad, D. M. Holt, and E. K. Hodson, Microprocessor-controlled time domain reflectometer for dynamic shock position measurements, *Rev. Sci. Instrum.*, **51**, 642-646, 1980.
- Wackerle, J., Shock-wave compression of quartz, *J. Appl. Phys.*, **33**, 922-937, 1962.
- Zel'dovich, Ya. B., and Yu. P. Raizer, *Physics of Shock Waves and High-Temperature Hydrodynamic Phenomena*, Academic, San Diego, Calif., 1967.

B. W. Callen, Department of Physics, Drury College, Springfield, MO 65802.

F. K. Lamb and J. D. Sullivan, Department of Physics, University of Illinois, Urbana-Champaign, Loomis Laboratory of Physics, 1110 W. Green Street, Urbana, IL 61801

(Received January 7, 1991,
revised July 30, 1991,
accepted September 10, 1991.)

The U.S. Government is authorized to reproduce and sell this report.
Permission for further reproduction by others must be obtained from
the copyright owner.

INSENSITIVE INTERVAL IN THE EVOLUTION OF SHOCK WAVES FROM EXPLOSIONS*

B. W. CALLEN, F. K. LAMB, and J. D. SULLIVAN

Department of Physics, University of Illinois at Urbana-Champaign, 1110 West Green Street, Urbana, IL 61801, U.S.A.

There is empirical evidence that the radius of the expanding shock front produced by an explosion in silicate rocks is relatively insensitive to the particular rock but fairly sensitive to the yield during part of the hydrodynamic phase. By using an approximate but relatively accurate analytical model for shock wave propagation, we show that the existence of this *insensitive interval* is likely a consequence of correlations between certain properties of silicate rocks.

1. INTRODUCTION

The initial speed of the shock wave generated by an underground explosion increases with the yield of the explosion, other things being equal. As a result, the radius of the shock front at a given time is greater for explosions of greater yield. Hence, measurements of the radius of the shock front using CORTEX¹ or other techniques can be used to estimate the yield, provided the dependence of the radius vs. time curve on the properties of the ambient geologic medium is understood. In practice, the yield of an explosion is estimated using an algorithm, by which we mean a particular procedure for comparing radius vs. time data with a model of the motion of the shock front. If there exists an interval in time during which the radii of shock waves in all media of interest are similar for explosions of a given yield, it is advantageous to use the data in such an *insensitive interval*.

In fact, there is empirical evidence that the radius of the shock front is relatively insensitive to the ambient medium toward the end of the hydrodynamic phase of shock wave evolution, for the rocks within U.S. nuclear test experience, which are mostly silicates. This is illustrated in Figure 1, which shows typical radius vs. time curves for explosions of the same yield in two such rocks. The curves approach each other gradually, cross, and then separate gradually. Because the curves intersect at a small angle, the insensitive interval is not sharply defined.

*Supported in part by DARPA through AFGL under Contract F-19628-88-K-0040.

Despite widespread use of algorithms that use data in the insensitive interval, the physical reason for the existence of such an interval and the extent to which it would persist for shock waves in a more diverse collection of geologic media has been unclear. We show that the existence of an insensitive interval is most likely a consequence of correlations between certain properties of the rocks in question. To demonstrate this we use an approximate, analytical model for the propagation of the shock wave.

2. ANALYTICAL MODEL

We consider here a simple model of the spherical shock wave produced by release of a very large amount of energy in an infinitesimal volume (a *point explosion*) in homogeneous rock. For many materials, the relation between the speed D of a shock front and the particle speed u just behind it is approximately linear for large u , that is

$$D_i \equiv \frac{dR_i}{dt} = A_i + B_i u, \quad (1)$$

where A_i and B_i are constants.² Here the subscript i denotes the material. We shall assume that $D(u)$ can be adequately represented by a single linear relation of the form (1) over the range of u that is of interest.

We shall also assume that the particle speed just behind the shock front is related to the yield W_i of the explosion by the expression^{3,4}

$$\frac{4\pi}{3} \rho_0 R_i^3(t) u^2(t) = f_i W_i, \quad (2)$$

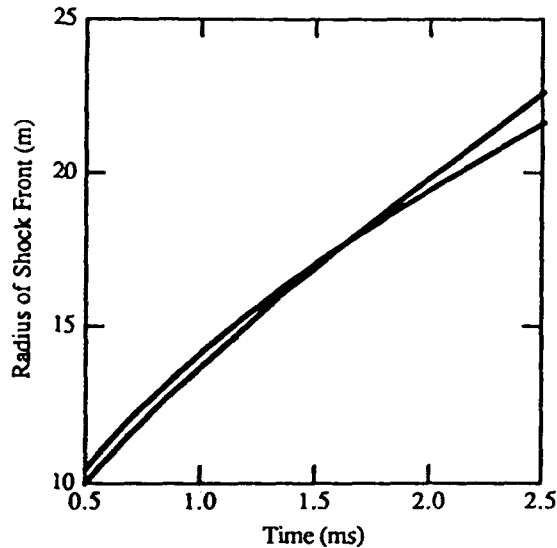


FIGURE 1

Radius vs. time curves for simulated explosions of the same yield in two different silicate rocks.

where $R_i(t)$ is the radius of the shock front at time t , ρ_{0i} is the mass density of the rock in its unshocked state, and f_i is a dimensionless factor that describes how the energy of the explosion is partitioned between kinetic energy of bulk motion and internal energy, and depends upon the variation with position of the velocity, density, and internal energy of the shocked material. In general, f_i is a constant when the shock wave is strong, but changes somewhat as the shock wave weakens.^{3,4} In this analysis, we shall assume that f_i can be treated as constant for the times of interest.

Given these assumptions, equation (1) with u given by equation (2) can be integrated analytically. First we rewrite equation (1) in terms of the dimensionless variables³

$$x = R_i/L_i \quad \text{and} \quad \tau = t/T_i, \quad (3)$$

where

$$L_i = \left(\frac{3f_i W_i B_i^2}{4\pi\rho_{0i} A_i^2} \right)^{1/3} \quad \text{and} \quad T_i = \frac{L_i}{A_i}. \quad (4)$$

In terms of the non-dimensional variables (3), equation (1) becomes

$$\frac{dx}{d\tau} = 1 + \frac{1}{x^{3/2}}. \quad (5)$$

The solution of equation (5) is³

$$\tau(x) = x + \frac{1}{3} \ln \left(\frac{x + 2\sqrt{x} + 1}{x - \sqrt{x} + 1} \right) - \frac{2}{\sqrt{3}} \left[\frac{\pi}{6} + \tan^{-1} \left(\frac{2\sqrt{x} - 1}{\sqrt{3}} \right) \right]. \quad (6)$$

At small radii ($x \ll 1$), this solution reduces to

$$x(\tau) \approx (5/2)^{2/5} \tau^{2/5}, \quad (7)$$

which is the behavior of a *strong, self-similar* shock wave.⁵ At large radii ($x \gg 1$), the solution becomes

$$x(\tau) \approx \text{const.} + \tau, \quad (8)$$

which describes a constant-speed plastic wave. Equation (6) agrees quite well with field data and numerical simulations.^{3,4,6,7}

Within the assumptions of the present model, any explosion is completely defined by its yield W_i and the four parameters characterizing the ambient medium: ρ_{0i} , A_i , B_i , and f_i . The radius vs. time curve for any explosion can be generated from the function (6) by applying the similarity transformation

$$R_i(t) = L_i x(t/T_i). \quad (9)$$

Equation (9) also implies that if the radius vs. time curve for explosion i is known, then the radius vs. time curve for any other explosion j can be generated, provided that ρ , A , B , f , and W are known for both explosions. The radius vs. time curve $R_j(t)$ for any explosion j is given in terms of the radius vs. time curve $R_i(t)$ for explosion i by the similarity transformation

$$R_j(t) = (L_j/L_i) R_i(T_i t/T_j). \quad (10)$$

The approach outlined below depends only on the existence of a similarity transformation of the form (10), and not on the particular values of the characteristic scales L and T , or the particular form of the function $x(\tau)$.

3. INSENSITIVE INTERVAL

To formulate a more precise definition of the insensitive interval, consider the shock waves produced by an explosion of the *same yield* in two *different media* i and j . The difference between the

resulting radius vs. time curves $R_i(t)$ and $R_j(t)$ at time t is

$$\Delta R_{ij}(t) \equiv R_i(t) - R_j(t). \quad (11)$$

We define the *insensitive time* t_0 as the time at which the yield estimate is least sensitive to the ambient medium, for media in the collection of interest. Given a criterion for the maximum acceptable yield error, the extent Δt of the "insensitive interval" can be calculated from the way in which $|\Delta R_{ij}(t)|^2$, averaged over the collection, varies with time about t_0 .

One can calculate t_0 and Δt for a collection of n different media by applying standard statistical techniques. However, analysis of a collection of two different media captures the most important features of the problem and is considerably more transparent; hence we summarize those results here.

We assume that $R_i(t)$ and $R_j(t)$ cross at one and only one point (cf. Figure 1). At the crossing point, any monotonically increasing function of $|\Delta R_{ij}(t)|$ is a minimum. Thus, the insensitive time t_{ij}^0 is the root of the equation

$$\Delta R_{ij}(t) = 0. \quad (12)$$

If the curves $R_i(t)$ and $R_j(t)$ are generated from a curve $x(\tau)$ by similarity transformations of the form (9), then

$$\Delta R_{ij} = L_i x(\tau_i) - L_j x(\tau_j), \quad (13)$$

where $\tau_i = t/T_i$ and $\tau_j = t/T_j$. Note that the dimensionless times τ_i and τ_j that correspond to the *same* time t are in general *different* for the two media.

If $x(\tau)$ varies sufficiently slowly in the region of interest, we can relate $x(\tau_j)$ and $x(\tau_i)$ by expanding both in a Taylor series about

$$\bar{\tau}_{ij} \equiv \frac{1}{2}(\tau_i + \tau_j). \quad (14)$$

Then to first order in $\tau_i - \bar{\tau}_{ij}$ and $\tau_j - \bar{\tau}_{ij}$, the condition $\Delta R_{ij}(t_{ij}^0) = 0$ becomes

$$\alpha(\bar{\tau}_{ij}^0) = M_{ij}, \quad (15)$$

where

$$\alpha(\tau) \equiv \frac{d \ln x}{d \ln \tau} \quad \text{and} \quad M_{ij} \equiv \frac{\bar{T}_{ij}}{L_{ij}} \frac{\Delta L_{ij}}{\Delta T_{ij}}, \quad (16)$$

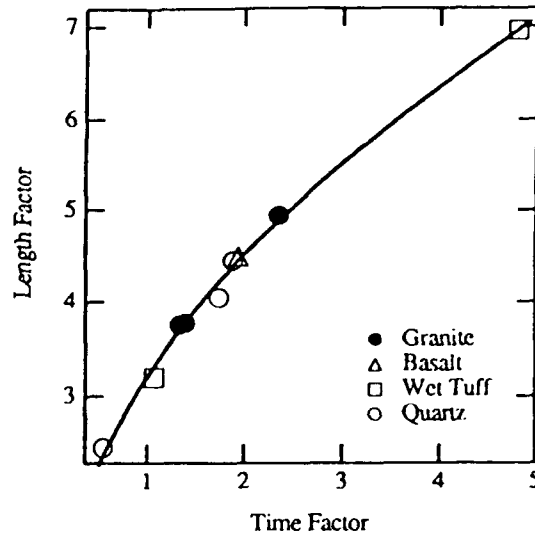


FIGURE 2

Plots of L_i vs. T_i for rocks typical of those found at U.S. nuclear test sites.

and

$$\Delta L_{ij} \equiv L_i - L_j \quad \text{and} \quad \bar{L}_{ij} \equiv \frac{1}{2}(L_i + L_j). \quad (17)$$

The definitions of ΔT_{ij} and \bar{T}_{ij} are similar to the definitions of ΔL_{ij} and \bar{L}_{ij} . Equation (15) determines the dimensionless time $\bar{\tau}_{ij}^0$. Note that the left side of equation (15) depends only on the properties of the medium-independent function $x(\tau)$, while the right side depends only on the properties of the two ambient media.

For the $x(\tau)$ given by equation (6), the logarithmic derivative $\alpha(\tau)$ increases monotonically from 0.4 to 1 as τ increases from 0 to ∞ [see eqs. (7) and (8)]. Thus, there can be at most one crossing point. The radius vs. time curves $R_i(t)$ and $R_j(t)$ cross if and only if

$$0.4 \leq M_{ij} \leq 1. \quad (18)$$

Figure 2 shows a plot of the characteristic lengths L_i vs. the characteristic times T_i , for a collection of silicate rocks typical of those found at U.S. nuclear test sites. The values were calculated from equations (4), assuming $f_i = 0.53$ for all the media.^{3,4,7,8} The data points all lie close to the curve $L = 3.20 T^{0.49}$, for which $d \ln L / d \ln T = 0.49$. This suggests that M_{ij} should be ~ 0.49 for

all pairs of media in this sample. In fact, the mean value of M_{ij} for the media in Figure 2 is 0.53; most of the M_{ij} cluster near this value and all lie in the range 0.3–0.7. Moreover, the second-order correction to $\alpha(\bar{\tau}_{ij})$ is 0.05 or less for these media. Thus, for a point explosion in homogeneous rock, the above analysis predicts an insensitive interval near the time when $\alpha(\bar{\tau}_{ij}) \approx 0.53$. This result is in good agreement with the empirical observation⁸ that there is an insensitive interval where $\alpha \approx 0.48$.

4. DISCUSSION AND CONCLUSIONS

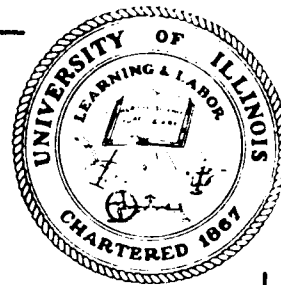
The analysis presented here is approximate in several respects. First, the solution (6) for a point explosion in a homogeneous medium is only approximate, although it agrees well with both particle speed data and with radius vs. time data over a broad interval in time. Second, in computing the values of L_i and T_i plotted in Figure 2 we have assumed that $f_i = 0.53$ for all these media. While the actual values of f_i may be similar for these rocks,⁴ they are not expected to be identical. The values of L_i and T_i can easily be corrected for differences in f_i once the best values of f_i have been determined. Third, actual shock waves are not produced by spherically symmetric point explosions. Although the shock wave produced by an aspherical source of finite size will evolve toward a spherically-symmetric, self-similar wave if the shock front envelops a mass much greater than that of the nuclear charge while the shock wave is still strong,⁹ even the shock waves produced by a 150 kt explosion weaken too quickly for this to occur, given current U.S. testing practices.⁸ Finally, the geologic media in which tests are conducted often are not homogeneous, but have layers, voids, and other structures that can affect the propagation of the shock wave.

Despite these complications, we think that the analysis presented here points to the physical reason for the existence of an insensitive interval for the rocks within U.S. nuclear test experience, namely, a correlation between the basic properties of these rocks (cf. Fig. 2). (Note that the existence of an insensitive interval *cannot* be attributed to strong, self-similar motion of the shock wave. For the reasons mentioned above, the shock

wave is not self-similar during the insensitive interval, for current test geometries and the yields permitted by the Threshold Test Ban Treaty. In fact, the shock wave is not even strong during this interval.⁸ If the shock wave were strong, $\partial \ln R / \partial \ln t$ during the insensitive interval would be⁵ 0.4, rather than the value ~ 0.48 that is observed.) We expect that the analytical approach described here can be used to predict whether an insensitive interval exists for collections that include media outside U.S. test experience.

REFERENCES

1. C.F. Virchow, G.E. Conrad, D.M. Holt, and E.K. Hodson, *Rev. Sci. Inst.* 51 (1980) 642.
2. Ya.B. Zel'dovich and Yu.P. Raizer, *Physics of Shock Waves and High-Temperature Hydrodynamic Phenomena* (Academic Press, New York, 1967).
3. F.K. Lamb, *ACDIS WP-2-87-2* (Univ. of Illinois Program in Arms Control, Disarmament, and International Security, Urbana, IL, 1987).
4. W.C. Moss, *J. Appl. Phys.* 63 (1988) 4771.
5. L.I. Sedov, *Similarity and Dimensional Methods in Mechanics* (Academic Press, New York, 1959).
6. F.K. Lamb, *An Independent Assessment of CORTEX*, Report prepared for the Congressional Office of Technology Assessment (1987).
7. F.K. Lamb, B.W. Callen, and J.D. Sullivan, "Insensitive Interval in the Evolution of Shock Waves from Underground Nuclear Explosions", *Rep. P/89/5/77* (UIUC Physics Dept., Urbana, IL, 1989).
8. F.K. Lamb, in *Nuclear Arms Technologies in the 1990s*, eds. D. Schroerer and D. Hafemeister (American Institute of Physics, New York, 1988) p. 109.
9. G.I. Barenblatt, *Similarity, Self-Similarity, and Intermediate Asymptotics* (Consultants Bureau, New York, 1979).



Insensitive Interval in the Evolution of Shock Waves
from Underground Nuclear Explosions

F. K. Lamb, B. W. Callen, and J. D. Sullivan

UNIVERSITY OF ILLINOIS AT URBANA-CHAMPAIGN
DEPARTMENT OF PHYSICS
LOOMIS LABORATORY OF PHYSICS
1110 W. GREEN STREET
URBANA, ILLINOIS 61801

INSENSITIVE INTERVAL IN THE EVOLUTION OF SHOCK WAVES FROM UNDERGROUND NUCLEAR EXPLOSIONS*

F. K. Lamb, B. W. Callen, and J. D. Sullivan

University of Illinois at Urbana-Champaign
Department of Physics
and

Program in Arms Control, Disarmament, and International Security
1110 West Green Street, Urbana, IL 61801, U.S.A.

ABSTRACT

The initial speed of the shock wave produced by an underground nuclear explosion increases with the yield of the explosion. Thus, techniques that measure the radius of the shock front as a function of time, such as CORRTEX, can be used to estimate the yield, provided the dependence of the radius vs. time curve on the properties of the ambient geologic medium is understood. For silicate rocks, there is empirical evidence that the radius of the shock front is relatively insensitive to the particular rock but fairly sensitive to the yield of the explosion during part of the hydrodynamic phase. This *insensitive interval* lies outside the strong shock region. The physical origin of this insensitivity and whether it would persist for a more diverse collection of geologic media has been unclear. We show that the existence of an insensitive interval is probably a consequence of correlations between certain properties of the rocks at U.S. test sites. We relate the radius of the shock front to these rock properties using an approximate solution for the propagation of the shock wave that assumes a linear relation between shock speed and particle speed and a scaling relation for the particle speed. This solution agrees well with particle speed and radius vs. time data. Given this solution, the radius vs. time curve for one rock can be generated by applying a similarity transformation to the radius vs. time curve for a different rock. When the relevant rock properties are correlated in a certain way, an insensitive interval appears. The relevant properties of the rocks found at U.S. test sites correlate in just this way. Remarkably, similar correlations exist among the relevant properties of other, quite different media.

*Presented at the 11th Annual AFGL/DARPA Seismic Research Symposium, San Antonio, TX, 2-4 May 1989. Work supported in part by DARPA through the Air Force Geophysics Research Laboratory under Contract F-19628-88-K-0040.

INSENSITIVE INTERVAL IN THE EVOLUTION OF SHOCK WAVES FROM UNDERGROUND NUCLEAR EXPLOSIONS

F. K. Lamb, B. W. Callen, and J. D. Sullivan
University of Illinois at Urbana-Champaign
Department of Physics and
Program in Arms Control, Disarmament, and International Security
1110 West Green Street, Urbana. IL 61801

Contract: F19628-88-K-0040

OBJECTIVE

The overall objective of this project is to improve analysis and interpretation of shock wave data that have been and may be gathered to help monitor agreed limitations on underground nuclear testing. Specific objectives are to explore the effects of the ambient geologic medium on yield estimates made using shock wave methods, to investigate the effects of different test geometries, and to explore the possibility of using shock wave methods to monitor yield limitations well below the current yield limit of 150 kt.

SUMMARY

During the six months since this project began, (1) equation of state data have been assembled for a variety of geologic media relevant to U.S. and Soviet test sites, (2) the usefulness and limitations of various simple high-pressure equations of state for geologic media have been explored, (3) the requirements for self-similar and intermediate asymptotic behavior of shock waves produced by underground nuclear explosions have been analyzed, and (4) the conditions under which so-called 'insensitive interval scaling' can be used to estimate reliably the yield of an underground nuclear explosion have been investigated. In this report we describe our results thus far on insensitive interval scaling.

Insensitive Interval Scaling

The initial speed of the shock wave generated by an underground nuclear explosion increases with the yield of the explosion, all other things being equal. As a result, the radius of the shock front at a given time is greater for explosions of greater yield. Hence measurements of the radius of the shock front using CORTEX (Virchow et al. 1980) or other techniques can be used to estimate the yield, provided the dependence of the radius vs. time curve on the properties of the ambient geologic medium is understood. In practice, the yield of an explosion is estimated using an algorithm, by which we mean a particular procedure for comparing radius vs. time data with a model of the motion of the shock front. One of the most commonly used algorithms, and the one that the United States has proposed to use in monitoring Soviet compliance with the Threshold Test Ban Treaty, is insensitive interval scaling.

An "insensitive interval" exists if, for explosions of a given yield, there is an interval in time during which the radii of shock waves in all media of interest are similar. In fact, there is empirical evidence that the radius of the shock front is relatively insensitive to the ambient medium toward the end of the hydrodynamic phase of shock wave evolution, for the rocks within U.S. test experience, which are mostly silicates. This is illustrated in the left panel of Figure 1, which shows typical radius vs. time curves for explosions of the same yield in two such rocks. The curves approach each other gradually, cross, and then separate gradually from one another. Because the curves intersect at a small angle, the insensitive interval is not sharply defined.

The insensitive interval scaling algorithm is based on this empirical evidence. It assumes that, during a certain interval in time and radius called the "algorithmic interval", the radius of the shock front produced by an explosion of a *given* yield is the same for all ambient media of interest. The algorithm assumes further that if the yield is varied, the location and extent of the algorithmic interval scale as the cube root of the yield. Stated differently, the insensitive interval scaling algorithm assumes that there is an interval in scaled elapsed time since the beginning of the explosion $\hat{t} \equiv t/W^{1/3}$ and scaled radius of the shock front $\hat{R} \equiv R/W^{1/3}$ during which $\hat{R}(\hat{t})$ is the same for all rocks of interest.

In using insensitive interval scaling, yield estimates are made by comparing a simple empirical formula, often called the Los Alamos Formula, to radius vs. time data collected in the algorithmic interval. This formula is (Bass and Larsen 1977)

$$\hat{R}(\hat{t}) = a \hat{t}^b, \quad (1)$$

where a and b are constants, and \hat{R} and \hat{t} are in units of $m/kt^{1/3}$ and $ms/kt^{1/3}$, respectively. This simple power law expression does not accurately describe the position of the shock front as a function of time in any medium. However, it may approximate the radius of the shock front over a certain time interval, if a and b are chosen appropriately. This is illustrated in the right panel of Figure 1, which compares the radius vs. time curve given by the Los Alamos Formula for $a = 6.29$ and $b = 0.475$ (Bass and Larsen 1977) with the radius vs. time curve from a model of the evolution of the shock wave produced in granite by a spherically-symmetric point explosion with a yield of 62 kt.

The values of a and b used in equation (1) are usually determined by fitting it to a collection of $\hat{R}(\hat{t})$ data obtained from many nuclear explosions in the different rocks of interest, over a selected interval of \hat{t} . In general, $\hat{R}(\hat{t})$ depends on the ambient medium, even within this interval. The resulting values of a and b , therefore, do not represent the best fit of equation (1) to the $\hat{R}(\hat{t})$ curve for any *single* medium, but rather the best fit to the pooled $\hat{R}(\hat{t})$ curves for *all* the media of interest, over the chosen interval in \hat{t} . Not surprisingly, different individuals and groups have found different best-fit values of a and b from different collections of explosions on different dates. The values of a and b used in this report are those noted above.

Within the assumptions of the insensitive interval scaling algorithm, a sequence of yield estimates W_q can be obtained for any explosion without regard to the particular medium in which it occurred by adjusting W in equation (1) so that it agrees with the shock front radii R_q measured at a sequence of times t_q in some prescribed "algorithmic interval" $\Delta \hat{t}$. A best estimate of the yield is then formed by combining the individual yield

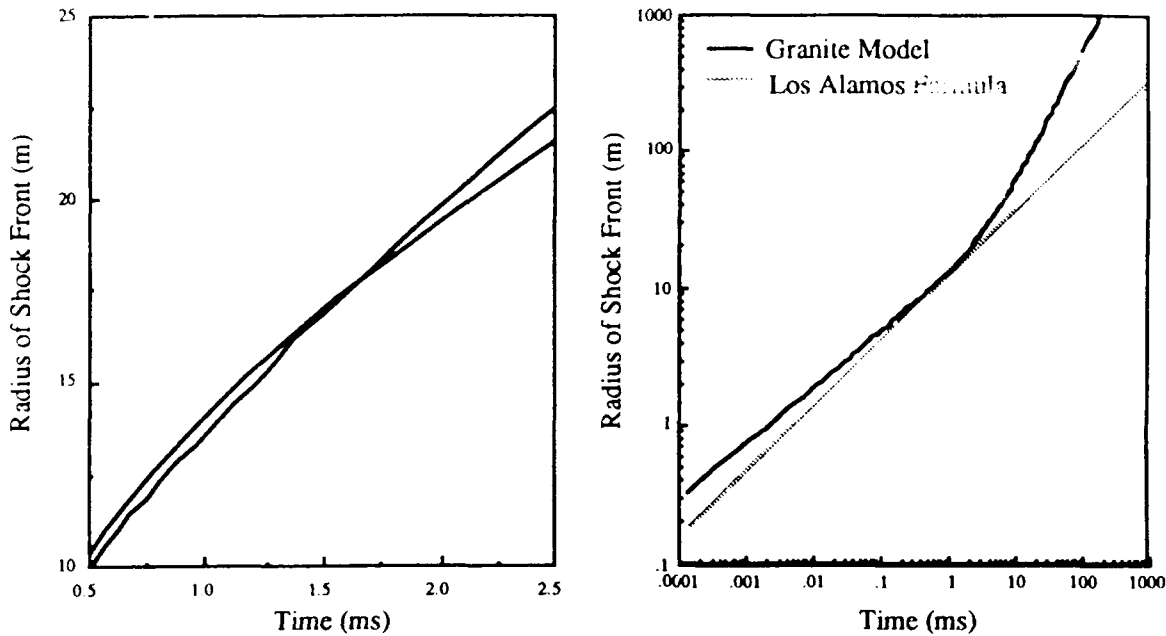


Fig. 1.—*Left*: Typical radius vs. time curves for two explosions of the same yield in two different silicate rocks, showing how the curves gradually approach each other, cross, and then gradually deviate from one another. *Right*: Comparison of the radius vs. time curve given by the Los Alamos Formula (1), for $a = 6.29$ and $b = 0.475$, with the radius vs. time curve from a model of the evolution of the shock wave produced in granite by a spherically-symmetric point explosion with a yield of 62 kt. The radius given by the Formula is close to the radius of the shock front for $t \approx 1$ ms, but deviates from the shock front radius at both earlier and later times.

estimates W_q in some way, for example by averaging them. Since the data to be combined are to be chosen from a prescribed interval in \hat{t} but the yield is unknown *a priori*, the yield estimates W_q must be constructed by an iterative process.

Any discrepancy $\Delta\hat{R}$ between the value of $\hat{R}(\hat{t})$ given by equation (1) and the true value of $\hat{R}(\hat{t})$ introduces an error

$$\frac{\Delta W}{W} \approx 3 \frac{\Delta\hat{R}}{\hat{R}} \quad (2)$$

in the yield. The extent in \hat{t} of the data that can be used in estimating the yield (i.e., the extent of the so-called "algorithmic interval") depends on how large an error in the yield can be tolerated and the diversity of materials that need to be considered. If a relatively large error is acceptable, the algorithmic interval can be relatively large. On the other hand, if only a very small error in the yield is acceptable, there may be no interval in \hat{t} that gives a yield estimate with the required accuracy.

From this discussion it is apparent that a critical requirement for successful use of the insensitive interval algorithm is that there exist an interval in \hat{t} during which $\hat{R}(\hat{t})$ depends weakly or not at all on the medium surrounding the explosion, for the media of interest. Despite widespread use of this algorithm, the physical reason for the existence of such an insensitive interval and the extent to which it would persist for shock waves in a more diverse collection of geologic media has been unclear. In this report we show that the existence of an insensitive interval is most likely a consequence of correlations between

certain properties of the rocks at the U.S. test sites. To demonstrate this we relate the scaled radius \hat{R} of the shock front at a given scaled time \hat{t} to these rock properties, using an approximate, analytical model for the propagation of the shock wave. This model is described in the next section. It agrees well with both particle speed and radius vs. time data from nuclear tests and numerical simulations. Within the assumptions of this model, the radius vs. time curve for an explosion in one rock can be used to generate the radius vs. time curve for an explosion of any yield in any rock by applying a certain similarity transformation. By studying these transformations, we show that an insensitive interval appears when the relevant rock properties are correlated in a certain way. We then show that the relevant properties of the rocks found at U.S. test sites correlate in just this way. However, this correlation does not extend to all rocks.

Analytical Model

In order to focus on the effect of the ambient medium on shock wave evolution, we consider here the spherical shock wave produced by release of a very large amount of energy in an infinitesimal volume (a so-called *point explosion*) in homogeneous rock. Some of the complications that can arise when the hydrodynamic source is of finite size and aspherical and the medium is inhomogeneous are mentioned at the end of this report. Our analysis assumes that the evolution of the shock wave is adequately described by the following model.

Studies of shock waves in solids (see Zel'dovich and Raizer 1967) have shown that for many materials, the relation between the speed D of a shock front and the particle speed u just behind it is approximately linear for large u , that is

$$D_i \equiv \frac{dR_i}{dt} = A_i + B_i u, \quad (3)$$

where A_i and B_i are constants. The subscript i denotes the material. In general, $D(u)$ will deviate from this relation as u decreases. In the present analysis we shall assume that $D(u)$ can be adequately represented by a single linear relation of the form (3) over the range of u that is of interest.

We shall also assume that the particle speed just behind the shock front is related to the yield W_i of the explosion by the expression (Lamb 1987a; Moss 1988)

$$\frac{4\pi}{3} \rho_{0i} R_i^3(t) u^2(t) = f_i W_i, \quad (4)$$

where $R_i(t)$ is the radius of the shock front at time t , ρ_{0i} is the mass density of the rock in its unshocked state, and f_i is a dimensionless factor that describes how the energy of the explosion is partitioned between kinetic energy of bulk motion and internal energy, and how the velocity, density, and internal energy of the shocked material vary with position. In general, f_i is a constant when the shock wave is strong, but changes somewhat as the shock wave weakens (Lamb 1987a). Expression (4) with f_i constant agrees relatively well with particle speed data over a broad interval in time (Moss 1988). In the present analysis, we shall assume that f_i can be treated as constant for the times of interest.

Given these assumptions, equation (3) with u given by equation (4) can be integrated analytically to yield a simple, closed expression for $R_i(t)$. First we rewrite equation (3) in terms of the dimensionless variables (Lamb 1987a)

$$x = R_i/L_i \quad \text{and} \quad \tau = t/T_i, \quad (5)$$

where

$$L_i = \left(\frac{3f_i W_i B_i^2}{4\pi \rho_{0i} A_i^2} \right)^{1/3} \quad \text{and} \quad T_i = \frac{L_i}{A_i}. \quad (6)$$

The properties of the medium enter the characteristic length L_i and the characteristic time T_i through the constants ρ_{0i} , A_i , B_i , and f_i , while the yield enters through W_i . The constants A_i and B_i are determined by the shock adiabat while f_i reflects the release adiabat.

In terms of the non-dimensional variables (5), equation (3) becomes

$$\frac{dx}{d\tau} = 1 + \frac{1}{x^{3/2}}. \quad (7)$$

The solution of equation (7) is (Lamb 1987a)

$$\tau(x) = x + \frac{1}{3} \ln \left(\frac{x + 2\sqrt{x} + 1}{x - \sqrt{x} + 1} \right) - \frac{2}{\sqrt{3}} \left[\frac{\pi}{6} + \tan^{-1} \left(\frac{2\sqrt{x} - 1}{\sqrt{3}} \right) \right]. \quad (8)$$

At small radii ($x \ll 1$), this solution reduces to

$$x(\tau) \approx (5/2)^{2/5} \tau^{2/5}, \quad (9)$$

which is the behavior of a *strong, self-similar shock wave* (Sedov 1959). At large radii ($x \gg 1$), the solution becomes

$$x(\tau) \approx \text{const.} + \tau, \quad (10)$$

which describes a constant-speed plastic wave. In the transition interval between these regimes, equation (8) provides a simple interpolation between the strong shock wave and the plastic wave that agrees quite well with field data and numerical simulations (Lamb 1987a,b; Moss 1988).

Within the assumptions of the present model, any explosion is completely defined by its yield W_i and the ambient medium. The ambient medium is completely specified by the quantities ρ_{0i} , A_i , B_i , and f_i . The radius vs. time curve for any explosion can be generated from the function (8) by applying the similarity transformation

$$R_i(t) = L_i x(t/T_i). \quad (11)$$

Conversely, this result implies that the yield of any explosion can be determined by comparing measured values of $R(t)$ with the values given by equation (11), if the quantities ρ_{0i} , A_i , B_i , and f_i are known.

The result (11) also implies that if the radius vs. time curve for explosion i is known, then the radius vs. time curve for any other explosion j can be generated, provided that ρ , A , B , f , and W are known for both explosions. More precisely, the radius vs. time curve $R_j(t)$ for any explosion j is given in terms of the radius vs. time curve $R_i(t)$ for explosion i by the similarity transformation

$$R_j(t) = (L_j/L_i) R_i(T_i t/T_j). \quad (12)$$

Before proceeding further, we note that the approach outlined in the following sections depends only on the existence of a similarity transformation of the form (12), and not on the values of the characteristic scales L and T , or the particular form of the function $x(\tau)$. Thus, even if the actual values of L_i and T_i differ somewhat from the values given by expression (6), or the actual functional form of $x(\tau)$ differs from that of equation (8), the approach outlined below is still valid.

Existence of an Insensitive Interval

In the present section we use the analytical model described in the previous section to explore the conditions under which an insensitive interval exists.

According to our earlier definition, an insensitive interval exists if, for explosions of the same yield, there is an interval in time Δt about some time t_0 during which the radii R_i of the shock waves in all the media in the collection of interest are nearly equal. When this is true, the yield of any explosion can be estimated approximately by applying equation (1), or an alternate formula, to the $R(t)$ data in this interval, without regard to the particular medium in which the explosion occurred.

To formulate a more precise definition of the insensitive interval, consider the shock waves produced by an explosion of the *same yield* in two *different media* i and j . The difference between the resulting radius vs. time curves $R_i(t)$ and $R_j(t)$ at time t is

$$\Delta R_{ij}(t) \equiv R_i(t) - R_j(t). \quad (13)$$

We define the *insensitive time* t_0 as the time at which the yield estimate is least sensitive to the ambient medium, for media in the collection of interest. If the yield is estimated by adjusting the value of W in formula (1) so that the radius given by this formula agrees with the measured radius, then the insensitive time t_0 is the time at which the average over the collection of media of some appropriate function of ΔR_{ij} , such as $|\Delta R_{ij}(t)|^2$, is a minimum. The size of $\langle |\Delta R_{ij}(t_0)|^2 \rangle$ is then a measure of the sensitivity to the ambient medium of yield estimates made at t_0 , and in general will not be zero. The extent Δt of the "insensitive interval" can be calculated from the way in which $\langle |\Delta R_{ij}(t)|^2 \rangle$ varies with time about t_0 , given a criterion for the maximum acceptable yield error.

With these definitions, one can calculate t_0 and Δt for a collection of n different media by applying standard statistical techniques (Lamb, Callen, and Sullivan 1989). However, analysis of a collection of two different media captures the most important features of the problem and is considerably more transparent. Therefore, for pedagogical purposes we shall treat a collection of just two different media in the present report. A collection of n media can be treated by a straightforward extension of the methods described here.

The radius vs. time curves for two different geologic media typically cross, as illustrated by the sample curves shown in the left panel of Figure 1. We first assume that $R_i(t)$ and $R_j(t)$ cross at one and only one point, and then discuss what happens if they do not cross at all (the case of more than one crossing, if relevant, can be treated by a generalization of the following analysis).

Any monotonically increasing function of $|\Delta R_{ij}(t)|$ is a minimum when $R_i(t)$ and $R_j(t)$ cross. Thus, the insensitive time t_{ij}^0 is the root of the equation

$$\Delta R_{ij}(t) = 0. \quad (14)$$

Now suppose the curves $R_i(t)$ and $R_j(t)$ are generated from a curve $x(\tau)$ by similarity transformations of the form (11). Then

$$\Delta R_{ij} = L_i x(\tau_i) - L_j x(\tau_j), \quad (15)$$

where $\tau_i = t/T_i$ and $\tau_j = t/T_j$. Note that the dimensionless times τ_i and τ_j that correspond to the *same* time t are in general *different* for the two media.

In order to make further progress, we need to relate $x(\tau_j)$ and $x(\tau_i)$. If $x(\tau)$ varies sufficiently slowly in the region of interest, we can relate $x(\tau_j)$ and $x(\tau_i)$ by expanding both in a Taylor series about

$$\bar{\tau}_{ij} \equiv \frac{1}{2}(\tau_i + \tau_j). \quad (16)$$

Keeping only the three leading terms, the result is

$$x(\tau_i) = x(\bar{\tau}_{ij}) + (\tau_i - \bar{\tau}_{ij}) x'(\bar{\tau}_{ij}) + \frac{1}{2}(\tau_i - \bar{\tau}_{ij})^2 x''(\bar{\tau}_{ij}), \quad (17)$$

with a similar expression for $x(\tau_j)$. The primes indicate differentiation with respect to τ . Substituting these expansions into equation (15), one finds

$$\Delta R_{ij} = \Delta L_{ij} x(\bar{\tau}_{ij}) - \bar{L}_{ij} \left(\frac{\Delta T_{ij}}{\bar{T}_{ij}} \right) \bar{\tau}_{ij} x'(\bar{\tau}_{ij}) + \frac{1}{8} \Delta L_{ij} \left(\frac{\Delta T_{ij}}{\bar{T}_{ij}} \right)^2 (\bar{\tau}_{ij})^2 x''(\bar{\tau}_{ij}), \quad (18)$$

where

$$\Delta L_{ij} \equiv L_i - L_j \quad \text{and} \quad \Delta T_{ij} \equiv T_i - T_j \quad (19)$$

are the differences in the characteristic lengths and times of the two explosions, and

$$\bar{L}_{ij} \equiv \frac{1}{2}(L_i + L_j) \quad \text{and} \quad \bar{T}_{ij} \equiv \frac{1}{2}(T_i + T_j) \quad (20)$$

are their averages. Note that expression (18) is not an expansion of ΔR_{ij} in powers of ΔL_{ij} or ΔT_{ij} [the coefficients of $\bar{\tau}_{ij} x'(\bar{\tau}_{ij})$ and $(\bar{\tau}_{ij})^2 x''(\bar{\tau}_{ij})$ are exact].

The left side of equation (18) vanishes at the insensitive time t_{ij}^0 [cf. eq. (14)]. Thus, the zero of the right side of this equation gives an estimate, accurate to second order in $\tau_i - \bar{\tau}_{ij}$ and $\tau_j - \bar{\tau}_{ij}$, of the corresponding dimensionless time $\bar{\tau}_{ij}^0$, from which one can calculate t_{ij}^0 using the expression

$$t_{ij}^0 = \frac{2\bar{\tau}_{ij}^0}{\frac{1}{T_i} + \frac{1}{T_j}}. \quad (21)$$

As we show below, for the rock collections of interest to us the third term on the right side of equation (18) is typically quite small compared to the first two terms, and we therefore neglect it in estimating $\bar{\tau}_{ij}^0$. With this approximation, $\bar{\tau}_{ij}^0$ is determined implicitly by the condition

$$\Delta L_{ij} x(\bar{\tau}_{ij}) = \bar{L}_{ij} \frac{\Delta T_{ij}}{\bar{T}_{ij}} \bar{\tau}_{ij} x'(\bar{\tau}_{ij}) \quad (22)$$

or, in a more compact form,

$$\alpha(\bar{\tau}_{ij}) = M_{ij}, \quad (23)$$

where

$$\alpha(\tau) \equiv \frac{d \ln x}{d \ln \tau} \quad \text{and} \quad M_{ij} \equiv \frac{\bar{T}_{ij}}{\bar{L}_{ij}} \frac{\Delta L_{ij}}{\Delta T_{ij}}. \quad (24)$$

Note that the left side depends only on the properties of the medium-independent function $x(\tau)$, while the right side of equation (23) depends only on the properties of the two ambient media. The radius vs. time curves cross, if at all, when the logarithmic derivative $\alpha(\bar{\tau}_{ij})$ equals M_{ij} .

The development to this point requires only that one be able to generate the radius vs. time curves $R(t)$ of different explosions from some function $x(\tau)$ by applying a similarity transformation of the form (11) to this $x(\tau)$. If $x(\tau)$ is given by equation (8), we can be more specific about the existence and location of a crossing point. For this $x(\tau)$, the logarithmic derivative $\alpha(\tau)$ increases monotonically from 0.4 to 1 as τ increases from 0 to ∞ [see eqs. (9) and (10)]. Thus, there can be at most one crossing point. The radius vs. time curves $R_i(t)$ and $R_j(t)$ cross if

$$0.4 \leq M_{ij} \leq 1. \quad (25)$$

They do not cross if M_{ij} lies outside this interval. To summarize these results for two media, we have shown that whether the radius vs. time curves for two different media cross, and the time of crossing if they do, is determined by the characteristic lengths and times defined by the properties of the two media.

To apply these results to explosions in a collection of many media, we first note that if two media are very similar, then ΔR_{ij} will be small over a broad interval in time. In this case the time of intersection is very sensitive to differences in the properties of the two media, but is of little interest, because the radius vs. time curves are almost the same over an extended interval in time. The crossing points of most interest are those for dissimilar media. In considering a collection of many media, we can say that the radius vs. time curves for the various media will all cross each other at about the same time if (1) M_{ij} has approximately the same value for all explosions i and j in the collection and (2) this value lies in the interval $[0.4,1]$. The optimal insensitive time t_0 for the collection of media is then determined implicitly by the appropriate generalization of equation (23) (Lamb, Callen, and Sullivan 1989). Even if the *time of intersection* for a pair of media in the collection is significantly different from t_0 , the *difference in the radii* of the shock fronts at t_0 may still be small, if the two media have properties near the average properties of the collection.

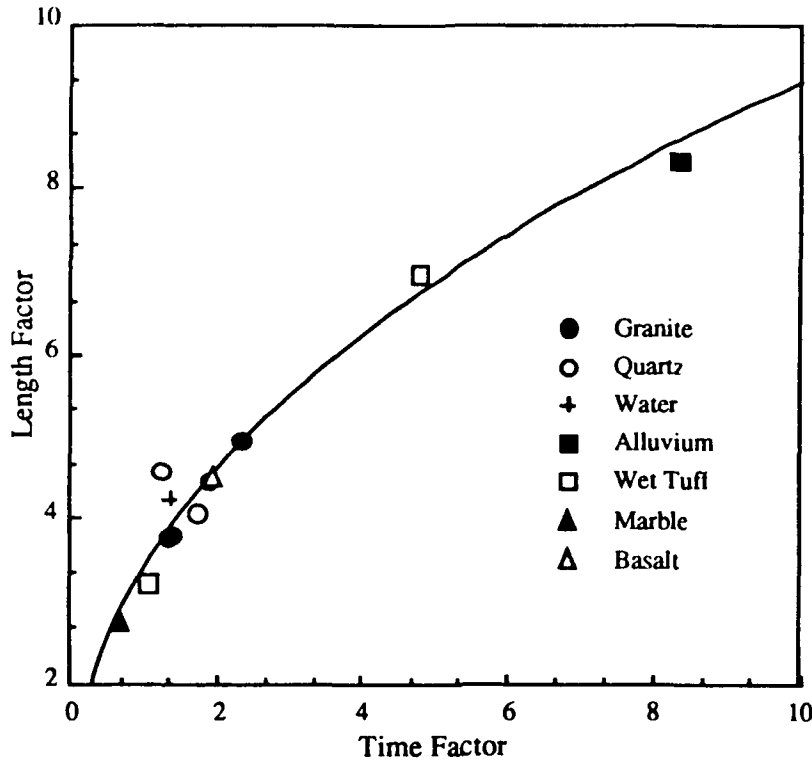


Fig. 2.—Plot of L_i vs. T_i calculated from equations (6) for the media listed in Table 1. Note that all the data points fall close to the curve $L = 3.39 T^{0.44}$.

Application to Rocks at U.S. Test Sites

Figure 2 shows a plot of the characteristic lengths L_i vs. the characteristic times T_i , for the collection of geologic media listed in Table 1. The values were calculated from equations (6), assuming $f_i = 0.53$ for all the media (see Lamb 1987a,b; Moss 1988). The materials listed in Table 1 are typical of the geologic media found at U.S. test sites.

The data points for these media all lie close to the curve $L = 3.39 T^{0.44}$, for which $d \ln L / d \ln T = 0.44$. This suggests that M_{ij} should be ~ 0.44 for all the media in this sample. In fact, the mean value of M_{ij} for the media in Table 1 is 0.53; most of the M_{ij} cluster near this value and all lie in the range 0.3–0.7. Moreover, the second-order correction to $\alpha(\bar{\tau}_{ij})$ is 0.05 or less for these media. Thus, for a point explosion in homogeneous rock, the analysis of the previous sections predicts an insensitive interval near the time when $\alpha(\bar{\tau}_{ij}) \approx 0.53$, or

$$\frac{\partial \ln R}{\partial \ln t} \approx 0.53. \quad (26)$$

This result is in good agreement with the empirical observation [cf. Fig. 1 and eq. (1)] that there is an insensitive interval near the time when

$$\frac{\partial \ln R}{\partial \ln t} \approx 0.48. \quad (27)$$

Discussion

The analysis presented here is approximate in several respects. First, the solution (8) for

TABLE 1
Equations of State^a

Rock	ρ_0 (g cm ⁻³)	A (km s ⁻¹)	B	Ref.
Westerly Granite	2.62	2.103	1.629	1
Granite	2.65	2.7	1.4	1
Granite	2.67	2.8	1.45	2
Quartz Crystal	2.65	2.35	1.56	1
Quartz Sand	1.6	2.32	1.04	1
Quartz (high u)	2.65	4.56	1.25	7
Vacaville Basalt	2.86	2.31	1.62	4
Dolomite	2.7	4.01	1.3	6
Wet Tuff	1.95	1.45	1.62	2
Wet Tuff	2.2	3.0	1.11	3
Dry Alluvium	1.78	1	1.4	5
Water	0.998	3.09	1.16	1

^aThe quantities ρ_0 , A , and B are the unshocked density and the parameters in the Hugoniot (3). ¹M. van Thiel (1977). ²W. C. Moss (1988), from fitting a Mie-Grüneisen equation of state to tabulated equations of state for granite (J. D. Johnson and S. P. Lyon 1985) and wet tuff (J. D. Johnson, unpublished). ³R. C. Bass (1966). ⁴A. H. Jones et al. (1968) and LLNL Equation-of-State File, S-Division (1964). ⁵W. R. Perret and R. C. Bass (1975). ⁶A. N. Dremin and G. A. Adadurov (1959). ⁷J. D. Johnson and S. P. Lyon (1985).

a point explosion in a homogeneous medium is only approximate, although it agrees well with both particle speed data and with radius vs. time data over a broad interval in time. Second, in computing the values of L_i and T_i for the media in Table 1 we have assumed that $f_i = 0.53$ for all these media. While the actual values of f_i may be similar for these rocks (Moss 1988), they are not expected to be identical. The values of L_i and T_i can easily be corrected for differences in f_i once the best values of f_i have been determined.

Third, actual shock waves are not produced by spherically symmetric point explosions. The emplacement holes currently used in U.S. tests have radii as large as 1.5 m and emplacement holes with larger radii are planned for the future. Moreover, the nuclear charge and diagnostic canisters may be many meters in length. As a result, the source of the shock wave is vapor and radiation filling a volume with a dimension of meters. Also, nuclear explosions are usually not spherically symmetric, causing the expanding shock wave to be aspherical initially. Although the shock wave produced by an aspherical source of finite size will evolve toward a spherically-symmetric, self-similar wave if the shock front envelops a mass much greater than that of the nuclear charge while the shock wave is still strong (Barenblatt 1979), even the shock waves produced by a 150 kt explosion weaken too quickly for this to occur, given current U.S. testing practices (Lamb 1988). Finally, the geologic media in which tests are conducted often are not homogeneous, but have layers, voids, and other structures that can affect the propagation of the shock wave.

Despite these complications, we think that the analysis presented here points to the physical reason for the existence of an insensitive interval for the rocks within U.S. test experience, namely, a correlation between the basic properties of these rocks (cf. Fig. 2).

The existence of an insensitive interval *cannot* be attributed to strong, self-similar motion of the shock wave. For the reasons mentioned above, the shock wave is not self-similar during the insensitive interval, for current test geometries and the yields permitted by the Threshold Test Ban Treaty. In fact, the shock wave is not even strong during this interval (Lamb 1988). If the shock wave were strong, the logarithmic derivative of the radius with respect to time during the insensitive interval would be 0.4 (Sedov 1959), rather than the value ~ 0.48 that is observed.

CONCLUSIONS AND RECOMMENDATIONS

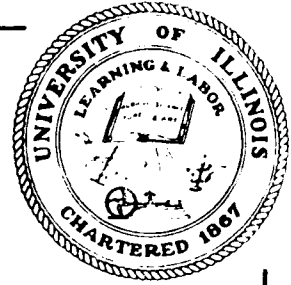
Using an approximate but relatively accurate analytical model of shock wave propagation, we have shown that the "insensitive interval" observed in nuclear explosions in the rocks within U.S. test experience is most likely due to correlations among certain properties of these rocks. We expect that the analytical approach described here can be used to predict whether an insensitive interval exists for collections of rocks that include media outside U.S. test experience.

We recommend that efforts be made to (1) improve the analytical model used here, (2) investigate the underlying physical basis for the observed correlation among the relevant properties of the rocks listed in Table 1, and (3) explore the evidence that similar correlations exist among other classes of media.

REFERENCES

- Barenblatt, G.I. 1979, *Similarity, Self-Similarity, and Intermediate Asymptotics* (New York: Consultants Bureau).
- Bass, R. C. 1966, *Rep. SC-RR-66-548*, (Albuquerque, NM: Sandia Corp.).
- Bass, R. C. and G. E. Larsen. 1977, *Rep. SAND 77-0402* (Albuquerque, NM: Sandia National Laboratories).
- Dremin, A. N. and G. A. Adadurov. 1959, *Soviet Physics-Doklady* 4, 972.
- Johnson, J. D. and S. P. Lyon. 1985, *Rep. LA-23391-MS* (Los Alamos, NM: Los Alamos National Laboratory).
- Jones, A. H., et al. 1968, *Interim Report, Contract NAS2-3427* (Warren, MI: General Motors Tech. Center).
- Lamb, F. K. 1987a, *ACDIS WP-2-87-2* (Urbana, IL: University of Illinois Program in Arms Control, Disarmament, and International Security, February, 1987).
- Lamb, F. K. 1987b, *An Independent Assessment of CORRTEX*, Report prepared for the Congressional Office of Technology Assessment (April, 1987).
- Lamb, F. K. 1988, in *Nuclear Arms Technologies in the 1990s*, edited by D. Schroerer and D. Hafemeister (New York: American Institute of Physics), p. 109.
- Lamb, F. K., B. W. Callen, and J. D. Sullivan. 1989, in preparation.
- Moss, W. C. 1988, *J. Appl. Phys.* 63, 4771.
- Perret, W. R. and R. C. Bass. 1975, *Rep. SAND 74-0252* (Albuquerque, NM: Sandia Corp.).

- Sedov, L. I. 1959, *Similarity and Dimensional Methods in Mechanics* (New York: Academic Press).
- van Thiel, M. 1977, *Rep. UCRL-50108* (Livermore, CA: Lawrence Livermore National Laboratory).
- Virchow, C. F., G. E. Conrad, D.M. Holt, and E.K. Hodson. 1980, *Rev. Sci. Inst.* **51**, 642.
- Zel'dovich, Ya. B. and Yu. P. Raizer. 1967, *Physics of Shock Waves and High-Temperature Hydrodynamic Phenomena* (New York: Academic Press).



Hydrodynamic Determination of the Yield
of Underground Nuclear Explosions

B. W. Callen, F. K. Lamb, and J. D. Sullivan

*Presented at the 12th Annual DARPA/GL Seismic Research Symposium,
Key West, Florida, 18-20 September 1990*

UNIVERSITY OF ILLINOIS AT URBANA-CHAMPAIGN

DEPARTMENT OF PHYSICS

LOOMIS LABORATORY OF PHYSICS

1110 W. GREEN STREET

URBANA, ILLINOIS 61801

HYDRODYNAMIC DETERMINATION OF THE YIELD OF UNDERGROUND NUCLEAR EXPLOSIONS

B. W. Callen, F. K. Lamb, and J. D. Sullivan
University of Illinois at Urbana Champaign
Department of Physics and
Program in Arms Control, Disarmament, and International Security
1110 West Green Street, Urbana, IL 61801

Contract: F19628-88-K-0040

OBJECTIVE

The overall objective of this project is to improve analysis and interpretation of shock wave data that have been and will be gathered to help monitor agreed limitations on underground nuclear testing. Specific objectives are to explore the effects of the ambient geologic medium on yield estimates made using shock wave methods, to investigate the effects of different test geometries, and to explore the possibility of using shock wave methods to monitor yield limitations well below the current yield limit of 150 kt.

SUMMARY

During the past year, we have (1) used an approximate analytical model for the evolution of the shock wave from an underground nuclear explosion, together with previously collected equation of state data for geologic media relevant to U. S. and Soviet test sites, to develop a method for estimating the yield of underground nuclear tests, (2) explored the usefulness and limitations of various simple high-pressure equations of state for geologic media, and (3) analyzed the requirements for scaling of shock waves produced by underground nuclear explosions and numerical simulations of such explosions. In this report we describe how a simple analytical model of the evolution of the shock wave can be used to produce relatively accurate estimates of the yield of underground nuclear explosions.

Hydrodynamic Methods for Yield Estimation

The strength of the shock wave generated by an underground nuclear explosion increases with the yield of the explosion, all other things being equal. As a result, the peak pressure, peak density, and shock speed at a given radius all increase monotonically with the yield. Hence, the yield of the explosion can be estimated by comparing measurements of these quantities with the values predicted by a model of the shock wave in the relevant geologic medium. Recently, the United States and the Soviet Union have signed new verification protocols (The White House 1990) that allow measurements of the radius of the shock front using the CORTEX technique (Virchow, *et al.* 1980) for treaty monitoring under some circumstances.

Most shock wave based algorithms for estimating the yield of underground nuclear explosions have focused on the so-called *hydrodynamic phase*, because the evolution of

the shock wave during this phase is relatively simple. The hydrodynamic phase of the explosion begins when the outward flow of energy via radiation becomes unimportant. This occurs about 10–100 μs after detonation, depending on the yield and the composition of the material surrounding the nuclear charge. The explosion can then be described using the equations of hydrodynamics alone. During the hydrodynamic phase, the radial stress produced by the shock wave greatly exceeds the critical stress at which the surrounding rock becomes plastic, and the shocked rock can be treated as a fluid. The shock wave weakens as it expands, and eventually the strength of the rock can no longer be neglected. This marks the end of the hydrodynamic phase. Yield estimation methods that use measurements taken during the hydrodynamic phase are called *hydrodynamic methods*.

Analytical Model

All hydrodynamic yield estimation methods require a model of the evolution of the shock wave. Models in recent or current use range in sophistication from an empirical power-law formula that assumes the evolution is completely independent of the medium (Bass and Larsen 1977; see also Heusinkveld 1982; Lamb 1988) to numerical simulations based on detailed equations of state (see Moss 1988; King, *et al.* 1989; Moran and Goldwire 1989). Although state-of-the-art numerical simulations are expected to be highly accurate for spherically symmetric, tamped explosions in homogeneous media, the detailed equation of state data needed for such calculations are only available for a few geologic media. Thus, a simple analytical model of the shock wave produced by such explosions can be quite useful, as it allows one to analyze how the evolution depends on the medium and the yield in a convenient manner. The particular analytical model we utilize in this paper has the additional virtue that it produces very good estimates of the yields of actual underground nuclear tests as we show below.

We summarize here an approximate analytical model of the hydrodynamic evolution of the shock wave produced by a point explosion in a homogeneous medium. Such a shock wave is necessarily spherically symmetric. In the model, the compression of the medium at the shock front is treated exactly, using the Rankine-Hugoniot jump conditions and the Hugoniot of the ambient medium. The rarefaction that occurs in material behind the advancing shock front is treated approximately, via an *ansatz* relating the specific kinetic energy of the fluid just behind the shock front to the mean specific energy within the shocked volume. This model was originally proposed by Lamb (1987), who showed that it is exact for strong, self-similar shock waves. The model was later proposed independently by Moss (1988). A detailed description and assessment of the model is given in Lamb, Callen, and Sullivan (1990).

We assume that the speed D of the shock front in a frame at rest with respect to the unshocked medium may be expressed in terms of the particle speed u just behind the shock front, that is,

$$D \equiv dR/dt = H(u), \quad (1)$$

where the Hugoniot $H(u)$ depends on the medium.

The specific kinetic energy of the fluid just behind the shock front can be related to

the mean specific energy within the shocked volume via the expression

$$u^2 = f \left(\frac{3W}{4\pi R^3 \rho_0} \right), \quad (2)$$

where W is the yield of the explosion, R is the radius of the shock front, ρ_0 is the mass density of the rock in its unshocked state, and f is a dimensionless factor that depends upon the velocity, density, and specific internal energy distributions within the shocked volume. In general, f is independent of R when the shock wave is strong, but it may vary as the shock wave weakens (Lamb 1987; Lamb, Callen, and Sullivan 1990).

In the model, f is assumed to be independent of the shock front radius R for all shock front radii of interest, including those for which the shock is no longer strong (Lamb 1987; Moss 1988; Lamb, Callen, and Sullivan 1990). Expression (2) with $f = 0.53$ agrees relatively well with particle speed data over a broad interval in time (Moss 1988; Lamb, Callen, and Sullivan 1990). In the present report, we shall use this value and assume that f can be treated as constant for the times of interest.

The assumption that f is independent of R leads to a simple approximate equation of motion for the shock front. With this assumption, the right side of equation (1) becomes a known function of R , and equation (1) becomes a first-order differential equation for R , namely

$$dR/dt = F(R). \quad (3)$$

This equation can be integrated directly to determine the radius of the shock front as a function of time, as pointed out by Lamb (1987) and Moss (1988).

Studies of shock waves in solids (see Zel'dovich and Raizer 1967) have shown that for many materials, the relation between the speed D of a shock front and the particle speed u just behind it is approximately linear for large u , that is

$$D \equiv \frac{dR}{dt} = A + Bu, \quad (4)$$

where A and B are constants. In general, $D(u)$ will deviate from this relation as u decreases. If we assume for the moment that $D(u)$ can be adequately represented by a single linear relation of the form (4) over the range of interest, we obtain an interesting and useful analytical solution to the differential equation (3).

Linear Hugoniot—First, we rewrite equation (4) in terms of the dimensionless variables (Lamb 1987; Lamb, Callen, and Sullivan 1990)

$$x = R/L \quad \text{and} \quad \tau = t/T, \quad (5)$$

where

$$L = \left(\frac{3fWB^2}{4\pi\rho_0 A^2} \right)^{1/3} \quad \text{and} \quad T = \frac{L}{A}. \quad (6)$$

The characteristic length L and the characteristic time T depend on the medium through the constants ρ_0 , A , B , and f , and also scale as the cube-root of the yield W . The

length L is the radius that separates the strong shock regime, where $D \propto R^{-3/2}$, from the low-pressure plastic wave regime, where $D \approx \text{const.}$ In terms of the non-dimensional variables (5), equation (4) becomes

$$\frac{dx}{d\tau} = 1 + \frac{1}{x^{3/2}}. \quad (7)$$

The solution of equation (7) is (Lamb 1987; Lamb, Callen, and Sullivan 1990)

$$\tau(x) = x + \frac{1}{3} \ln \left(\frac{x + 2\sqrt{x} + 1}{x - \sqrt{x} + 1} \right) - \frac{2}{\sqrt{3}} \left[\frac{\pi}{6} + \tan^{-1} \left(\frac{2\sqrt{x} - 1}{\sqrt{3}} \right) \right]. \quad (8)$$

At small radii ($x \ll 1$), this solution reduces to

$$x(\tau) \approx (5/2)^{2/5} \tau^{2/5}, \quad (9)$$

which is the behavior of a *strong, self-similar* shock wave (Sedov 1959). At large radii ($x \gg 1$), the solution becomes

$$x(\tau) \approx \text{const.} + \tau, \quad (10)$$

which describes a constant-speed plastic wave. In the transition interval between these regimes, equation (8) provides a simple interpolation between the strong shock wave and the plastic wave that agrees quite well with field data and numerical simulations (Lamb 1987; Moss 1988; Lamb, Callen, and Sullivan 1990).

Within the assumptions of the present model, any explosion is completely defined by its yield W and the ambient medium, which in turn is completely defined by the quantities ρ_0 , A , B , and f . The shock front radius vs. time curve for any explosion can be generated from the function $x(\tau)$ by applying the similarity transformation

$$R(t) = L x(t/T). \quad (11)$$

Conversely, this result implies that the yield of any explosion can be determined by comparing measured values of $R(t)$ with the values given by equation (11), if the quantities ρ_0 , A , B , and f are known. In particular, since the characteristic length and time L and T scale as the cube-root of the yield, the radius vs. time curve (11) automatically satisfies cube-root scaling. That is, if $R = g(t)$ is the radius vs. time curve for an explosion with a yield of 1 kt, then the curve for an explosion with a yield of W kt in the same medium is given by

$$R = W^{1/3} g(t/W^{1/3}). \quad (12)$$

Radius vs. time curves for various yields are generated by using the cube-root scaling exhibited by the model.

The curve (11) also satisfies a more general scaling that involves the material properties, as shown by equations (6). The result (11) also implies that if the radius vs. time curve for explosion i is known, then the radius vs. time curve for any other explosion j can be generated, provided that ρ_0 , A , B , f , and W are known for both explosions. More

precisely, the radius vs. time curve $R_j(t)$ for any explosion j is given in terms of the radius vs. time curve $R_i(t)$ for explosion i by the similarity transformation

$$R_j(t) = (L_j/L_i) R_i(T_i t/T_j). \quad (13)$$

This similarity transformation was previously exploited to show that the existence of an 'insensitive interval' in the evolution of shock waves in materials at U. S. test sites is most likely the result of correlations between the properties of those materials (Lamb, Callen, and Sullivan 1989).

Arbitrary Hugoniot. Although for many materials the Hugoniot at high particle speeds (or equivalently, at high pressures) is well-described by a single linear relation of the form (4), the Hugoniot at lower particle speeds usually deviates from the high-speed relation. Even if the Hugoniot is not linear over the range of u of interest, it can always be represented to any desired accuracy by a sequence of piecewise-linear segments. In this case, the differential equation (7) still describes the motion of the shock front within each segment of the Hugoniot, but at each break in $D(u)$ new Hugoniot parameters A and B must be introduced. It is possible to write the radius vs. time curve for a piecewise-linear Hugoniot as a sum of standard functions; however, in practice it is more convenient to integrate the differential equation numerically. The radius vs. time curve predicted by the model for any physically allowed Hugoniot obeys the cube-root scaling (12).

Yield Estimation

We now use the model discussed above to estimate yields by comparing the radius vs. time curve it predicts with data from four underground nuclear tests conducted by the United States. The four tests are *Piledriver*, *Cannikin*, *Chiberta*, and a test that we call *NTS-X*, since its name has not been reported in the open literature. (A more detailed discussion of these four events, and of the utility of this model in yield estimation, can be found in Lamb, Callen, and Sullivan [1990]). The radius vs. time data from the first three events were obtained using the so-called SLIFER technique (Heusinkveld and Holzer 1964). These data were kindly provided to us by M. Heusinkveld (1987, private communication); see also Heusinkveld (1986). The radius vs. time data from the event *NTS-X* were taken from Heusinkveld (1979); the technique used to obtain it was not reported. To our knowledge, no radius vs. time measurements made using the more recently developed CORTEX technique (Virchow, *et al.* 1980) are publicly available. We first briefly describe each event.

Piledriver.—The *Piledriver* event was an explosion conducted in granite at the Nevada Test Site on 1966 June 2 and had a yield of 62 kt (U. S. Department of Energy 1987).

Cannikin.—The *Cannikin* event was an explosion conducted in basalt at Amchitka Island, Alaska, on 1971 November 6. The official yield of this event remains classified; the U. S. Department of Energy (1987) has said only that it was less than 5 megatons. The data from *Cannikin* that were given to us had been scaled by dividing both the radius and the time measurements by the cube-root of the official yield. If cube-root scaling were exact, this would make the radius vs. time curve appear identical to the curve that would result from detonation of a 1 kt device in the same medium. As explained in Lamb, Callen, and Sullivan (1990), the validity of cube-root scaling for underground nuclear explosions

needs to be investigated more carefully. However, since the simple analytical model we are exploring exhibits exact cube-root scaling, comparisons of this model with scaled and unscaled data will give the same result. We therefore treat the data from this explosion as though it had been produced by a 1 kt explosion.

Chiberta. The *Chiberta* event was an explosion conducted in wet tuff at the Nevada Test Site on 1975 December 20. The official yield of this explosion remains classified; the U. S. Department of Energy (1987) has said only that it was between 20 and 200 kilotons. Using seismic data, Dahlman and Israelson (1977) estimate that the yield of *Chiberta* was 160 kt. Like the data from *Cannikin*, the radius vs. time data from *Chiberta* that were given to us had been scaled by the cube-root of the official yield. We therefore treat the data from *Chiberta* as though it had been produced by a 1 kt explosion.

NTS-X. The event we call *NTS-X* was an explosion conducted at the Nevada Test Site. Radius vs. time data from this explosion were reported by Heusinkveld (1979), who states that the official yield was 54.2 kt. Heusinkveld surmises that the ambient medium is saturated wet tuff, the ambient medium of most tests conducted at the Nevada Test Site. In modeling *NTS-X*, we assumed that the explosion did occur in wet tuff.

The analytical model outlined in the previous section describes a point explosion in a homogeneous medium, which necessarily produces a spherically symmetric shock wave. In reality, the shock wave produced by an underground nuclear test evolves from an aspherical source of finite size surrounded by a medium that is inhomogeneous, at least to some extent. We have investigated the conditions under which cube-root scaling is likely to be valid for shock waves produced by spherically symmetric sources of finite size (Lamb, Callen, and Sullivan 1990) and find that the requirements for cube-root scaling are unlikely to be satisfied for underground nuclear tests conducted according to current U. S. testing practices. Thus, cube-root scaling is at best only approximately valid during the hydrodynamic phase. Despite our lack of detailed knowledge of the conditions under which the above tests were conducted and the data collected, we find that the model provides a remarkably good description of the field data considered here.

In comparing the model with the data, we assumed that the sensing cable from which the radius vs. time data were obtained was crushed by the shock wave, and not by an elastic precursor (Lamb 1988).

The inputs to the model are the Hugoniot, the density and the parameter f for the ambient medium in which the event occurred. The Hugoniot can be determined from laboratory measurements made on samples removed from the emplacement and satellite holes. If such measurements were made for the four events analyzed here, they were not made available to us. Therefore, we used generic Hugoniot data for the ambient media of each explosion (see Fig. 1). For *Piledriver*, we used a piecewise-linear representation of the data on polycrystalline quartz compiled by King, *et al.* (1989). We assumed that the granite surrounding the nuclear device emplacement had a density equal to the standard density of quartz, namely 2.65 gm/cm^3 . For *Cannikin*, we used the data on Vacaville basalt obtained by Jones, *et al.* (1968) and Ahrens and Gregson (1964). We assumed that the density was 2.86 gm/cm^3 , equal to that of the samples measured by Jones, *et al.* For *Chiberta* and *NTS-X*, we used the wet tuff Hugoniot data of King, *et al.* (1989), and the density of 1.95 gm/cm^3 given by these authors.

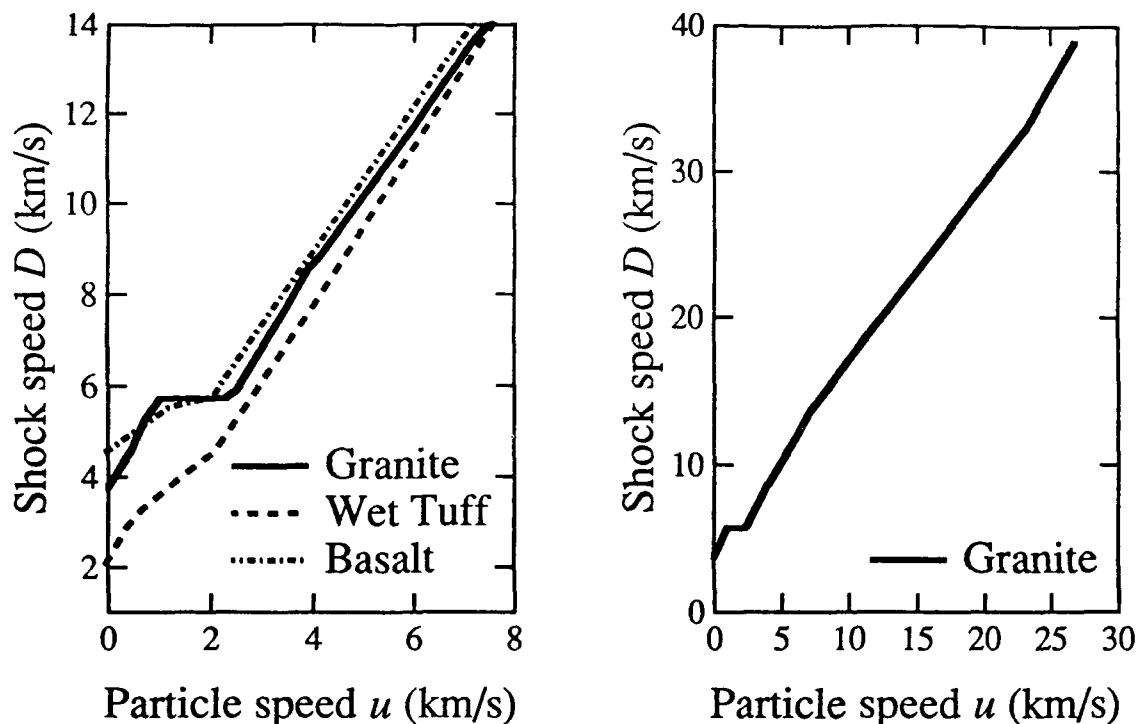


Fig. 1.—*Left*: Low-pressure shock speed–particle speed relations for granite, basalt, and wet tuff. The curves are piecewise-linear representations of Hugoniot data. *Right*: High-pressure shock speed–particle speed relation for granite. The high pressure relations for basalt and wet tuff are extensions of the linear segment at high u in the left figure. Data for granite are taken from the compilation of polycrystalline quartz data by King, *et al.* (1989). Data for basalt are taken from Jones, *et al.* (1968) and Ahrens and Gregson (1964). Wet tuff data are from King, *et al.* (1989)

To determine the yield, we found the model radius vs. time curve that minimized the quantity

$$\frac{1}{N} \sum_i (R(t_i) - R_{\text{model}}(t_i))^2 = 0, \quad (14)$$

where the sum runs over those data points used in the yield estimate. The model is valid only during the hydrodynamic phase, that is, as long as the strength of the ambient medium can be neglected. We chose the radius at which the predicted post-shock pressure p_1 falls below 150 kbar as end of the nominal hydrodynamic phase in all three media, and used only data taken at smaller radii. (150 kbar is roughly three times the critical stress at which granite and basalt become plastic. Although the critical stress for saturated wet tuff is unknown, wet tuff is also a silicate; thus, 150 kbar may be a reasonable estimate for the end of the hydrodynamic phase in this material as well.)

The resulting yield estimates are presented in Table 1. The quantities listed are the

TABLE 1
Yield Estimates^a

Event	Hydrodynamic Only				Full Data Set			
	W_{est} (kt)	N	ΔR_{rms} (m)	$\Delta R_{\text{rms}}/W_{\text{est}}^{1/3}$ (m/kt ^{1/3})	W_{est} (kt)	N	ΔR_{rms} (m)	$\Delta R_{\text{rms}}/W_{\text{est}}^{1/3}$ (m/kt ^{1/3})
<i>Piledriver</i>	62.5	25	0.312	0.079	59.1	33	0.370	0.095
<i>Cannikin</i>	0.92	158	0.020	0.021	0.92	158	0.020	0.021
<i>NTS-X</i>	58.5	34	0.087	0.022	71.5	141	0.320	0.077
<i>Chiberta</i>	0.93	47	0.021	0.021	1.00	108	0.045	0.045

^a W_{est} is the estimated yield in kilotons, N is the number of RVT data points used in the yield estimation, and $\Delta R_{\text{rms}} = [\sum (R_{\text{data}} - R_{\text{model}})^2 / N]^{1/2}$. The RVT data for *Cannikin* and *Chiberta* were scaled to 1 kt. The official yield of *Piledriver* is 62 kt. The yield of *NTS-X* is given by Heusinkveld (1978) as 54.2 kt. For the hydrodynamic yield estimates, data from regions where $p_1 < 150$ kbar were omitted.

estimated yield W_{est} , the number N of data points used in the estimate, and the quantity

$$\Delta R_{\text{rms}} = \left[\frac{1}{N} \sum_i (R(t_i) - R_{\text{model}}(t_i))^2 \right]^{1/2}, \quad (15)$$

which is simply the square root of the quantity (14). Also listed is $\Delta R_{\text{rms}}/W_{\text{est}}^{1/3}$, which can be used to compare the quality of the fits. The first four columns in each table describe the yield estimates obtained by using the data from the hydrodynamic phase (as defined above), whereas the second four columns describe the estimates obtained by fitting the entire data set. For *Piledriver* and *NTS-X*, the estimates are given to the nearest 0.1 kt, whereas for *Cannikin* and *Chiberta*, the estimates are given to the nearest 0.01 kt.

The yield estimates made using only data from the hydrodynamic phase differ from the official yields by 1% for *Piledriver*, 8% for *Cannikin*, 8% for *NTS-X*, and 7% for *Chiberta*. If *all* the data are used to estimate the yield, the results are still quite accurate for three of the four events. The yield estimate for *Cannikin* is unchanged, since all the data lie within the hydrodynamic region. The resulting yield estimate for *Piledriver* is relatively unaffected by the small amount of data outside the hydrodynamic region and differs by 5% from the official yield. For *Chiberta*, the resulting $\Delta W/W$ is $\lesssim 0.5\%$. The resulting yield estimate of *NTS-X*, however, differs by 32% from the yield reported by Heusinkveld (1979). The large difference in sensitivity to the 150 kbar cutoff for *Chiberta* and *NTS-X* is somewhat surprising, since both events supposedly took place in the same medium (although the medium and yield for *NTS-X* are not known for certain) and the data from both events cover the same interval in scaled time (up to ~ 0.6 ms/ $W^{1/3}$). Beyond the hydrodynamic region, the material strength begins to contribute to the speed of the shock front, which therefore moves faster than it would if it were hydrodynamic (see Lamb 1988). This is the direction in which the late-time data from *NTS-X* differs

from the model. However, other features of the model may also be invalid in this region. For example, the assumption that the dimensionless factor f is constant may be a poor approximation beyond the hydrodynamic phase.

CONCLUSIONS AND RECOMMENDATIONS

The approximate analytical model described above gives yield estimates that are within 8% of the official yields of underground nuclear explosions in granite and basalt, and two explosions in wet tuff. For comparison, the U. S. Department of State (1986a,b) has claimed that hydrodynamic methods are accurate to within 15% (at the 95% confidence level) of radiochemical yield estimates for explosions with yields greater than 50 kt in the geologic media in which tests have been conducted at the Nevada Test Site (see also U. S. Congress, Office of Technology Assessment 1988; Lamb 1988). The present model provides yield estimates that are competitive with other hydrodynamic models. We plan to investigate the constancy of the parameter f during the hydrodynamic phase and the dependence of f on the medium, using hydrodynamic simulations.

REFERENCES

- Ahrens, T. J., and V. G. Gregson, Jr. (1964). Shock compression of crustal rocks: data for quartz, calcite, and plagioclase rocks, *J. Geophys. Res.* **69**, 4839.
- Bass, R. C., and G. E. Larsen (1977). Rep. SAND 77-0402 (Albuquerque, NM: Sandia National Laboratories).
- Dahlman, O., and H. Israelson (1977). *Monitoring Underground Nuclear Explosions* (Amsterdam: Elsevier).
- Heusinkveld, M., and F. Holzer (1964). Method of continuous shock front position measurement, *Rev. Sci. Inst.* **35**, 1105.
- Heusinkveld, M. (1979). Analysis of SLIFER data from underground nuclear explosions, Rep. UCRL-52648 (Livermore, CA: Lawrence Livermore National Laboratory).
- Heusinkveld, M. (1982). Analysis of shock wave arrival time from underground nuclear explosions, *J. Geophys. Res.* **87**, 1891.
- Heusinkveld, M. (1986). Shock arrival times in granite, Mem. 0004A (Livermore, CA: Lawrence Livermore National Laboratory).
- Jones, A. H., et al. (1968). Material properties measurements for selected materials, *Interim Report, Contract NAS2-3427* (Warren, MI: General Motors Technical Center).
- King, D. S., B. E. Freeman, D. D. Eilers, and J. D. Johnson (1988). The effective yield of a nuclear explosion in a small cavity in geologic material, *J. Geophys. Res.* **94**, 12375.
- Lamb, F. K. (1987). An approximate solution for ground shock propagation, ACDIS WP-2-87-2 (Urbana, IL: University of Illinois Program in Arms Control, Disarmament, and International Security).
- Lamb, F. K. (1988). Monitoring yields of underground nuclear tests using hydrodynamic methods, in *Nuclear Arms Technologies in the 1990s*, edited by D. Schroerer and D. Hafe-meister (New York: American Institute of Physics), p. 109.
- Lamb, F. K., B. W. Callen, and J. D. Sullivan (1989). Insensitive interval in the evolution of shock waves from underground nuclear explosions, Rep. P/89/5/77 (Urbana, IL: Department of Physics).

- Lamb, F. K., B. W. Callen, and J. D. Sullivan (1990). Shock waves from underground nuclear explosions: I. An approximate analytical model (submitted to *Journal of Geophysical Research*).
- Moran, B. and H. C. Goldwire, Jr. (1989). Effect of source modelling on the inferred yield from an underground nuclear explosion, in *Shock Compression of Condensed Matter 1989*, edited by S. C. Schmidt, J. N. Johnson, and L. W. Davison (Amsterdam: North-Holland), p. 645.
- Moss, W. C. (1988). A method to estimate the yield of an underground nuclear explosion, *J. Appl. Phys.* **63**, 4771.
- Sedov, L. I. (1959). *Similarity and Dimensional Methods in Mechanics* (New York: Academic Press).
- U. S. Congress, Office of Technology Assessment (1988). *Seismic Verification of Nuclear Testing Treaties*, OTA ISC-361 (Washington, D C: Government Printing Office).
- U. S. Department of Energy (1987). *Announced United States Nuclear Tests, July 1945 through December 1986*, NVO-209 (Rev. 7), Nevada Operations Office.
- U. S. Department of State, Bureau of Public Affairs (1986a). U. S. policy regarding limitations on nuclear testing, *Special Report No. 150*.
- U. S. Department of State, Bureau of Public Affairs (1986b). Verifying nuclear testing limitations: possible U. S.-Soviet cooperation, *Special Report No. 152*.
- Virchow, C. F., G. E. Conrad, D. M. Holt, and E. K. Hodson (1980). Microprocessor-controlled time domain reflectometer for dynamic shock position measurements, *Rev. Sci. Inst.* **51**, 642.
- The White House, Office of the Press Secretary, June 1, 1990. *Fact Sheet: The Nuclear Testing Protocols*. (This document is reproduced in *The New York Times*, June 2, 1990, p. 8).
- Zel'dovich, Ya. B. and Yu. P. Raizer (1967). *Physics of Shock Waves and High-Temperature Hydrodynamic Phenomena* (New York: Academic Press).

Effects of Source Parameters on Hydrodynamic Yield Estimation and New Results on the Insensitive Interval

B. W. Callen*, R. A. Fiedler†, F. K. Lamb‡, and J. D. Sullivan

*Department of Physics
and
Program in Arms Control, Disarmament, and International Security
University of Illinois at Urbana-Champaign
1110 West Green Street, Urbana, IL 61801*

Presented at the 13th Annual PL/DARPA Seismic Research Symposium
8-10 October 1991, Keystone, CO

*Current Address: Dept. of Physics, Drury College, 900 North Benton Avenue, Springfield, MO 65802.

†Also, National Center for Supercomputing Applications, University of Illinois at Urbana-Champaign, 605 East Springfield Avenue, Champaign, IL 61820.

‡Also, Dept. of Astronomy, University of Illinois at Urbana-Champaign, 1110 West Green Street, Urbana, IL 61801.

**EFFECTS OF SOURCE PARAMETERS
ON HYDRODYNAMIC YIELD ESTIMATION
AND NEW RESULTS ON THE INSENSITIVE INTERVAL**

B. W. Callen, R. A. Fiedler, F. K. Lamb, and J. D. Sullivan

Department of Physics
and
Program in Arms Control, Disarmament, and International Security
University of Illinois at Urbana-Champaign
1110 West Green Street, Urbana, IL 61801

Contract No. F19628-88-K-0040

ABSTRACT

We explore the accuracy of yield estimation algorithms based on cube-root scaling by computing the apparent yields of a collection of simulated underground nuclear explosions with the same yield but different source parameters. We find that the yield inferred using cube-root scaling can vary by as much as 25% at 0.1 scaled ms for reasonable source parameters. This variation in the inferred yield appears to be due to variation in the fraction of the initial source energy that is transformed into hydrodynamic motion by the time the yield is estimated. Using the empirical result that the pressure in the source region is insensitive to the source parameters at late times, we obtain a simple expression for the energy remaining in the source region. We show that the variation in the energy remaining in the source given by this expression accurately accounts for the dependence of the inferred yield on the initial radius and on the effective adiabatic index of the source material. We also present new results on the location and extent of the "insensitive interval" (that part of the hydrodynamic phase during which the shock front location is relatively insensitive to the ambient medium but is sensitive to the yield) for silicate and carbonate geologic media.

OBJECTIVES

The initial speed of the shock front produced by an underground nuclear explosion increases with the yield (see Lamb, Callen, & Sullivan, 1991). Therefore, measurements of the front radius R as a function of time t can be used to estimate the yield, provided the dependence of the radius vs. time (RVT) curve on the ambient geologic medium is known. The overall objective of this project is to improve the analysis and interpretation of shock wave data that have been and will be gathered to help monitor agreed limitations on underground nuclear testing. Specific objectives are to investigate the effects of different

test geometries and different ambient geologic media. In this paper, we examine the effect of source parameters on the accuracy of yield estimates made using algorithms based on cube-root scaling. We also explore how the interval in the shock front RVT data that minimizes the uncertainties of yield estimates for silicate and carbonate geologic media may be determined.

RESEARCH ACCOMPLISHED

1. Source Effects

1.1. *The Zeus hydrodynamics code*

The work described here extends the work of Moran & Goldwire (1990), who studied the effect of varying the source parameters on yield estimates for a series of simulated explosions in rhyolite. In their computations, the yield was fixed while the source mass, initial radius, and equation of state (EOS) were independently varied. The source material was taken to be either an ideal gas or iron gas, and EOS tables were utilized for the ambient medium and for iron gas.

In this study, EOS tables based on the SESAME Library and obtained from S-Cubed Corporation were used for granite, wet tuff, and aluminum. We solved the ideal fluid equations appropriate for the hydrodynamic regime using the Zeus code developed by M. L. Norman and J. M. Stone at the National Center for Supercomputing Applications at the University of Illinois at Urbana-Champaign. Details of the methods used and numerical tests of the basic Zeus code are described in Norman (1980), Norman, Wilson, & Barton (1980), Norman & Winkler (1986), and Stone & Norman (1992).

The Zeus code uses the method of finite differences and a two-step, operator-split, explicit time-integration scheme. The computational meshes for the momentum components are staggered (offset) with respect to the mesh for the density and energy density in order to reduce the amount of interpolation needed to compute fluxes through the sides of mesh cells. The conservative, monotonicity-preserving advection scheme of van Leer (1977) is employed, and shocks are spread over several cells by introducing an artificial viscosity term (von Neumann & Richtmeyer, 1950). Truncation error terms in this method are second order in time and space. Interfaces between different media are handled in Zeus by the first-order-accurate method of J. M. LeBlanc (private communication, 1974).

For the work reported here, it was necessary to modify the original Zeus program to conserve exactly the total (kinetic plus internal) energy of the system. This was done by choosing the total energy density (rather than the internal energy density) as one of the dependent variables, and rewriting the term representing the work done by pressure forces as a surface integral over each mesh cell. We also modified the Zeus code in order to use EOS data in tabulated form.

All simulations presented here employ a fixed mesh with 200 spherical cells within a

region 40 meters in radius. The ratio of neighboring cell thicknesses is constant throughout the mesh. The radius of the innermost cell is 0.04 meters, and there are 22 cells within one meter of the origin.

1.2. Test case: Sedov-Taylor solution

The explosion produced by a finite, spherically symmetric source in an ideal gas should asymptotically approach the Sedov-Taylor self-similar solution for a point explosion at late times. In one test of our code, we simulated such an explosion. The ambient medium and source material were both taken to be ideal gasses with adiabatic index $\gamma = 1.4$. Initially, the source region had radius $R_s = 1.0$ m and density $\rho_s = 1.4$ kg m⁻³. For simplicity, the yield $W = 125$ kt was assumed to be distributed uniformly throughout the source. The ambient medium initially had density $\rho_0 = 1.4$ kg m⁻³ and pressure $P_0 = 10^5$ Pa.

Figure 1 shows the relative difference $(R - R_{\text{Sedov}})/R_{\text{Sedov}}$ between the shock front radius R predicted by the Zeus code and the radius R_{Sedov} given by the Sedov-Taylor solution. This difference is less than 0.4% beyond $R = 3.3$ m. Figure 2 displays the density profiles for the Zeus results and for the Sedov-Taylor solution at times $t_1 = 5.1 \times 10^{-5}$ ms and $t_2 = 0.35$ ms. The locations of the density peaks at the shock fronts in the numerical simulation and the Sedov-Taylor solution agree very well, despite the spreading of the density peak in the simulation (due to artificial viscosity) as the shock front encounters larger and larger cells. Peak position was found to be virtually independent of the viscosity coefficient assumed. The density profiles agree accurately from the radius of the material interface (about 16 m at time t_2) to the radius of the shock front. Comparable agreement was found between the pressure, energy density, and velocity profiles.

1.3. Explosions in granite

To explore the accuracy of cube-root scaling algorithms, we compared a series of twelve simulated explosions of a 125 kt device in granite. The source material, initial source radius, and source mass were varied in our studies. The parameters of all twelve source models are listed in Table 1; the first was arbitrarily chosen as the reference case. The ambient medium had density $\rho_0 = 2670$ kg m⁻³ and temperature $T_0 = 300$ K for all cases. In the reference case, the explosion is produced by an ideal gas source with adiabatic index $\gamma = 1.4$, initial radius 1.0 m, and mass 10 Mg. The energy of the explosion is initially uniformly distributed within the source. Figures 3, 4, and 5 show the density, velocity, and pressure profiles for the reference explosion at 0, 1.6×10^{-4} , 9.0×10^{-3} , 0.024, 0.12, 0.45, and 1.1 scaled ms (the actual time divided by the cube root of the yield in kilotons). For clarity, the velocity is displayed only at the three latest times.

At early times, the pressure gradient drives a shell of source material outward into the surrounding granite and a rarefaction wave travels inward toward the center of the

explosion. The rarefaction wave eventually reflects from the origin. At late times, there is a steep rise in the density at the interface between the source and the ambient medium. In time the pressure and density in the source region become nearly uniform, whereas the velocity profile in the source region remains jagged due to the presence of trapped waves. At late times, the results for runs with different source parameters are very similar (but not identical) to those for the reference case.

Figures 6, 7, and 8 show the relative inferred yield W/W_{ref} , computed by cube-root scaling the radius vs. time data (typically 75 different values) of the reference explosion so that they agree with the RVT data of the explosion of interest. Note that the scale along the vertical axis is different in each figure. These figures show that the inferred yield is quite sensitive to the effective adiabatic index γ of the source material (see Table 1). For example, the inferred yield is only 74% of the actual yield at 0.1 scaled ms when γ is reduced from 1.4 to 1.2. For ideal gas sources, the inferred yield is nearly independent of source mass. This result is expected since, for such a source, the pressure is independent of the mass density. We obtain similar results for explosions in wet tuff.

For an aluminum source, changing the source mass from 10 to 1 Mg increases the inferred yield by nearly 6%. Similar results were obtained by Moran & Goldwire (1990) for explosions with an iron gas source in rhyolite.

1.4. *Energy remaining in the source region*

RVT data are sensitive only to the fraction of the yield that has been converted from internal energy of the source, where it resides initially, into the shock wave at the time the radius measurements are made. We therefore expect that variations in the internal energy E_s remaining in the source region, which are caused by differences in the initial source radius and the equation of state of the source material, will produce variations in the inferred yield. (The kinetic energy remaining in the source region at late times is negligible compared to the internal energy. For example, we find that the internal energy in the source region of the reference explosion is 7 kt at 1 scaled ms, whereas the kinetic energy in the source region is less than 4×10^{-4} kt.)

To test this hypothesis, we computed E_s at 1 scaled ms for each explosion by numerically integrating the internal energy $\rho \epsilon$ over the source volume V_s . These computations show that the dependence of the inferred yield on the properties of the source is well accounted for by the variation in the energy remaining in the source region at the time of the yield measurement. For example, $E_s = 7$ kt at 1 scaled ms for the reference explosion, whereas for the explosion with source parameters identical to the reference explosion except that $\gamma = 1.2$, $E_s = 26$ kt. We therefore expect the ratio of the apparent yields at 1 scaled ms to be $(125 \text{ kt} - 26 \text{ kt}) / (125 \text{ kt} - 7 \text{ kt}) = 0.84$, which is close to the value 0.82 found from cube-root scaling (see Table 1). Similarly, for the explosion with $M_s = 10$ Mg,

$\gamma = 1.2$, and $R_s = 0.5$ m, we find $E_s = 18$ kt at 1 scaled ms. We therefore expect the apparent yield of this explosion at 1 scaled ms to be a fraction $107 \text{ kt}/118 \text{ kt} = 0.91$ of the yield of the reference explosion; the fraction found by cube-root scaling is 0.87 (again, see Table 1).

An approximate expression for the dependence of the inferred yield on the properties of an ideal-gas source can be derived by considering the adiabatic expansion of the source from its initially uniform state with volume $V_{s,i}$ and pressure $P_{s,i}$. At sufficiently late times in our simulations, the source pressure and density are again nearly uniform, and it is then meaningful to refer to the source pressure P_s . At these times

$$P_s V_s^\gamma = P_{s,i} V_{s,i}^\gamma = (\gamma - 1) W V_{s,i}^{(\gamma - 1)}, \quad (1)$$

and hence

$$E_s = \frac{P_s}{(\gamma - 1)} V_s = \frac{P_s}{(\gamma - 1)} \left[\frac{(\gamma - 1)W}{P_s} V_{s,i}^{(\gamma - 1)} \right]^{(1/\gamma)}. \quad (2)$$

Moreover, we find empirically that at late times P_s is insensitive to the initial properties of the source. Using the appropriate value of P_s in equation (2) therefore allows us to estimate the dependence of E_s , and hence the inferred yield, on the adiabatic index γ of the source material and the initial source volume $V_{s,i}$. The values of E_s at 1 scaled ms (when P_s is approximately 2.2×10^9 Pa) predicted by equation (2) agree with the results from direct numerical integration to within 1%.

2. Insensitive Interval

In using RVT data to estimate the yield of an underground nuclear explosion, one must combine an accurate model of shock wave propagation in the ambient medium with knowledge of the parameters that characterize the response of the medium to the shock wave. Since uncertainties in the parameters describing the ambient medium lead to errors in the estimated yield, it is of interest to find the interval in time (or, equivalently, in radius) that minimizes the error in the yield due to incomplete or inaccurate knowledge of the medium.

Empirical evidence from nuclear explosions in silicate rocks at the Nevada Test Site has shown that the shock front RVT curves from several geologic media are relatively insensitive to the particular ambient medium, yet fairly sensitive to the yield, during a certain interval in time. Using a simple model and a limited set of media, we have previously shown in a first-order analysis (Lamb, Callen, & Sullivan 1989) that this insensitivity is likely a result of correlations among media properties, particularly the initial density ρ_0 and the parameters A and B that describe the high-pressure Hugoniot of a given medium. These three parameters can be combined to form a characteristic length L and a characteristic time T for each medium. When the logarithmic derivative of L with respect to T

is a constant (i.e., when L varies with T according to a power law), an insensitive interval is predicted by the model within the accuracy of the first-order analysis. In actual applications of hydrodynamic methods of verification, if such an insensitive interval exists, data from that interval should be given higher weight in any yield estimation algorithm, since errors resulting from improper characterization of the medium are thereby minimized.

The above analysis suggested a method for predicting the existence of an insensitive interval for any collection of media: from equation-of-state information, calculate the characteristic length L and characteristic time T for each member of the collection, and check for a power law relation between L and T . Table 2 lists equation-of-state information for an improved collection of silicates. As Figure 9 shows, for these media L and T are well described by the power law relation $L = 3.31 T^{0.44}$, confirming our previous results. Similar equation-of-state information for a collection of carbonate materials is listed in Table 3. The characteristic times and lengths for these materials are also well fit by a power law relation, as Figure 10 shows. These latter results suggest that an insensitive interval may also exist for explosions in carbonate materials.

Our previous work (Lamb, Callen, & Sullivan 1989) showed how to find the crossing point for a pair of RVT curves, and suggested a process for determining an interval in which the variation in shock front radius would be minimized for explosions of equal yield in a collection of three or more media. Stated differently, this latter problem consists of finding the particular interval that minimizes the variation in yield estimates for explosions of equal yield in a given collection of ambient media. To solve this problem, we must go beyond the first-order approximation used in our earlier work.

To proceed, we use the analytical model of Lamb (1987), combined with the simple linear Hugoniot listed in Tables 2 and 3, to generate shock front RVT curves for 100 kt explosions in each material in the collections of silicates and carbonates. A more complete analysis would use piecewise linear approximations to the Hugoniot (see Lamb, Callen, & Sullivan 1992). The resulting RVT curves are shown in Figures 11 and 12. The curves in each collection follow each other relatively closely for a limited interval in time, but diverge at later times. For silicate materials, this similarity is greatest for times near 0.5 ms; for the carbonates, the corresponding similarity occurs near 0.8 ms. This convergence of the RVT curves suggests the optimal interval for yield estimation is near these times.

To determine the optimal interval, we employed the following procedure. We examined all $n_p = n_m(n_m - 1)$ ordered pairs of RVT curves in a given collection of n_m media at equally spaced times during the overall interval from 0 to 2.32 ms (corresponding to a scaled time interval of 0.0 to 0.5 scaled ms). The first curve of the pair was assumed to be a standard with a yield of 100 kt, and cube-root scaling was used to find the yield of the second explosion. Next, the square $(\Delta W)^2$ of the difference in yields was computed for each ordered pair of curves. The differences were then summed over all ordered pairs in

the collection. This process was repeated for each time point in the overall interval from 0 to 2.32 ms.

We then used these individual sums to evaluate all possible candidate intervals $t_1 \leq t \leq t_2$. For each candidate interval, $\sum(\Delta W)^2/N$ was calculated, where the sum was over all N time points within the candidate interval. If N is treated as an adjustable parameter, this sum is minimized for $N = 1$, namely that time for which $|\Delta W|$ was smallest. If instead the length N of the measurement interval is regarded as fixed, the optimal location of the interval can be determined. Figures 13 and 14 show the optimal location of the interval as a function of N . For silicates, these intervals are roughly centered about 0.5 ms, whereas for carbonates, the optimal intervals are centered near 0.8 ms. These results are consistent with the locations of the necks in the RVT curves shown in Figures 11 and 12, and suggest that merely identifying the ambient medium as a silicate or a carbonate can be used to estimate the optimal interval for yield estimation.

The procedure just described does not determine a unique optimal interval because the RVT curves used were generated from a model, and thus do not include the errors and uncertainties that would be present in experimental shock-front RVT data. If such uncertainties were part of the RVT record, the procedure described above would allow the determination of the optimal length N as well as the optimal location of the interval for yield estimation in a given collection of media. To illustrate the procedure, we model experimental error by including a second term $n_p(\delta W)^2/N$ in the quantity to be minimized, where δW is a characteristic fractional error in the yield. Incorporating this term does not change the location of the best interval for a given interval length, i.e., the intervals shown in Figures 13 and 14 remain the best choices. It does, however, allow a determination of the optimal interval length, and hence the overall best interval.

We examine the results for several values of the fractional yield error δW . For each value of δW , the optimal interval is determined by minimizing the quantity

$$\frac{1}{N} \left[\sum(\Delta W)^2 + n_p(\delta W)^2 \right].$$

The results for $\delta W = 0, 10, 20, 30, 50, 80,$ and 100 kt are shown for silicates in Figure 15 and for carbonates in Figure 16. For $\delta W = 0$, the optimal interval has length 0 ($N = 1$); that is, the minimum occurs for a single point in time and not an extended interval, as expected. For $\delta W > 0$, there is an optimal interval of non-zero length, whose size depends on δW . For explosives in silicates, for example, the optimal interval for $\delta W = 30$ kt has length $\simeq 0.46$ ms, and begins at $t_1 \simeq 0.33$ ms.

CONCLUSIONS

We find that variations in the effective adiabatic index of the source material can cause the inferred yield of spherically symmetric explosions to vary by as much as 26%

at 0.1 scaled ms. These variations may be a significant source of uncertainty in hydrodynamic yield estimates when the hydrodynamic method is used in a treaty-verification context, since detailed properties of the source are not expected to be available to the treaty monitoring party. Our results for explosions in granite agree generally with those of Morar & Goldwire (1990) for explosions in rhyolite. The pressure profiles within the source region of all the explosions we simulated are very similar at late times. Using this empirical result, we constructed a simple formula for the dependence of the inferred yield on the effective adiabatic index and the initial radius of an ideal-gas source by considering the energy that remains trapped in the source region at the time the yield is estimated.

In studying further the issue of an optimal interval for yield estimation, we find that a simple examination of equation-of-state data can help to determine what interval of shock front RVT data should be used to minimize the uncertainty in a given hydrodynamic yield estimate. For the collections of silicates and carbonates examined here, there is an interval during which yield estimates are relatively insensitive to the medium, yet still sensitive to the yield. The procedure described in this paper could be improved by replacing the simple linear Hugoniot used to generate the RVT curves for each medium with more accurate piecewise-linear Hugoniot. A more accurate statistical analysis would require detailed simulation of the errors present in experimental RVT curves, the uncertainties in the properties of the ambient media and the source, and the correlations present in the radius vs. time data.

ACKNOWLEDGEMENTS

We thank Steve Peyton and Jim Baker of S-CUBED Corporation for kindly providing the modified SESAME equation of state tables used in our simulations. We also thank Bill Moran for helpful discussions regarding numerical equations of state, source parameters, and yield estimation and Tom Ahrens for helpful discussion of Hugoniot and the equations of state of geologic media.

TABLE 1
Source Parameters and Inferred Yield^a

Model	M_s (Mg)	R_s (m)	EOS ^b	Relative Yield	
				0.1 scaled ms	1.0 scaled ms
1 ^c	10	1.0	1.4	1.00	1.00
2	1	1.0	1.4	0.99	1.01
3	10	0.5	1.4	1.01	0.99
4	1	0.5	1.4	1.00	0.99
5	10	1.0	1.2	0.74	0.82
6	1	1.0	1.2	0.74	0.83
7	10	0.5	1.2	0.81	0.86
8	1	0.5	1.2	0.82	0.87
9	10	1.0	Al	0.95	0.94
10	1	1.0	Al	1.04	0.99
11	10	0.5	Al	0.98	0.95
12	1	0.5	Al	1.00	0.98

^a For all cases, the ambient medium was granite.

^b Numerical values are adiabatic indices for ideal gas; Al indicates aluminum EOS table from S-CUBED Corp.

^c Reference calculation

TABLE 2
Silicate Equations of State^a

Rock	ρ_0 (kg m ⁻³)	A (km s ⁻¹)	B	Reference
Westerly granite	2627	2.103	1.629	<i>McQueen et al.</i> [1967]
Weathered granite	2631	2.66	1.49	<i>Ahrens et al.</i> [1991]
Granite	2600	3.75	1.28	<i>Trunin et al.</i> [1988]
Biotite-chlorite granite	2680	2.22	1.63	<i>van Thiel</i> [1977]
Quartz (high u)	2650	4.659	1.226	<i>Trunin et al.</i> [1971a], <i>Al'tshuler et al.</i> [1977]
Fused quartz	2200	1.143	1.603	<i>Wackerle</i> [1962], <i>Jones et al.</i> [1968], <i>Trunin et al.</i> [1971b]
Vacaville basalt	2860	2.31	1.615	<i>Jones et al.</i> [1968]
Tuff	2740	2.69	1.556	<i>Trunin et al.</i> [1988]
Wet tuff	2200	3.0	1.11	<i>Bass</i> [1966]
Dry tuff	1600	0.4	1.3	<i>Bass</i> [1966]
Dry alluvium	1780	1	1.4	<i>Perret and Bass</i> [1975]

^aThe quantities ρ_0 , A , and B are the unshocked density and the parameters in the Hugoniot $D = A + Bu$.

TABLE 3
Carbonate Equations of State^a

Rock	ρ_0 (kg m ⁻³)	A (km s ⁻¹)	B	Reference
Polycrystalline calcite	2665	3.70	1.44	<i>Kalashnikov et al.</i> [1973]
Polycrystalline calcite	2020	1.74	1.61	<i>Kalashnikov et al.</i> [1973]
Polycrystalline calcite	1705	1.15	1.60	<i>Kalashnikov et al.</i> [1973]
Dover chalk	1400	0.67	1.60	<i>Tyburczy & Ahrens</i> [1986]
Solenhofen limestone	2620	3.269	1.796	<i>Tyburczy & Ahrens</i> [1986]
Solenhofen limestone	2585	3.62	1.39	<i>van Thiel</i> [1977]
Kaibab limestone	2220	1.89	1.597	<i>Jones et al.</i> [1968]
Dolomite	2703	3.99	1.32	<i>Adadurov et al.</i> [1961]
Dolomite	2840	4.99	1.24	<i>Trunin et al.</i> [1988]
Aragonite	2930	5.02	1.30	<i>Vizgirda & Ahrens</i> [1982]

^aThe quantities ρ_0 , A , and B are the unshocked density and the parameters in the Hugoniot $D = A + Bu$.

REFERENCES

- Adadurov, G. A., D. B. Balashov, and A. N. Dremin, A study of the volumetric compressibility of marble at high pressures, *Bull. Acad. Sci. USSR Geophys. Ser.*, 5, 463-466, 1961.
- Ahrens, T. J., A. M. Rubin, T. S. Duffy, and T. Sekine, Shock propagation in crustal rock. Chapter I: compression and isentropic release of granite, Final Technical Report, Contract F19628-88-K-0034, Geophysics Laboratory, Hanscom Air Force Base, April 1991. PL-TR-91-2096, ADA239548
- Al'tshuler, L. V., N. N. Kalitikin, L. V. Kuzmina, and B. S. Chekin, Shock adiabats for ultrahigh pressures, *Sov. Phys.-JETP* 45, 167-171, 1977.
- Bass, R. C., Rep. SC-RR-66-548, Sandia Corp., Albuquerque, N. M., 1966.
- Jones, A. H., W. M. Isbell, F. H. Shipman, R. D. Perkins, S. J. Green, and C. J. Maiden, Material properties measurements for selected materials, Interim report, Contract NAS2-3427, General Motors Technical Center, Warren, Mich., April 1968.
- Kalashnikov, N. G., M. N. Pavlovskiy, G. V. Simakov, and R. F. Trunin, Dynamic compressibility of calcite-group minerals, *Izv. Acad. Sci. USSR Phys. Solid Earth*, 2, 23-29, 1973.
- Lamb, F. K., An approximate solution for ground shock propagation, *University of Illinois Program in Arms Control, Disarmament, and International Security, Rep. WP-2-87-2*, February 1987.
- Lamb, F. K., B. W. Callen, and J. D. Sullivan, Insensitive interval in the evolution of shock waves from underground nuclear explosions, *Dept. of Physics, University of Illinois at Urbana-Champaign, Rep. P/89/5/77*, May 1989.
- Lamb, F. K., B. W. Callen, and J. D. Sullivan, An approximate analytical model of shock waves from underground nuclear explosions, *J. Geophys. Res.*, 97, 515-535, 1992.
- McQueen, R. G., S. P. Marsh, and J. N. Fritz, Hugoniot equation of state for twelve rocks, *J. Geophys. Res.*, 72, 4999-5036, 1967.
- Moran, B., and H. C. Goldwire, Jr., Effect of source modeling on the inferred yield from an underground nuclear explosion, in *Shock Compression of Condensed Matter--1989*, edited by S. C. Schmidt, J. N. Johnson, and L. W. Davison, pp. 645-648, North Holland, New York, 1990.
- Norman, M. L., Ph.D. thesis, University of California at Davis, *Lawrence Livermore Natl. Lab. Report UCRL-52946*, 1980.
- Norman, M. L., J. Wilson, and R. Barton, A new calculation on rotating protostar collapse, *Astrophys. J.*, 239, 968-981, 1980.
- Norman, M. L., and K.-H. Winkler, in *Astrophysical Radiation Hydrodynamics*, edited by K.-H. Winkler and M. Norman, Reidel, Dordrecht, 1986.

- Perret, W. R., and R. C. Bass, Free-field ground motion induced by underground explosions, *Sandia National Laboratory, Rep. SAND74-0252*, February 1975.
- Stone, J. M., and M. L. Norman, ZEUS-2D: A radiation hydrodynamics code for astrophysical flows in two spatial dimensions. I. the hydrodynamics algorithms and tests, *Astrophys. J. Suppl.*, *80*, no. 2, June 1992.
- Trunin, R. F., G. V. Simakov, I. P. Dudoladov, G. S. Telegin, and I. P. Trusov, Rock compressibility in shock waves, *Izv. Acad. Sci. USSR Phys. Solid Earth*, *24*, 38-42, 1988.
- Trunin, R. F., G. V. Simakov, and M. A. Podurets, Compression of porous quartz by strong shock waves, *Izv. Acad. Sci. USSR Phys. Solid Earth*, *7*, 102-106, 1971b.
- Trunin, R. F., G. V. Simakov, M. A. Podurets, B. N. Moiseyev, and L. V. Popov, Dynamic compressibility of quartz and quartzite at high pressures, *Izv. Acad. Sci. USSR Phys. Solid Earth*, *7*, 8-12, 1971a.
- Tyburczy, J. A., and T. J. Ahrens, Dynamic compression and volatile release of carbonates, *J. Geophys. Res.*, *91*, 4730-4744, 1986.
- van Leer, B., Towards the ultimate conservative difference scheme. IV. A new approach to numerical convection, *J. Comp. Phys.*, *23*, 276-299, 1977.
- van Thiel, M., J. Shaner, and E. Salinas, *Rep. UCRL-50108*, vol. 3, Lawrence Livermore National Laboratory; Livermore, Calif., 1977.
- Vizgirda, J., and T. J. Ahrens, Shock compression of aragonite and implications for the equation of state of carbonates, *J. Geophys. Res.*, *87*, 4747-4758, 1982.
- von Neumann, J., and R. D. Richtmeyer, A method for the numerical calculation of hydrodynamic shocks, *J. Appl. Phys.*, *21*, 232-237, 1950.
- Wackerle, J., Shock-wave compression of quartz, *J. Appl. Phys.* *33*, 922-937, 1962.

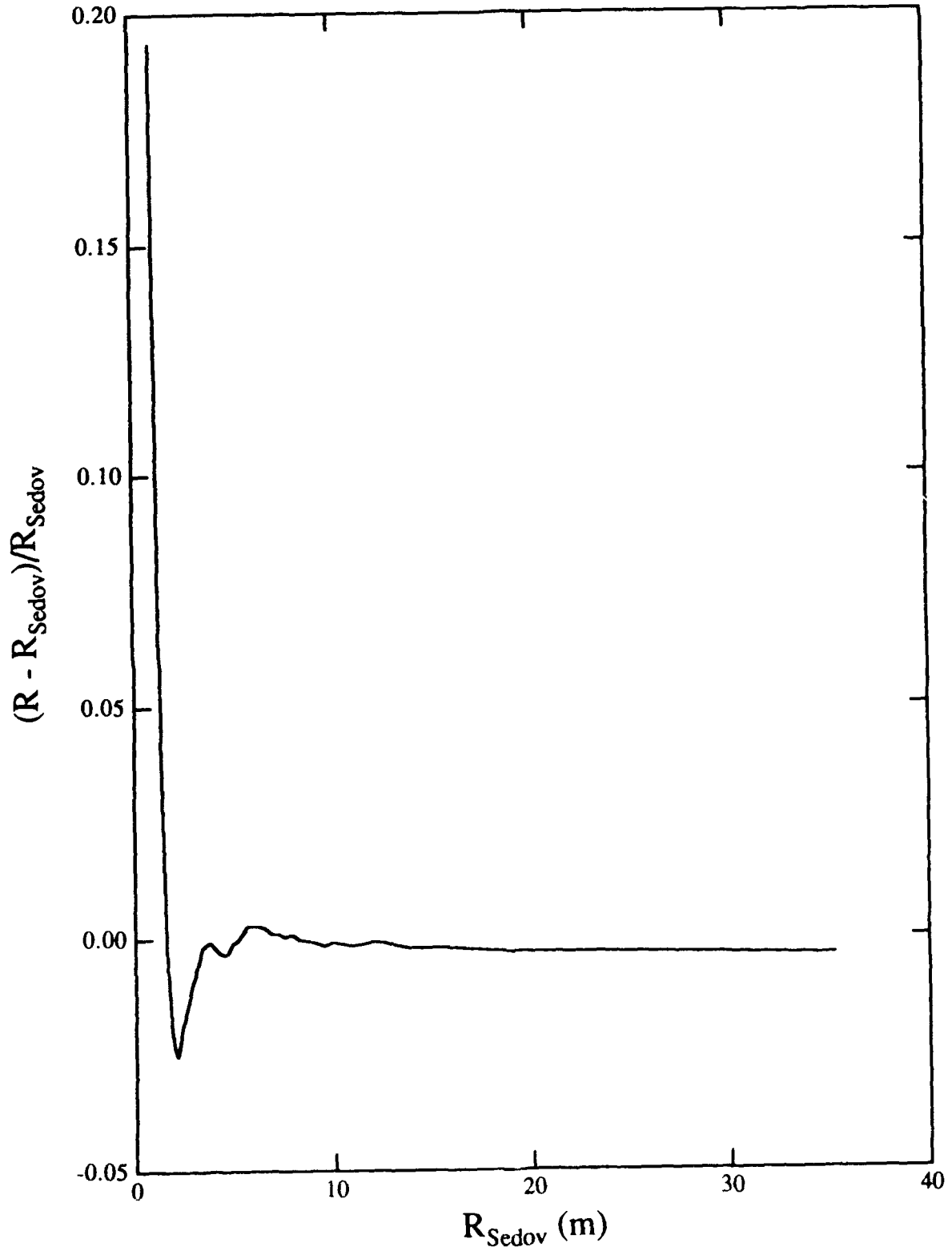


Figure 1

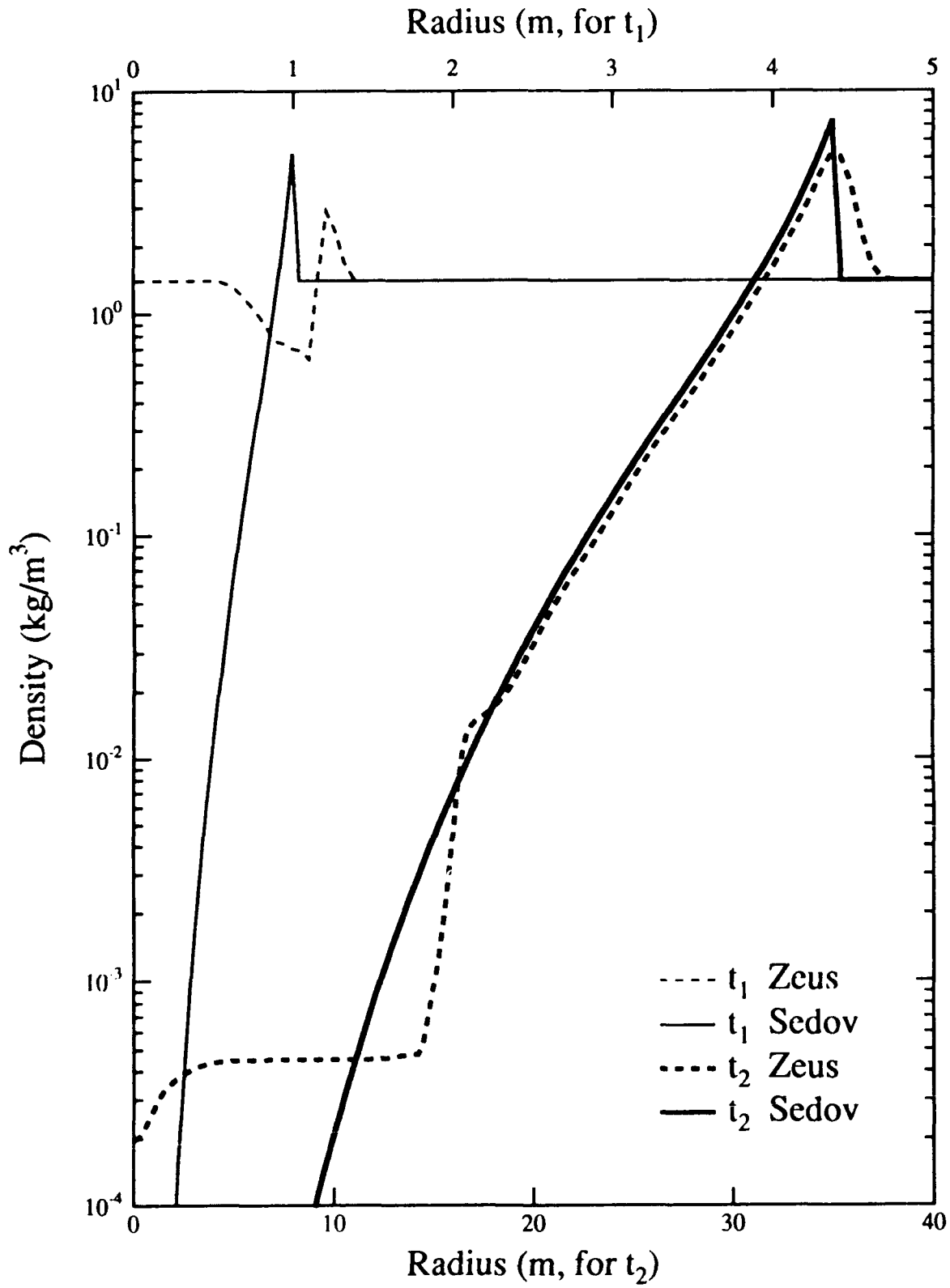


Figure 2

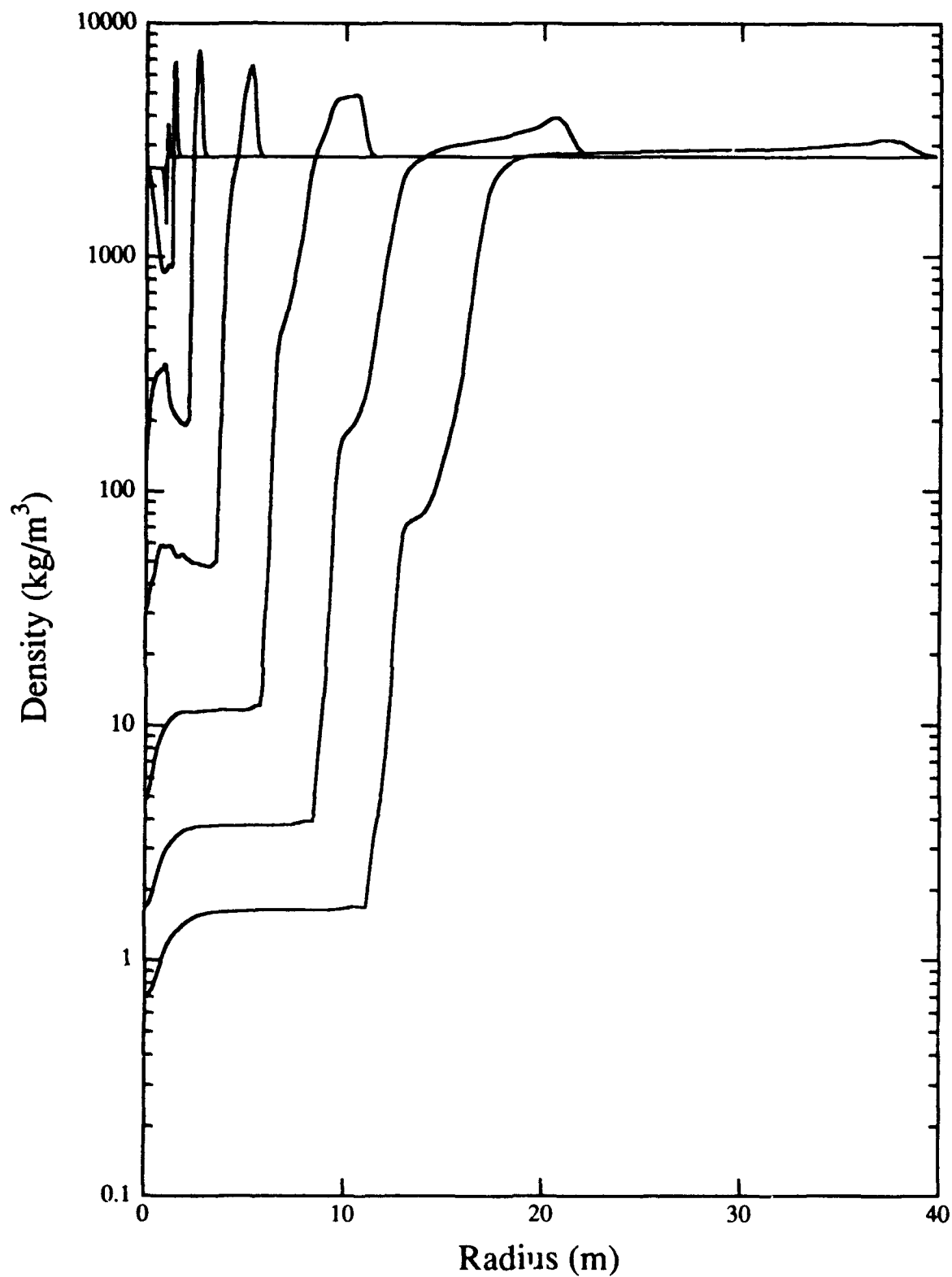


Figure 3

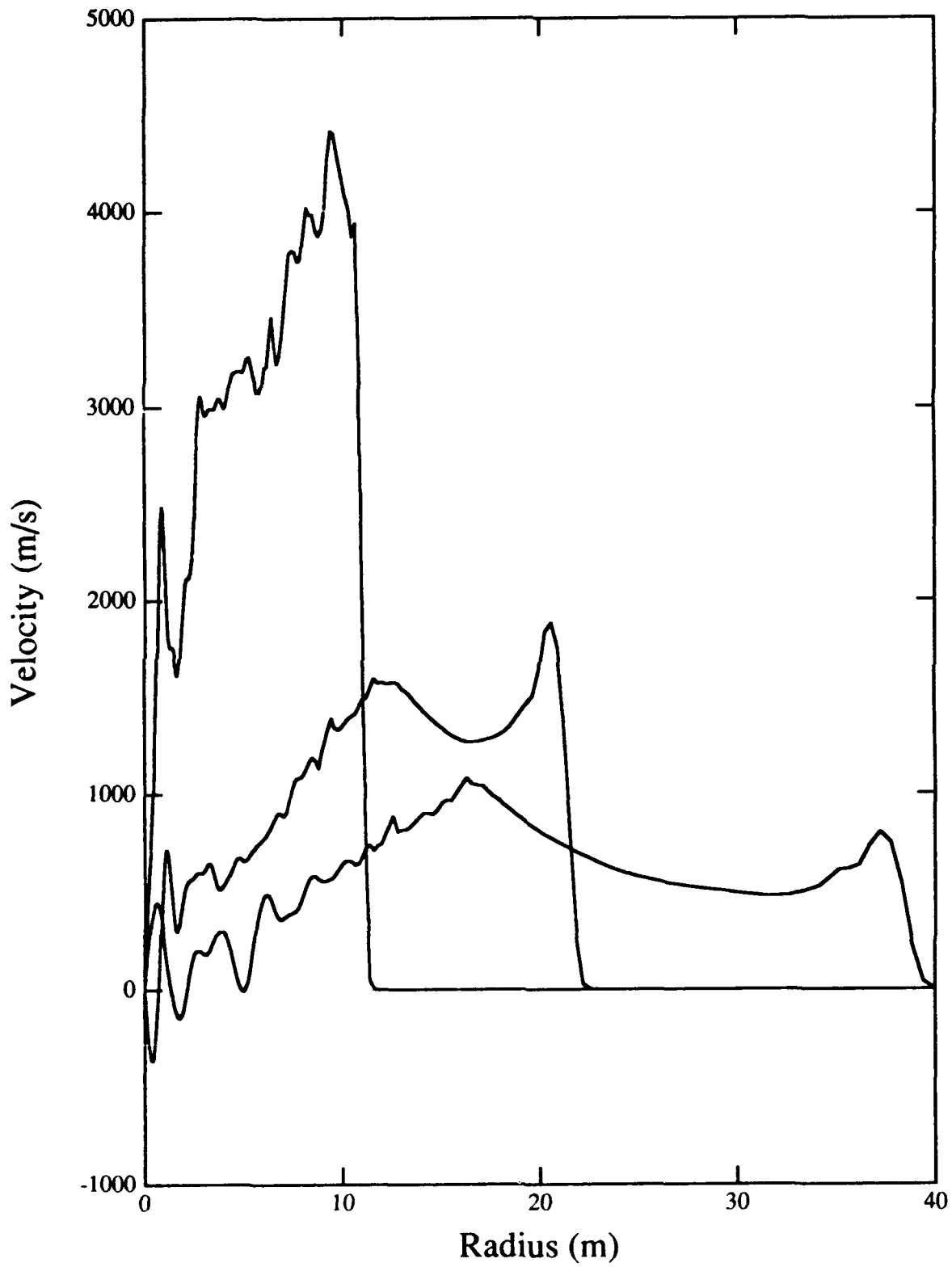


Figure 4

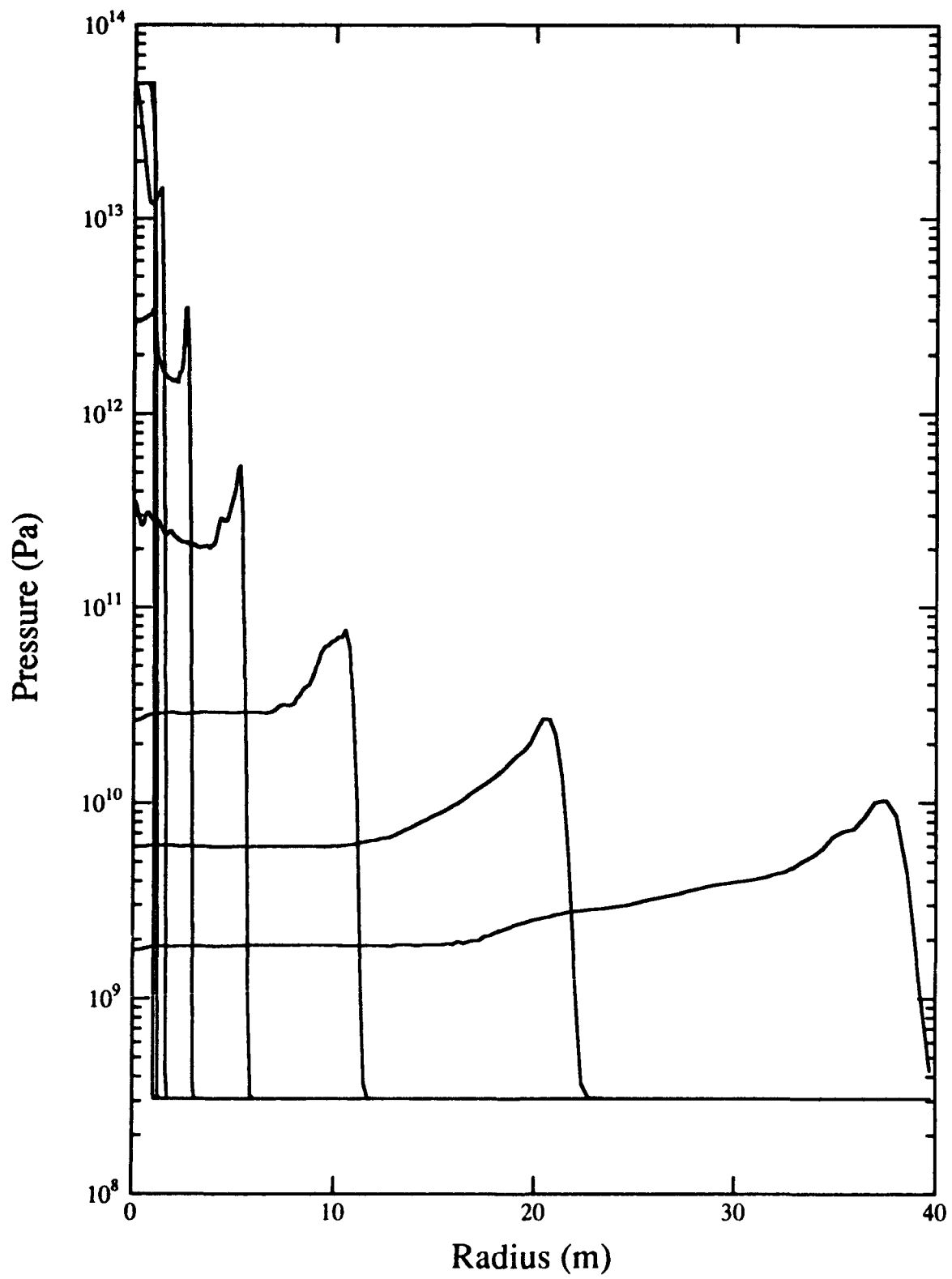


Figure 5

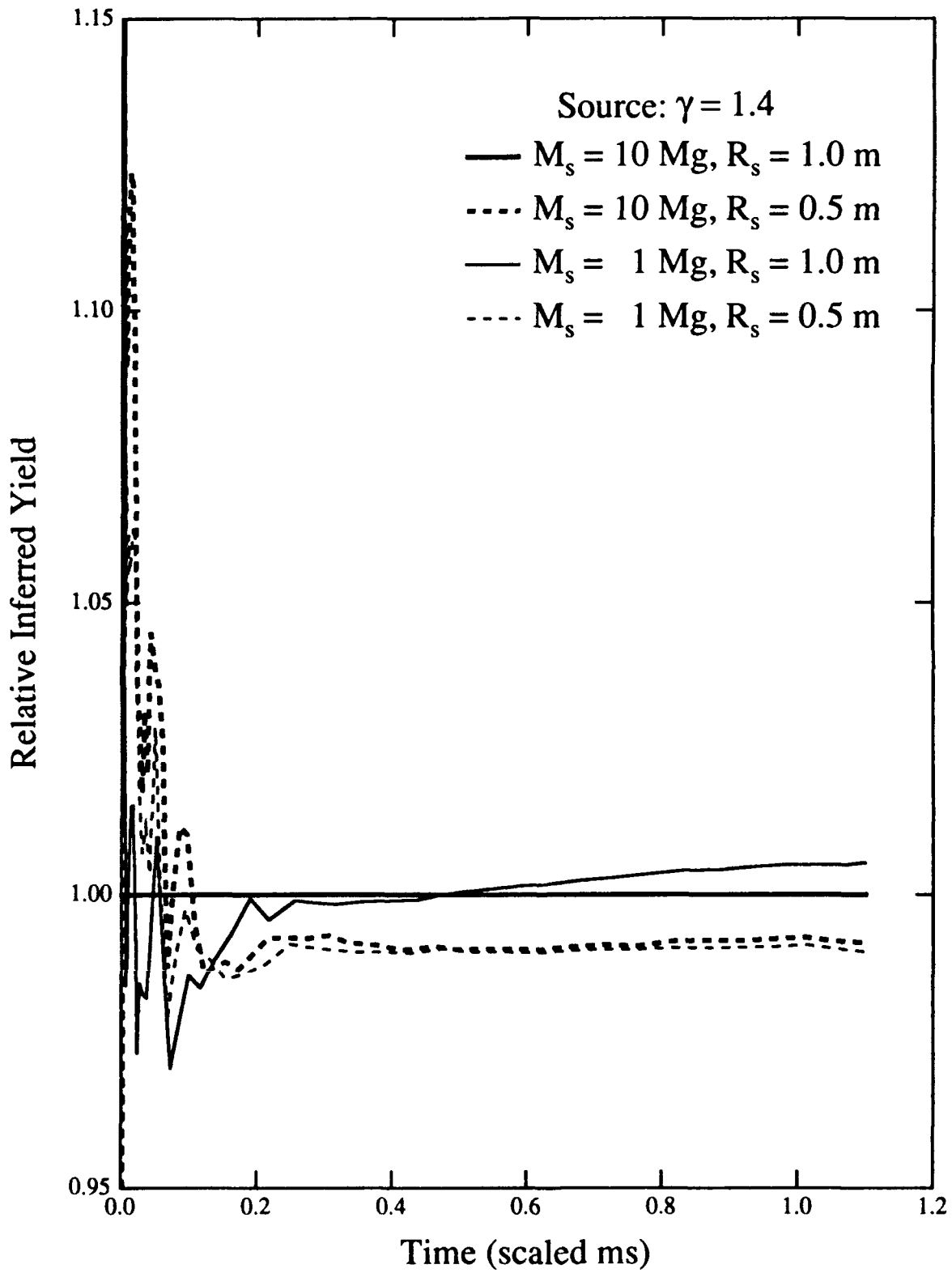


Figure 6

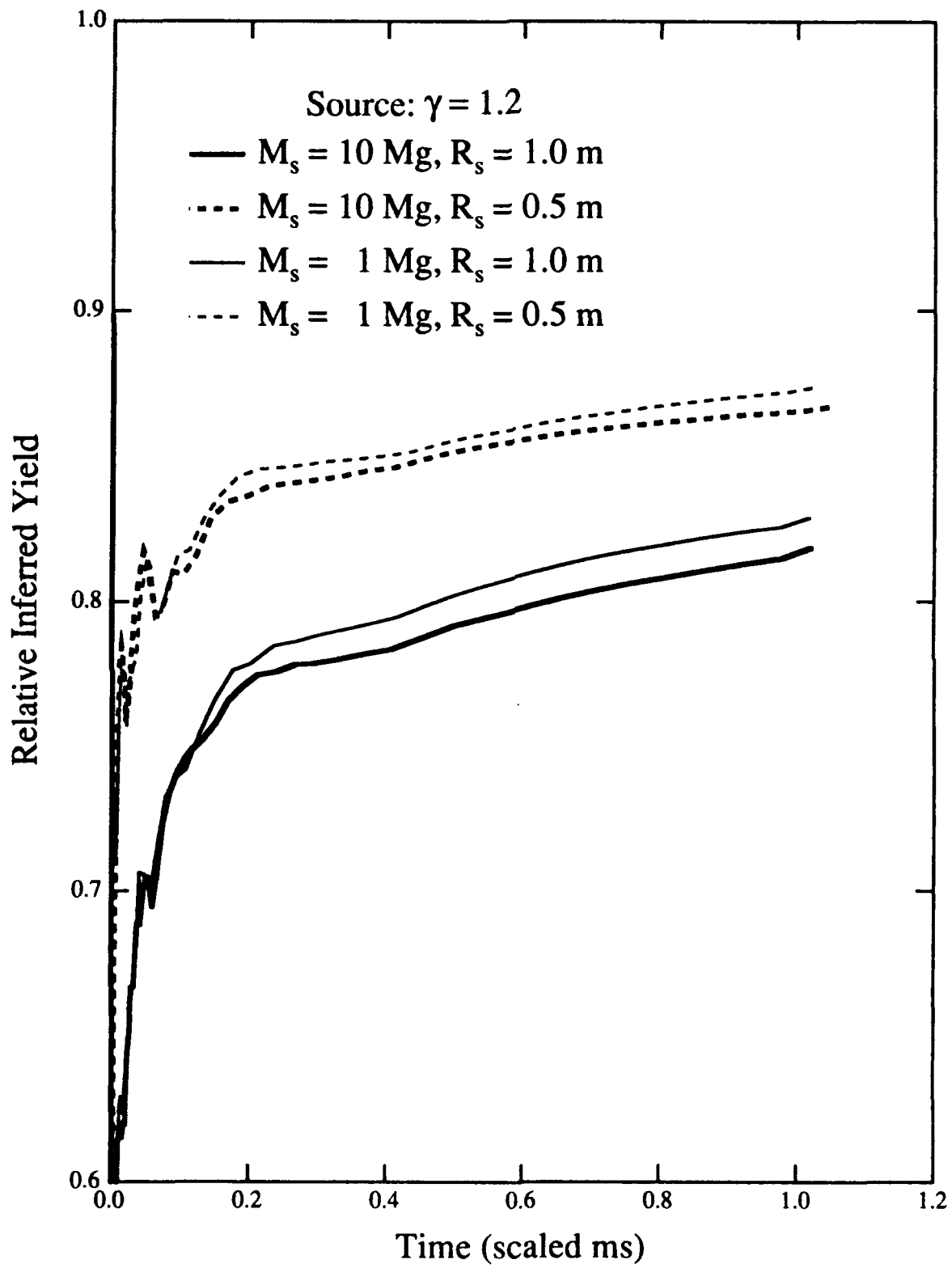


Figure 7

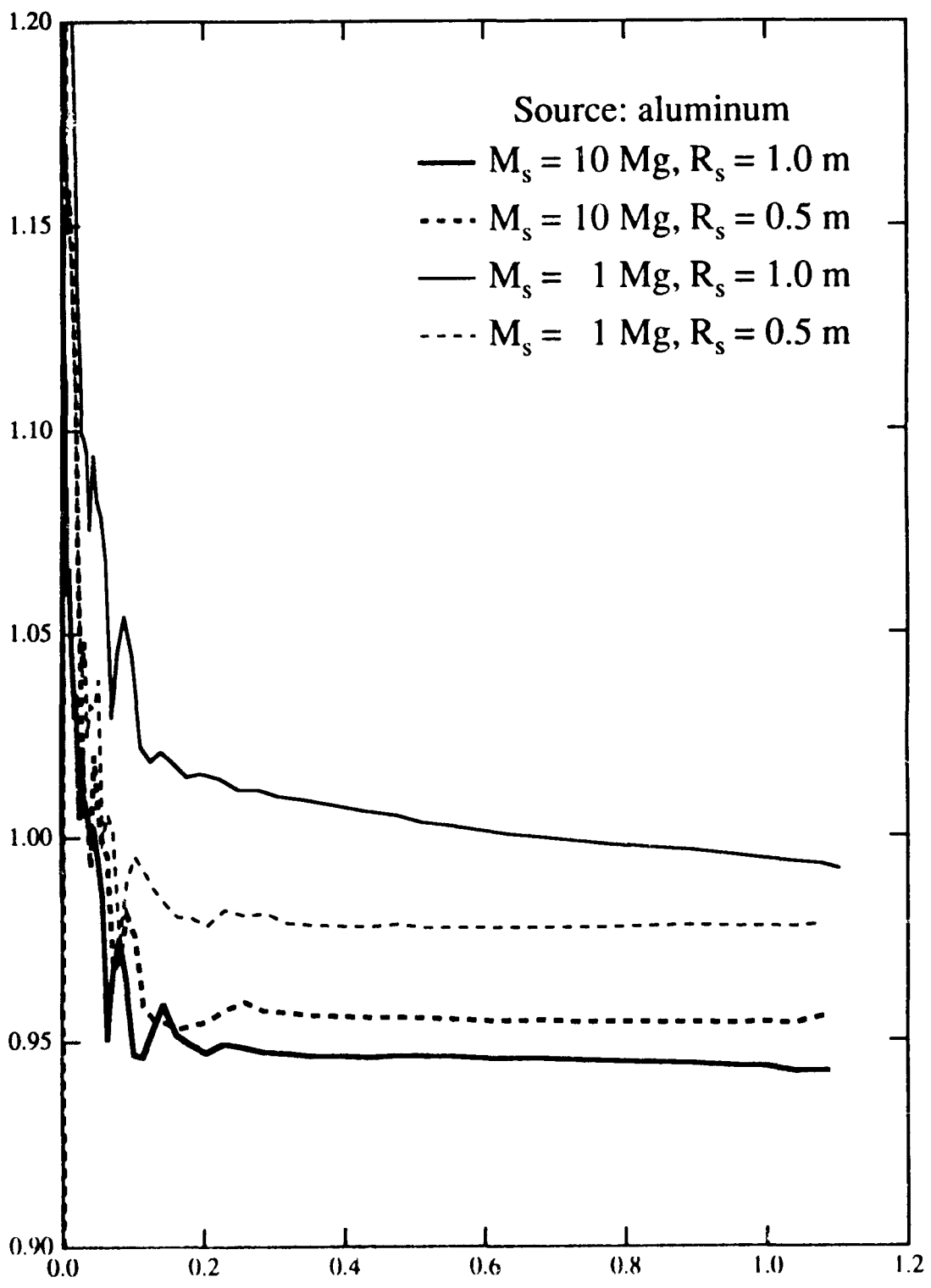


Figure 8

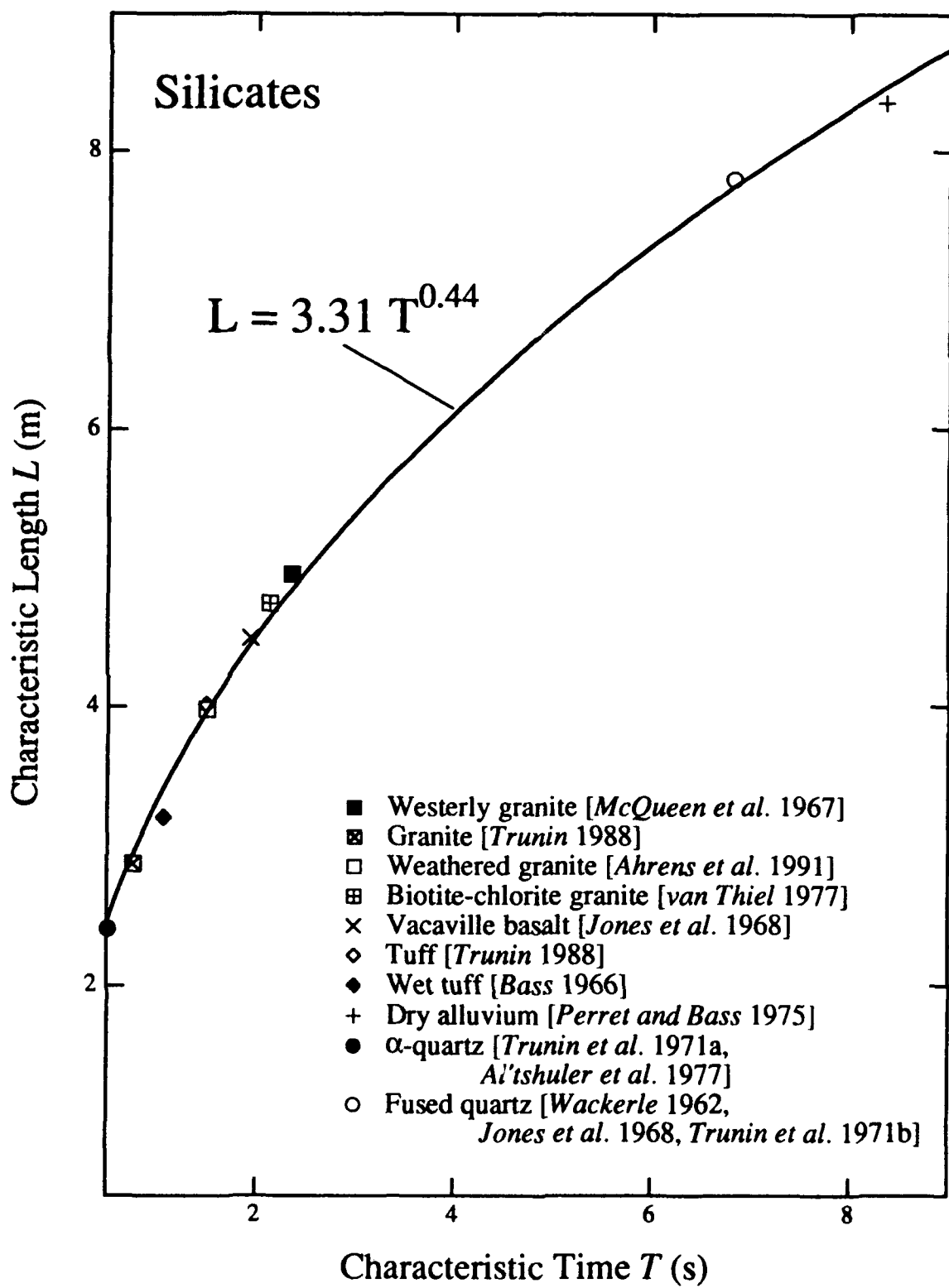


Figure 9

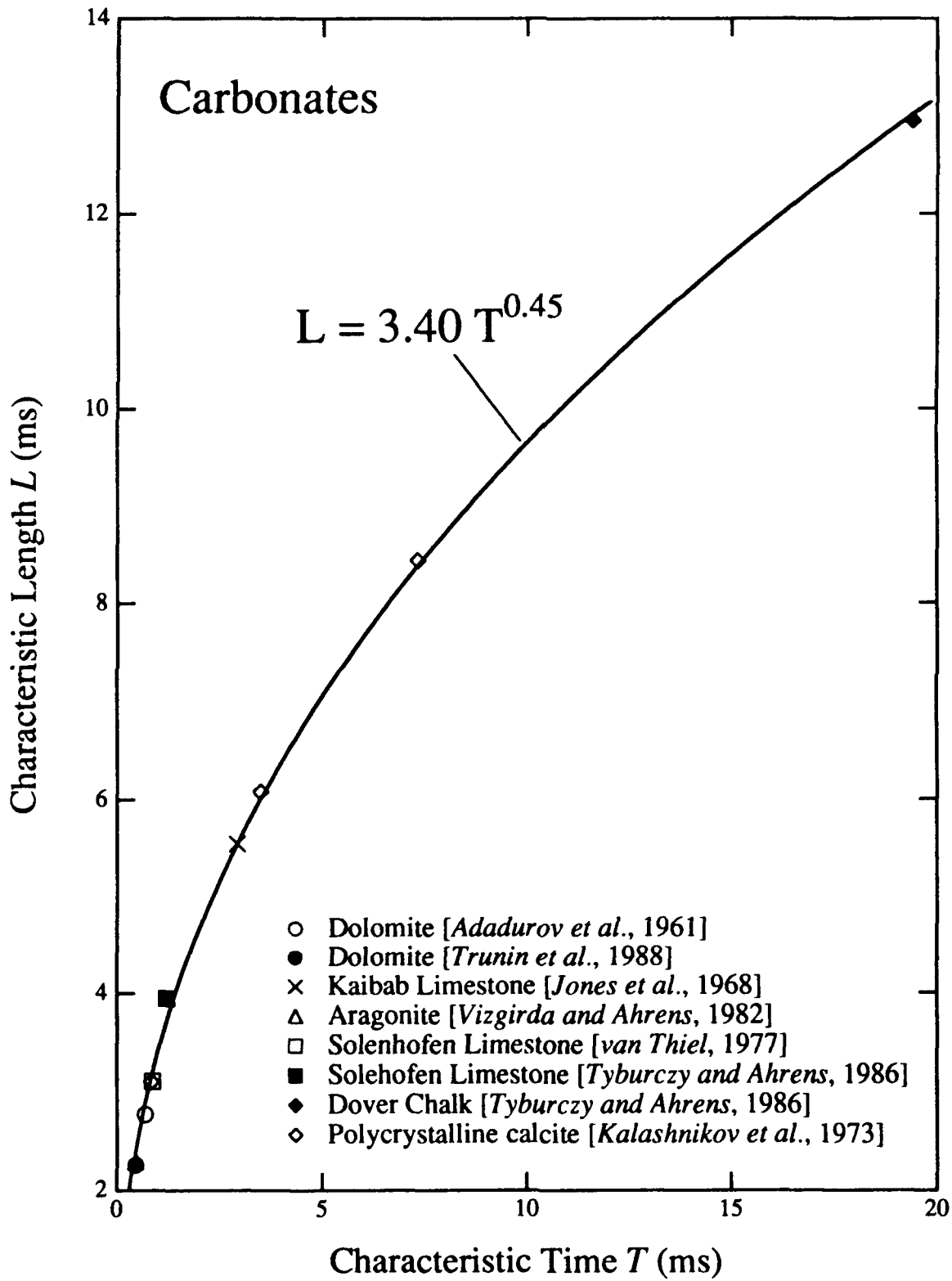


Figure 10

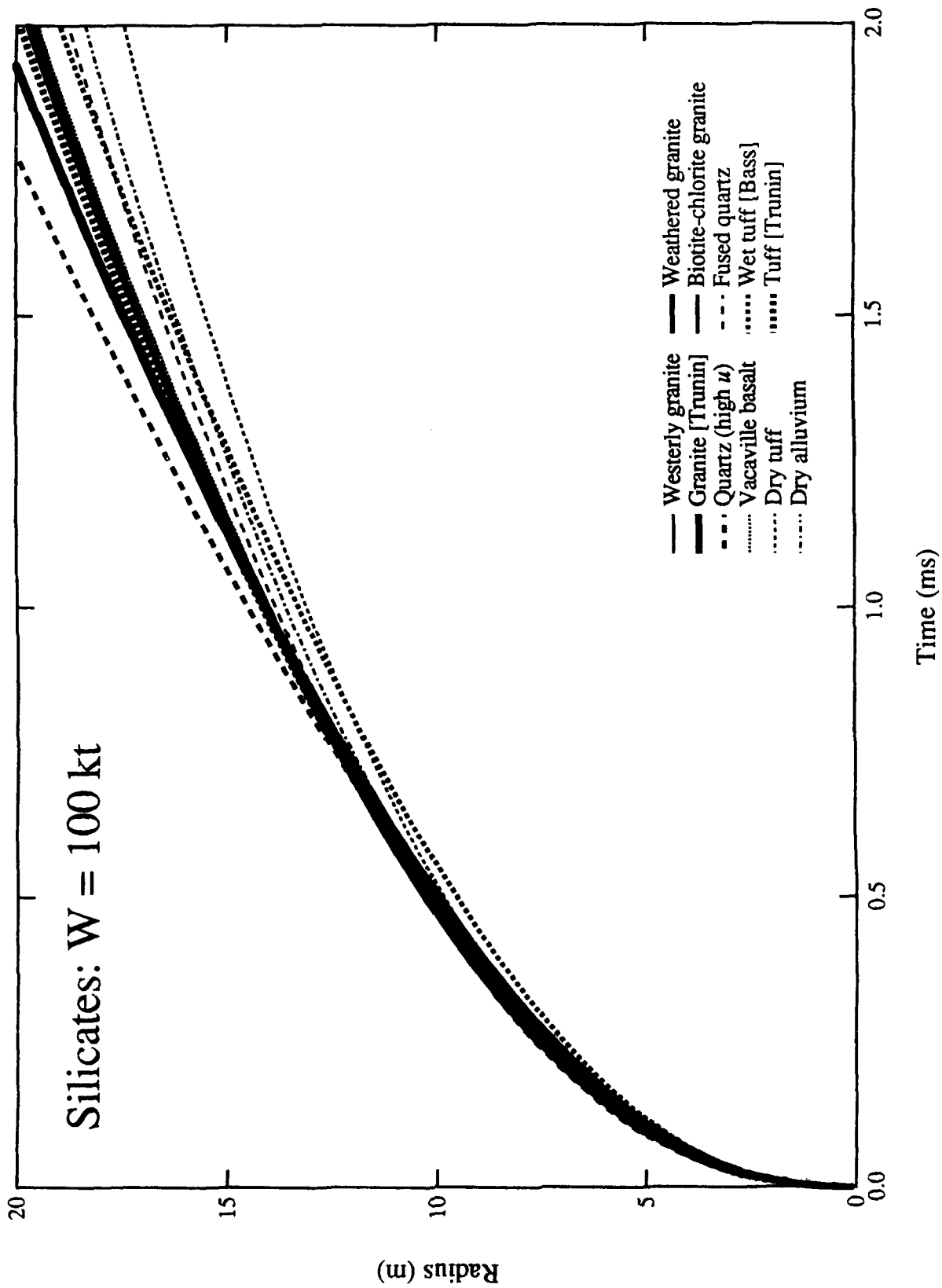


Figure 11

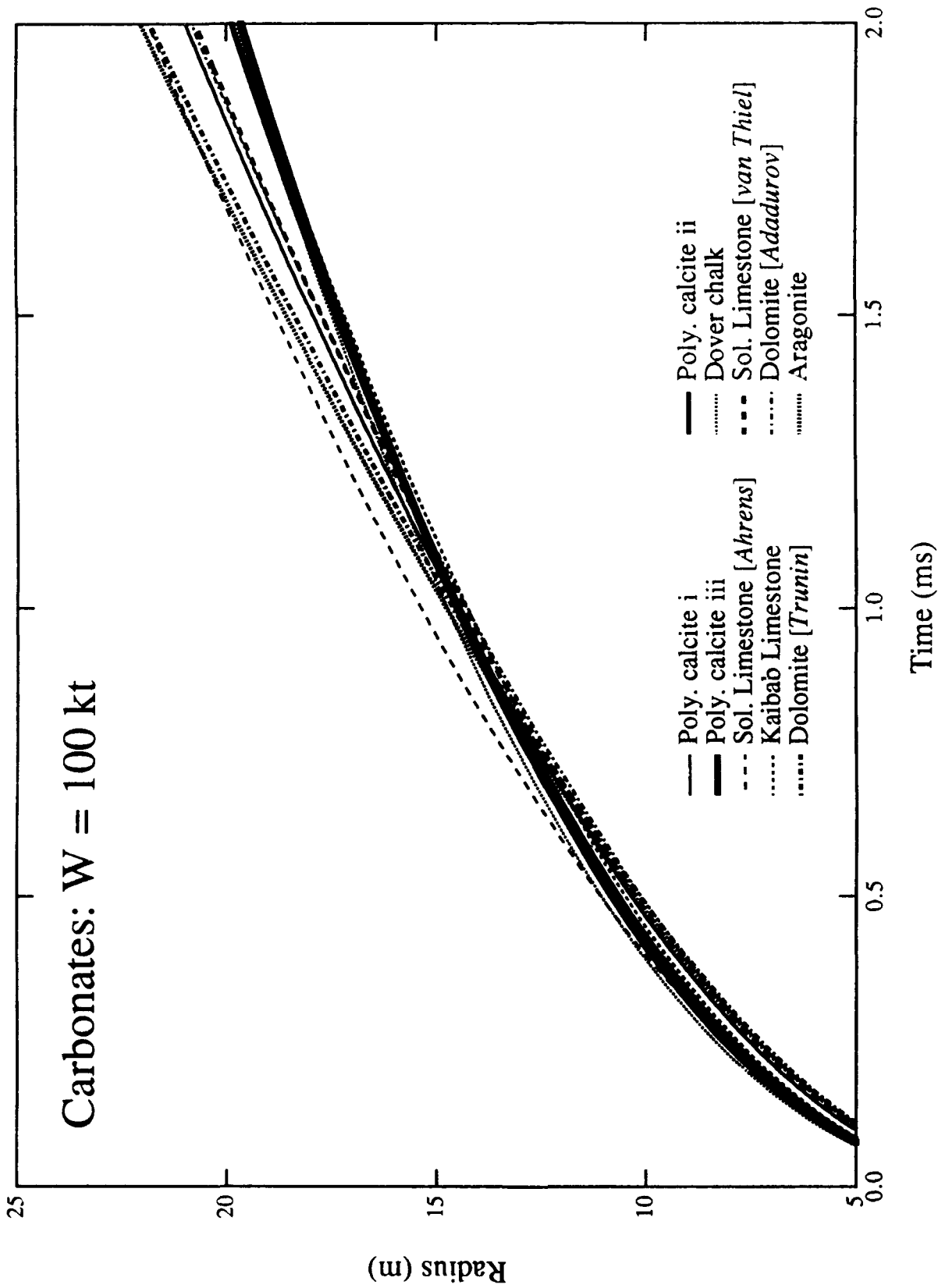


Figure 12

Silicates: Position vs. length of interval

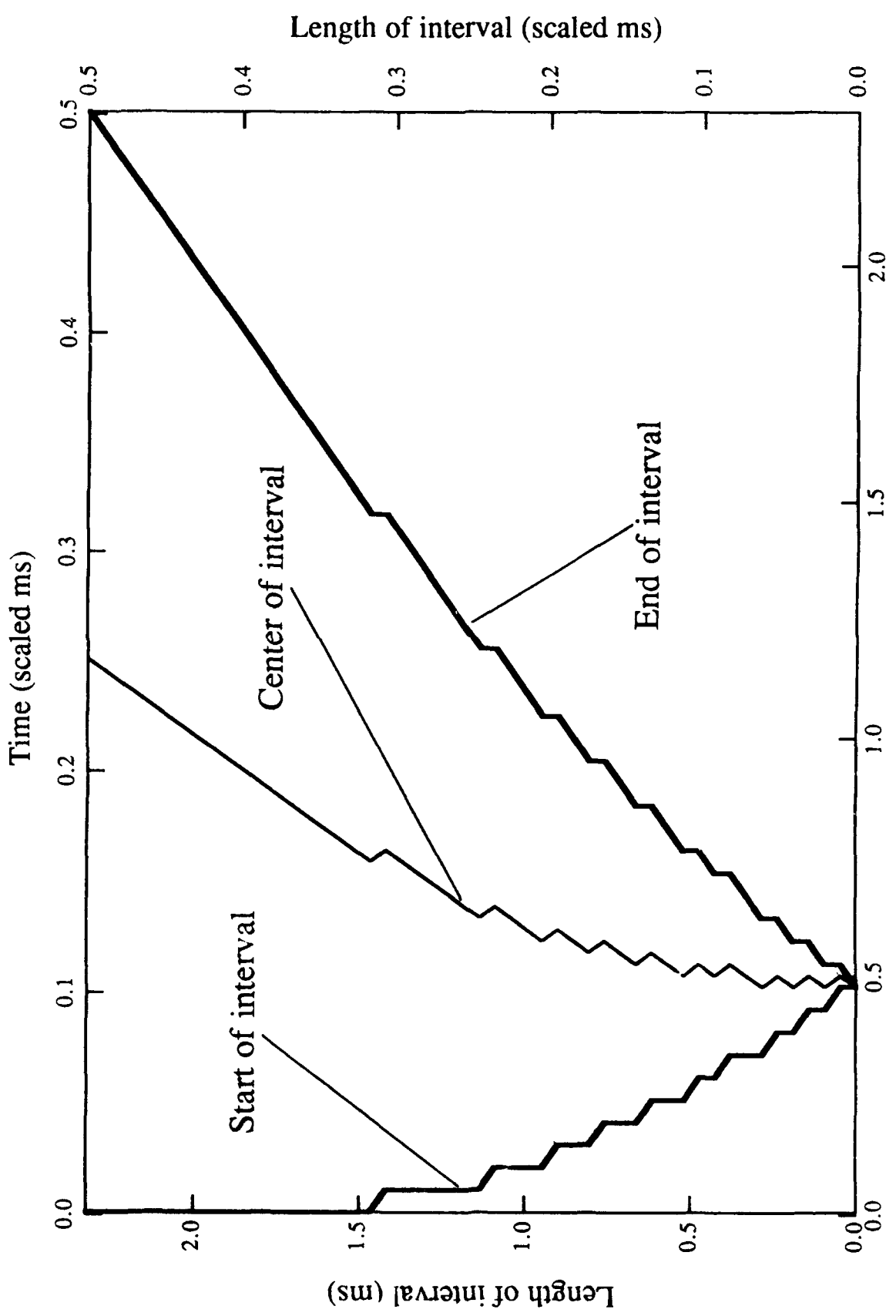
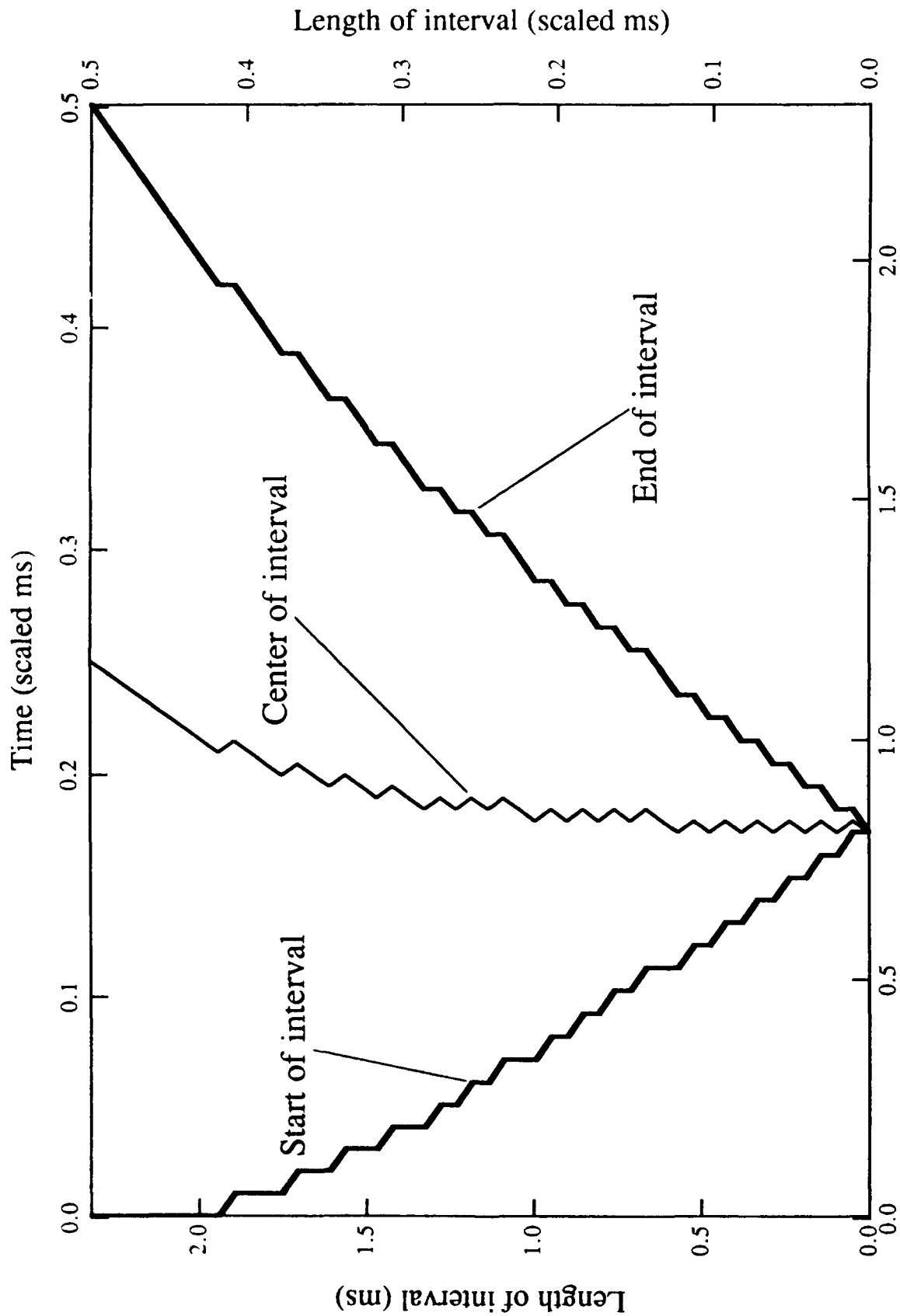


Figure 13

Carbonates: Position vs. length of interval



Time (ms)

Figure 14

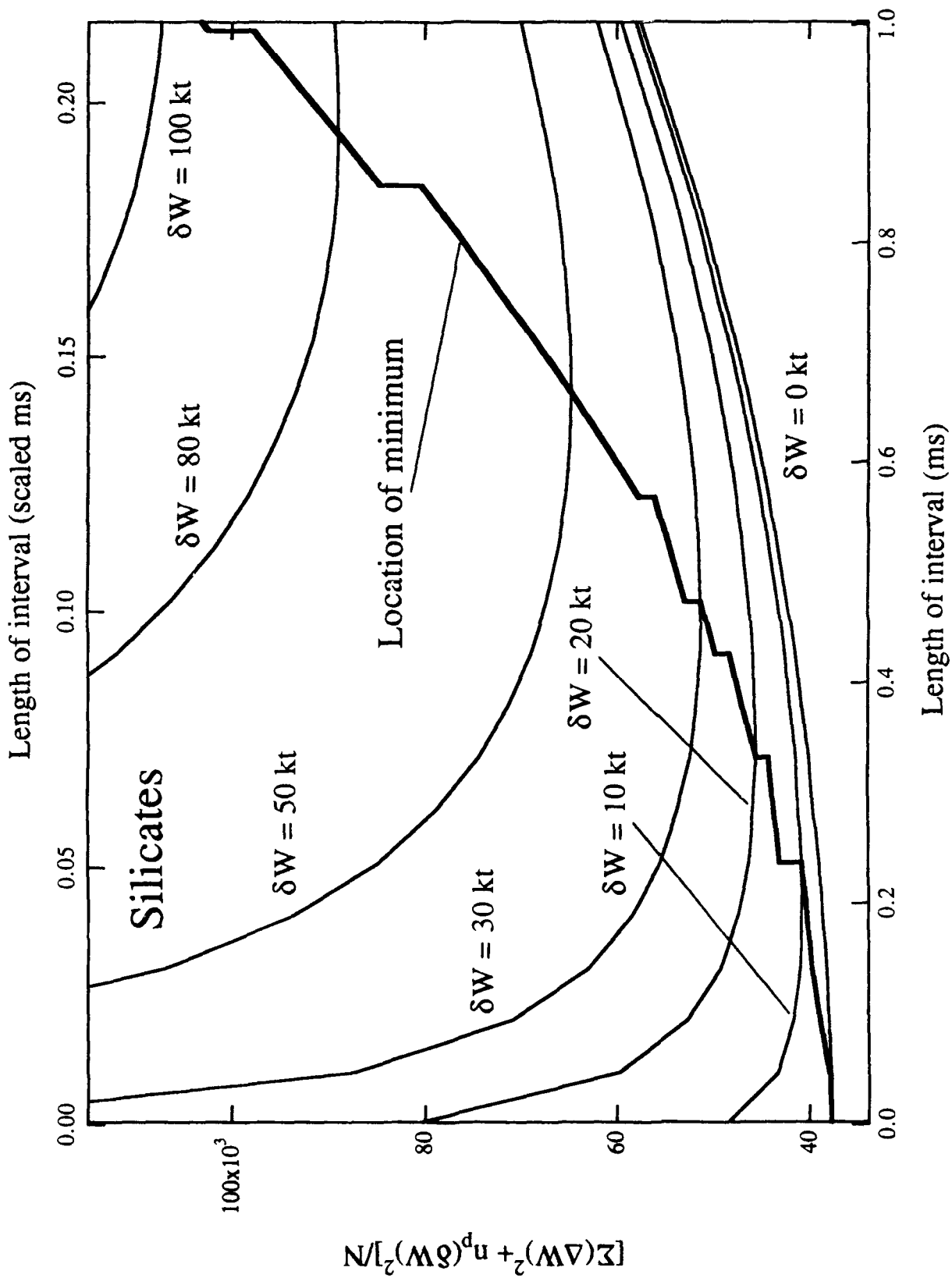


Figure 15

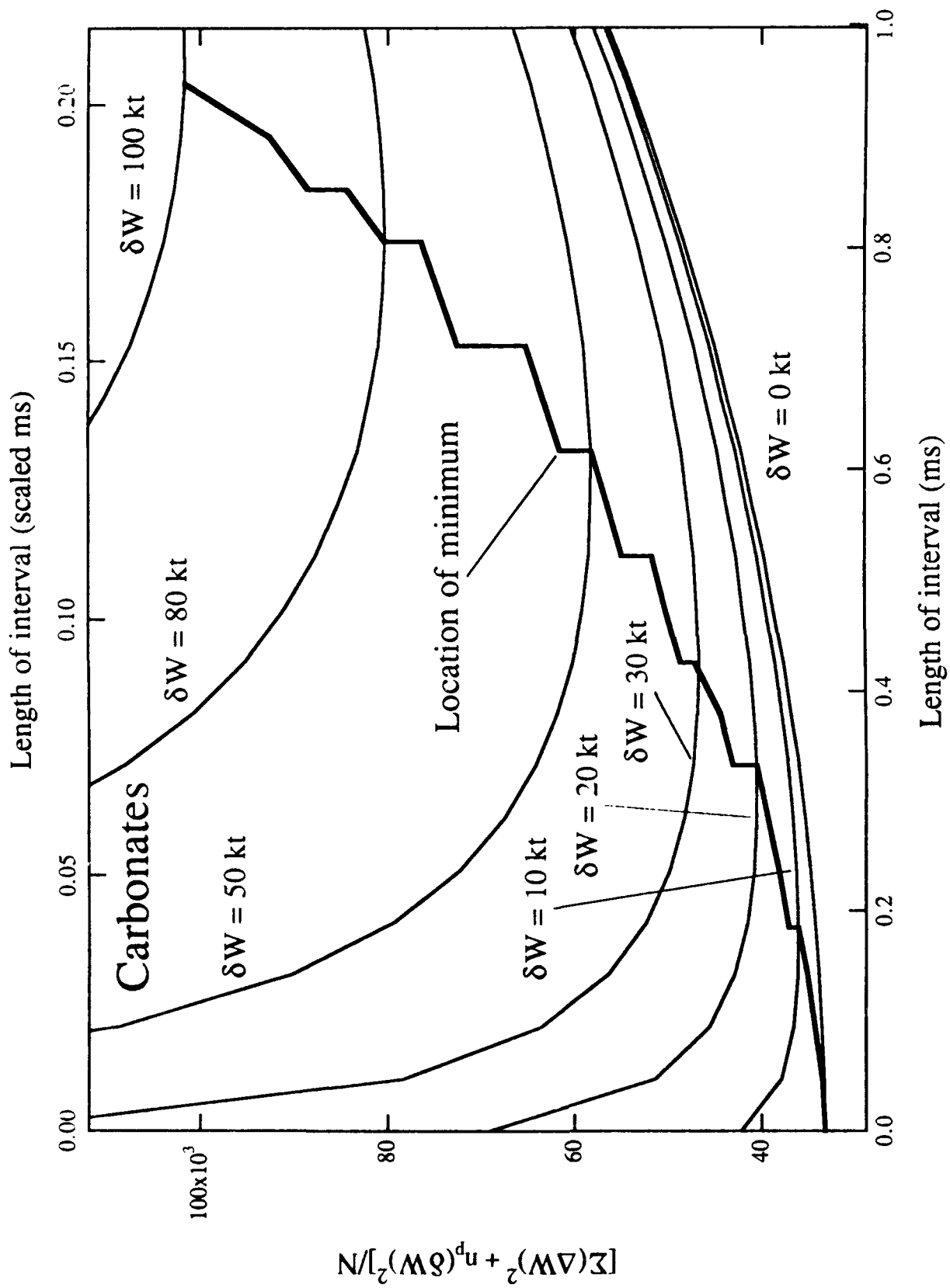


Figure 16

DISTRIBUTION LIST

Prof. Thomas Ahrens
Seismological Lab, 252-21
Division of Geological & Planetary Sciences
California Institute of Technology
Pasadena, CA 91125

Prof. Keiiti Aki
Center for Earth Sciences
University of Southern California
University Park
Los Angeles, CA 90089-0741

Prof. Shelton Alexander
Geosciences Department
403 Deike Building
The Pennsylvania State University
University Park, PA 16802

Dr. Ralph Alewine, III
DARPA/NMRO
3701 North Fairfax Drive
Arlington, VA 22203-1714

Prof. Charles B. Archambeau
CIRES
University of Colorado
Boulder, CO 80309

Dr. Thomas C. Bache, Jr.
Science Applications Int'l Corp.
10260 Campus Point Drive
San Diego, CA 92121 (2 copies)

Prof. Muawia Barazangi
Institute for the Study of the Continent
Cornell University
Ithaca, NY 14853

Dr. Jeff Barker
Department of Geological Sciences
State University of New York
at Binghamton
Vestal, NY 13901

Dr. Douglas R. Baumgardt
ENSCO, Inc
5400 Port Royal Road
Springfield, VA 22151-2388

Dr. Susan Beck
Department of Geosciences
Building #77
University of Arizona
Tucson, AZ 85721

Dr. T.J. Bennett
S-CUBED
A Division of Maxwell Laboratories
11800 Sunrise Valley Drive, Suite 1212
Reston, VA 22091

Dr. Robert Blandford
AFTAC/TT, Center for Seismic Studies
1300 North 17th Street
Suite 1450
Arlington, VA 22209-2308

Dr. G.A. Bollinger
Department of Geological Sciences
Virginia Polytechnical Institute
21044 Derring Hall
Blacksburg, VA 24061

Dr. Stephen Bratt
Center for Seismic Studies
1300 North 17th Street
Suite 1450
Arlington, VA 22209-2308

Dr. Lawrence Burdick
Woodward-Clyde Consultants
566 El Dorado Street
Pasadena, CA 91109-3245

Dr. Robert Burrige
Schlumberger-Doll Research Center
Old Quarry Road
Ridgefield, CT 06877

Dr. Jerry Carter
Center for Seismic Studies
1300 North 17th Street
Suite 1450
Arlington, VA 22209-2308

Dr. Eric Chael
Division 9241
Sandia Laboratory
Albuquerque, NM 87185

Prof. Vernon F. Cormier
Department of Geology & Geophysics
U-45, Room 207
University of Connecticut
Storrs, CT 06268

Prof. Steven Day
Department of Geological Sciences
San Diego State University
San Diego, CA 92182

Marvin Denny
J.S. Department of Energy
Office of Arms Control
Washington, DC 20585

Dr. Cliff Frolich
Institute of Geophysics
8701 North Mopac
Austin, TX 78759

Dr. Zoltan Der
ENSCO, Inc.
1400 Port Royal Road
Springfield, VA 22151-2388

Dr. Holly Given
IGPP, A-025
Scripps Institute of Oceanography
University of California, San Diego
La Jolla, CA 92093

Prof. Adam Dziewonski
Hoffman Laboratory, Harvard University
Dept. of Earth Atmos. & Planetary Sciences
20 Oxford Street
Cambridge, MA 02138

Dr. Jeffrey W. Given
SAIC
10260 Campus Point Drive
San Diego, CA 92121

Prof. John Ebel
Department of Geology & Geophysics
Boston College
Chestnut Hill, MA 02167

Dr. Dale Glover
Defense Intelligence Agency
ATTN: ODT-1B
Washington, DC 20301

Eric Fielding
SNEE Hall
INSTOC
Cornell University
Ithaca, NY 14853

Dr. Indra Gupta
Teledyne Geotech
314 Montgomery Street
Alexandria, VA 22314

Dr. Mark D. Fisk
Mission Research Corporation
735 State Street
P.O. Drawer 719
Santa Barbara, CA 93102

Dan N. Hagedorn
Pacific Northwest Laboratories
Battelle Boulevard
Richland, WA 99352

Prof Stanley Flatte
Applied Sciences Building
University of California, Santa Cruz
Santa Cruz, CA 95064

Dr. James Hannon
Lawrence Livermore National Laboratory
P.O. Box 808
L-205
Livermore, CA 94550

Dr. John Foley
NER-Geo Sciences
1100 Crown Colony Drive
Quincy, MA 02169

Dr. Roger Hansen
HQ AFTAC/TTR
Patrick AFB, FL 32925-6001

Prof. Donald Forsyth
Department of Geological Sciences
Brown University
Providence, RI 02912

Prof. David G. Harkrider
Seismological Laboratory
Division of Geological & Planetary Sciences
California Institute of Technology
Pasadena, CA 91125

Dr. Art Frankel
U.S. Geological Survey
922 National Center
Reston, VA 22092

Prof. Danny Harvey
CIRES
University of Colorado
Boulder, CO 80309

Prof. Donald V. Helmberger
Seismological Laboratory
Division of Geological & Planetary Sciences
California Institute of Technology
Pasadena, CA 91125

Prof. Eugene Herrin
Institute for the Study of Earth and Man
Geophysical Laboratory
Southern Methodist University
Dallas, TX 75275

Prof. Robert B. Herrmann
Department of Earth & Atmospheric Sciences
St. Louis University
St. Louis, MO 63156

Prof. Lane R. Johnson
Seismographic Station
University of California
Berkeley, CA 94720

Prof. Thomas H. Jordan
Department of Earth, Atmospheric &
Planetary Sciences
Massachusetts Institute of Technology
Cambridge, MA 02139

Prof. Alan Kafka
Department of Geology & Geophysics
Boston College
Chestnut Hill, MA 02167

Robert C. Kemerait
ENSCO, Inc.
445 Pineda Court
Melbourne, FL 32940

Dr. Max Koontz
U.S. Dept. of Energy/DP 5
Forrestal Building
1000 Independence Avenue
Washington, DC 20585

Dr. Richard LaCoss
MIT Lincoln Laboratory, M-200B
P.O. Box 73
Lexington, MA 02173-0073

Dr. Fred K. Lamb
University of Illinois at Urbana-Champaign
Department of Physics
110 West Green Street
Urbana, IL 61801

Prof. Charles A. Langston
Geosciences Department
403 Deike Building
The Pennsylvania State University
University Park, PA 16802

Jim Lawson, Chief Geophysicist
Oklahoma Geological Survey
Oklahoma Geophysical Observatory
P.O. Box 8
Leonard, OK 74043-0008

Prof. Thorne Lay
Institute of Tectonics
Earth Science Board
University of California, Santa Cruz
Santa Cruz, CA 95064

Dr. William Leith
U.S. Geological Survey
Mail Stop 928
Reston, VA 22092

Mr. James F. Lewkowicz
Phillips Laboratory/GPEH
Hanscom AFB, MA 01731-5000(2 copies)

Mr. Alfred Lieberman
ACDA/VI-OA State Department Building
Room 5726
320-21st Street, NW
Washington, DC 20451

Prof. L. Timothy Long
School of Geophysical Sciences
Georgia Institute of Technology
Atlanta, GA 30332

Dr. Randolph Martin, III
New England Research, Inc.
76 Olcott Drive
White River Junction, VT 05001

Dr. Robert Masse
Denver Federal Building
Box 25046, Mail Stop 967
Denver, CO 80225

Dr. Gary McCartor
Department of Physics
Southern Methodist University
Dallas, TX 75275

Prof. Thomas V. McEvilly
Seismographic Station
University of California
Berkeley, CA 94720

Dr. Art McGarr
U.S. Geological Survey
Mail Stop 977
U.S. Geological Survey
Menlo Park, CA 94025

Dr. Keith L. McLaughlin
S-CUBED
A Division of Maxwell Laboratory
P.O. Box 1620
La Jolla, CA 92038-1620

Stephen Miller & Dr. Alexander Florence
SRI International
333 Ravenswood Avenue
Box AF 116
Menlo Park, CA 94025-3493

Prof. Bernard Minster
IGPP, A-025
Scripps Institute of Oceanography
University of California, San Diego
La Jolla, CA 92093

Prof. Brian J. Mitchell
Department of Earth & Atmospheric Sciences
St. Louis University
St. Louis, MO 63156

Mr. Jack Murphy
S-CUBED
A Division of Maxwell Laboratory
11800 Sunrise Valley Drive, Suite 1212
Reston, VA 22091 (2 Copies)

Dr. Keith K. Nakanishi
Lawrence Livermore National Laboratory
L-025
P.O. Box 808
Livermore, CA 94550

Dr. Carl Newton
Los Alamos National Laboratory
P.O. Box 1663
Mail Stop C335, Group ESS-3
Los Alamos, NM 87545

Dr. Bao Nguyen
HQ AFTAC/TTR
Patrick AFB, FL 32925-6001

Prof. John A. Orcutt
IGPP, A-025
Scripps Institute of Oceanography
University of California, San Diego
La Jolla, CA 92093

Prof. Jeffrey Park
Kline Geology Laboratory
P.O. Box 6666
New Haven, CT 06511-8130

Dr. Howard Patton
Lawrence Livermore National Laboratory
L-025
P.O. Box 808
Livermore, CA 94550

Dr. Frank Pilotte
HQ AFTAC/TT
Patrick AFB, FL 32925-6001

Dr. Jay J. Pulli
Radix Systems, Inc.
2 Taft Court, Suite 203
Rockville, MD 20850

Dr. Robert Reinke
ATTN: FCTVID
Field Command
Defense Nuclear Agency
Kirtland AFB, NM 87115

Prof. Paul G. Richards
Lamont-Doherty Geological Observatory
of Columbia University
Palisades, NY 10964

Mr. Wilmer Rivers
Teledyne Geotech
314 Montgomery Street
Alexandria, VA 22314

Dr. George Rothe
HQ AFTAC/TTR
Patrick AFB, FL 32925-6001

Dr. Alan S. Ryall, Jr.
DARPA/NMRO
3701 North Fairfax Drive
Arlington, VA 22209-1714

Dr. Richard Sailor
TASC, Inc.
55 Walkers Brook Drive
Reading, MA 01867

Prof. Charles G. Sammis
Center for Earth Sciences
University of Southern California
University Park
Los Angeles, CA 90089-0741

Prof. Christopher H. Scholz
Lamont-Doherty Geological Observatory
of Columbia University
Palisades, CA 10964

Dr. Susan Schwartz
Institute of Tectonics
1156 High Street
Santa Cruz, CA 95064

Secretary of the Air Force
(SAFRD)
Washington, DC 20330

Office of the Secretary of Defense
DDR&E
Washington, DC 20330

Thomas J. Sereno, Jr.
Science Application Int'l Corp.
10260 Campus Point Drive
San Diego, CA 92121

Dr. Michael Shore
Defense Nuclear Agency/SPSS
6801 Telegraph Road
Alexandria, VA 22310

Dr. Matthew Sibol
Virginia Tech
Seismological Observatory
4044 Derring Hall
Blacksburg, VA 24061-0420

Prof. David G. Simpson
IRIS, Inc.
1616 North Fort Myer Drive
Suite 1440
Arlington, VA 22209

Donald L. Springer
Lawrence Livermore National Laboratory
L-025
P.O. Box 808
Livermore, CA 94550

Dr. Jeffrey Stevens
S-CUBED
A Division of Maxwell Laboratory
P.O. Box 1620
La Jolla, CA 92038-1620

Lt. Col. Jim Stobie
ATTN: AFOSR/NL
Bolling AFB
Washington, DC 20332-6448

Prof. Brian Stump
Institute for the Study of Earth & Man
Geophysical Laboratory
Southern Methodist University
Dallas, TX 75275

Prof. Jeremiah Sullivan
University of Illinois at Urbana-Champaign
Department of Physics
1110 West Green Street
Urbana, IL 61801

Prof. L. Sykes
Lamont-Doherty Geological Observatory
of Columbia University
Palisades, NY 10964

Dr. David Taylor
ENSCO, Inc.
445 Pineda Court
Melbourne, FL 32940

Dr. Steven R. Taylor
Los Alamos National Laboratory
P.O. Box 1663
Mail Stop C335
Los Alamos, NM 87545

Prof. Clifford Thurber
University of Wisconsin-Madison
Department of Geology & Geophysics
1215 West Dayton Street
Madison, WS 53706

Prof. M. Nafi Toksoz
Earth Resources Lab
Massachusetts Institute of Technology
42 Carleton Street
Cambridge, MA 02142

Dr. Larry Turnbull
CIA-OSWR/NED
Washington, DC 20505

DARPA/RMO/SECURITY OFFICE
3701 North Fairfax Drive
Arlington, VA 22203-1714

Dr. Gregory van der Vink
IRIS, Inc.
1616 North Fort Myer Drive
Suite 1440
Arlington, VA 22209

HQ DNA
ATTN: Technical Library
Washington, DC 20305

Dr. Karl Veith
EG&G
5211 Auth Road
Suite 240
Suitland, MD 20746

Defense Intelligence Agency
Directorate for Scientific & Technical Intelligence
ATTN: DTIB
Washington, DC 20340-6158

Prof. Terry C. Wallace
Department of Geosciences
Building #77
University of Arizona
Tuscon, AZ 85721

Defense Technical Information Center
Cameron Station
Alexandria, VA 22314 (2 Copies)

Dr. Thomas Weaver
Los Alamos National Laboratory
P.O. Box 1663
Mail Stop C335
Los Alamos, NM 87545

TACTEC
Battelle Memorial Institute
505 King Avenue
Columbus, OH 43201 (Final Report)

Dr. William Wortman
Mission Research Corporation
8560 Cinderbed Road
Suite 700
Newington, VA 22122

Phillips Laboratory
ATTN: XPG
Hanscom AFB, MA 01731-5000

Prof. Francis T. Wu
Department of Geological Sciences
State University of New York
at Binghamton
Vestal, NY 13901

Phillips Laboratory
ATTN: GPE
Hanscom AFB, MA 01731-5000

AFTAC/CA
(STINFO)
Patrick AFB, FL 32925-6001

Phillips Laboratory
ATTN: TSML
Hanscom AFB, MA 01731-5000

DARPA/PM
3701 North Fairfax Drive
Arlington, VA 22203-1714

Phillips Laboratory
ATTN: SUL
Kirtland, NM 87117 (2 copies)

DARPA/RMO/RETRIEVAL
3701 North Fairfax Drive
Arlington, VA 22203-1714

Dr. Michel Bouchon
I.R.I.G.M.-B.P. 68
38402 St. Martin D'Herès
Cedex, FRANCE

Dr. Michel Campillo
Observatoire de Grenoble
I.R.I.G.M.-B.P. 53
38041 Grenoble, FRANCE

Dr. Jorg Schlittenhardt
Federal institute for Geosciences & Nat'l Res.
Postfach 510153
D-3000 Hannover 51, GERMANY

Dr. Kin Yip Chun
Geophysics Division
Physics Department
University of Toronto
Ontario, CANADA

Dr. Johannes Schweitzer
Institute of Geophysics
Ruhr University/Bochum
P.O. Box 1102148
4360 Bochum 1, GERMANY

Prof. Hans-Peter Harjes
Institute for Geophysics
Ruhr University/Bochum
P.O. Box 102148
4630 Bochum 1, GERMANY

Prof. Eystein Husebye
NTNF/NORSAR
P.O. Box 51
N-2007 Kjeller, NORWAY

David Jepsen
Acting Head, Nuclear Monitoring Section
Bureau of Mineral Resources
Geology and Geophysics
G.P.O. Box 378, Canberra, AUSTRALIA

Ms. Eva Johannisson
Senior Research Officer
National Defense Research Inst.
P.O. Box 27322
S-102 54 Stockholm, SWEDEN

Dr. Peter Marshall
Procurement Executive
Ministry of Defense
Blacknest, Brimpton
Reading FG7-FRS, UNITED KINGDOM

Dr. Bernard Massinon, Dr. Pierre Mechler
Societe Radiomana
27 rue Claude Bernard
75005 Paris, FRANCE (2 Copies)

Dr. Svein Mykkeltveit
NTNT/NORSAR
P.O. Box 51
N-2007 Kjeller, NORWAY (3 Copies)

Prof. Keith Priestley
University of Cambridge
Bullard Labs, Dept. of Earth Sciences
Madingley Rise, Madingley Road
Cambridge CB3 0EZ, ENGLAND